# LARGE-AREA SINGLE-CRYSTAL DIAMOND FILMS VIA HOT FILAMENT CHEMICAL VAPOR DEPOSITION

---

A Dissertation

Presented to

The Faculty of the Graduate School

At the University of Missouri

---

In Partial Fulfillment

Of the Requirements for the Degree

Doctor of Philosophy

---

By

PAUL MASON

Dr. Mark Prelas, Dissertation Supervisor

MAY 2014

The undersigned, appointed by the dean of the Graduate School,

have examined the Dissertation entitled

LARGE-AREA SINGLE-CRYSTAL DIAMOND FILMS VIA HOT FILAMENT CHEMICAL VAPOR DEPOSITION

Presented by Paul Mason

A candidate for the degree of

Doctor of Philosophy

And hereby certify that, in their opinion, it is worthy of acceptance.

---

Professor Mark Prelas

---

Professor Sudarshan Loyalka

---

Professor Tushar Ghosh

---

Professor Robert Tompson

---

Professor Stephen Montgomery-Smith

The work is dedicated to my wife Sherri who reminds me that anything is possible. I would also like to thank my daughter, whom I learn from every day. Their support is an ongoing effort that never fails to inspire me.

# ACKNOWLEDGEMENTS

I would like to thank my advisor, Professor Mark Prelas. His willingness to explore new avenues and constant stream of new ideas were instrumental to my success.

The faculty members and staff at the Nuclear Science and Engineering Institute foster the spirit of academic freedom. This spirit has provided the environment necessary for my work as well as the many students before me.

Finally, I would like to thank Brian Samuels who was vital to the development of the equipment design.

# TABLE OF CONTENTS

# LIST OF FIGURES

Figure Page

# LIST OF TABLES

# LIST OF SYMBOLS

| | |
|---|---|
| $\rho$ | Density |
| $\vec{\boldsymbol{v}}$ | Velocity vector |
| $\vec{T}$ | Viscous stress tensor |
| $g$ | Gravitational constant |
| $P$ | Pressure |
| $\mu$ | Viscosity |
| $\delta_{ij}$ | Kronecker's delta |
| $c_p$ | Heat capacity |
| $\sum_{i=1}^{R}$ | Sum of number of reactions |
| $\sum_{g=1}^{G}$ | Sum of number of gas species in reactions |
| $H_g$ | Molar enthalpy for species g |
| $v_{ig}$ | Stoichiometric coefficient for the $i^{th}$ gas species in the $g^{th}$ gas reaction |
| $r_{g,f}^{g}$ | Reaction rate, forward of the $g^{th}$ gas reaction |
| $r_{g,r}^{g}$ | Reaction rate, reverse of the $g^{th}$ gas reaction |
| $T$ | Temperature |
| $m_i$ | Molar mass |
| $\vec{J}_i$ | Diffusive mas flux |
| $k$ | Thermal conductivity |
| $R$ | Ideal gas law constant |
| $D_i^T$ | Thermal diffusion coefficient |
| $f_i$ | Species molar fraction for gas species i |

# ABSTRACT

Production advances have spurred further investigation into identifying properties of synthetic diamond films in high-purity form. These properties have provided evidence that films of exceptionally high quality can be used as a heat sink, as a sensor material in electro-chemistry, and as a neutron sensor. This discussion focuses on purposing a diamond film production method that may be used as a sensor material. To be utilized as a sensor material competitive with existing neutron detectors, these diamond films must be single crystals that are nearly completely free of lattice defects; possess high electron and hole mobility; demonstrate a high response rate to neutron interactions; and be comprised of sufficient cross section to interact with a large number of incident neutrons.

The notion of producing diamond films for this purpose is gaining significant ground. As can be seen in the recent experiments at CERN, Element Six© diamond crystals were used as detection media during the Higgs Boson experiments. Other sensors have been created in which small diamond wafers were multiplexed into a larger detection cross-section through parallel wire bonding. Aside from multiplexing, which is challenging from a cost and fabrication perspective, the resulting cross sectional area is the most significant limitation with using these wafers as sensors. Realistically, the largest diamond film that can be purchased commercially as a neutron detector is a square chip 3.5 mm by 3.5 mm by 0.5 mm thick. However, while prohibitively expensive for commercialization, there are crystals with cross sections as

large as 1 $cm^2$. Improving the probability of interaction of diamond with neutrons can be accomplished by increasing the cross sectional area of the film. The current research effort is aimed at producing a single-crystal diamond wafer that is 5 cm in diameter by 200 µm thick utilizing Hot Filament Chemical Vapor Deposition (HFCVD). This is a twenty-fold increase in cross-sectional area and therefore, an increase by the same amount in the probability of interaction with incident neutrons. Two hundred micrometers is estimated as the minimum thickness required for a resultant semiconductor grade wafer that can be used as a substrate in Microwave Plasma-Assisted Chemical Vapor Deposition (MPACVD).

The use of Hot Filament Chemical Vapor Deposition (HFCVD) resulted in a large-area single-crystal diamond wafer measuring 4.4 cm in diameter, 370 µm thick by using a 90/10 platinum/iridium foil substrate coated in a mixture of 0-2 µm and 5-8 µm natural diamond powder. This was covered with a 5 cm diameter boron nitride ring to alter the incoming gas flow to the optimum velocity necessary for growth. Diamond nucleation and subsequent homoepitaxial growth formed on the diamond seed crystals. Growth began near the ring and progressed symmetrically and radially inward. Coalescing nucleation points from the Pt/Ir foil and seed crystals merged without visible distinction between the individual structures. Diamond growth mimicked the surface topography of the foil and piping (µm-sized holes) was present in the final film. Optical and microanalysis were used to determine that the entire 4.4 cm diameter underside of the film is one crystal.

# 1. INTRODUCTION

The properties of diamond films of exceptionally high quality make them ideal for use as a heat sink, as a sensor material in electro-chemistry, as a neutron sensor, for infrared transparent films, or for scanning probe microscopy.[1-4]

This research aims to produce a single-crystal diamond wafer 4.5 cm in diameter and at least 200 µm thick utilizing Hot Filament Chemical Vapor Deposition (HFCVD): This represents a twenty-fold increase in cross-sectional area over previously produced wafers of electronic grade quality. Electronic grade by manufacturers such as Element Six© is defined as containing less than 5 parts per billion (ppb) nitrogen and less than 1 ppb boron. The resultant wafer must be a minimum thickness of 200 µm to be used as a substrate in Microwave Plasma-Assisted Chemical Vapor Deposition (MPCVD). Polishing requires removal of 50 µm total; film thickness of over 100 µm can be mechanically polished without fracture.

Other CVD methods used to achieve diamond growth include combustion flame, laser ablation, plasma-jet and microwave plasma assisted CVD (MPCVD). Each is subject to inherent advantages and limitations. Combustion flame-assisted method is limited by the stoichiometric ratio of the flame material (usually acetylene). HFCVD (Hot Filament Chemical Vapor Deposition), unlike MPCVD, is limited by thickness of the diamond growth, uniformity of the hot filament temperature across multiple wires, film growth rate, and steady state operation of the reactor.[5-8]

MPCVD substrate surface area is limited by lower microwave frequency (as low as 915 MHz) and size of the standing wave cavity.[6, 9] Substrate growth must be heteroepitaxial at 5 cm or larger (with the exception of mosaics) due to a lack of large area diamond substrates available.[10, 11] However, at 915 MHz, microwave chambers that can accommodate substrates as large as 16 cm are being constructed.[12]

There is a great demand and multiple applications for larger crystals than can currently be produced, on example being infrared transparent (7-15 μm wavelength) windows for military applications. Existing technology for creating diamond wafers above 1 $cm^2$ allow defects caused by contamination or lattice offset that result in crystallite formation.[13] To date, the largest diamond wafer usable in microwave CVD without the use of mosaic methods is 1 $cm^2$.[6, 14] However, utilizing the tiling/mosaic method has yielded monocrystalline wafers (as defined by the authors) as large as 1 $in^2$ and theoretically as large as 4 inches in diameter using Ir/YSZ/Si (001) heteroepitaxial growth.[13, 15] Wafers created using the mosaic technique lack uniformity in purity concentrations and growth planes are visible at the interfaces between the adjacent single crystals used in the mosaic. Diamond wafers using the Ir/YSZ/Si (001) substrate have poor homogeneity. Contamination and boundaries present in the final film make these crystals unsuitable for semiconductor applications. The pyramidal-shape substrate technique aims to reduce these challenges by growing wafers as thick is 1 mm which will reduce these errors as it grows.[16] Even diamond wafers purchased by our

research department from suppliers, when tested, possessed required specifications but results of electron and hole mobility testing were lower than quoted.

With MPCVD, crystallites present in the diamond substrate replicate during growth whereas irregular dopant or atomic holes can be repaired. DC Arc Plasma Jet CVD produces growth rates as high as 17.4 μm/hr., but like MPCVD, requires a large area diamond.[17] Using non-diamond materials (heteroepitaxy) to grow diamond has made progress.[15, 18] However, to date a single-crystal diamond of large surface area is required to grow an electronic grade diamond of similar surface area using any method.[6, 11] Recent attempts at a mosaic technique where single crystal plates are placed edge-to-edge have been successful but have not proven to eliminate boundary growth and contamination issues.[13, 19]

Due to interference with merging growth planes, heteroepitaxial growth on areas larger than 1 $cm^2$ produces crystalline defects which can lead to polycrystalline growth.[11] Homoepitaxial growth on single crystal substrates in MPCVD chambers does not produced lattice mismatches and seems to possess the ability to merge growth planes into a monocrystalline diamond. This suggests it may be possible for scale-up problems found in MPCVD growth to be corrected by using a larger than 1 $cm^2$ diamond substrate created using coalescing methods.[11] The need for large single crystal substrates in MPCVD is the basis for this work.

# 2. ANALYSIS

In contrast to other HFCVD reactors that use 1-8 wires, 13 wires were strung across the surface of the substrate for a total coverage distance of 5 cm and a vertical distance of 4-8 mm. Gasses in predefined proportions were introduced 2.30 cm above the wires with a 0.64 cm diameter nozzle. Approximately 15 amps per wire were applied to attain a temperature of approximately 2000 C. However, the current requirements change as the tungsten filaments age and resistance in the wires increases. Only hydrogen and methane gases at 99% +/- 1% and 1.00% +/- 0.01% respectively were used during the one hour bias enhanced nucleation (BEN) stage. Molar gas fractions for hydrogen, oxygen, and methane were applied after nucleation at 99% +/- 1%, 0.10% +/- 0.01%, and 0.99% +/- 0.01% respectively. Errors in flow rates are based on performance information in equipment literature. Calculated errors were found to be 0.5% in hydrogen, 0.01% in oxygen, and 0.01% in methane flow.

A 100 µm thick polished platinum/iridium foil coated with 0-2 and 5-8 µm natural diamond powder served as the substrate. This plate was polished with the 0-2 µm natural diamond powder that was aligned with a fluidized technique discussed in section 5.3. A DC positive bias was applied to the substrate during the experiment such that the breakdown current was maintained at 50 mA. The filament temperature during the one-hour nucleation phase was 2200 C and afterward 2000 C. Film closure was confirmed by visual inspection during the run which required 17 days of continuous operation. Upon removing the film from the chamber, it separated from the substrate

due to the differences in thermal expansion between the metal and diamond, yielding a single crystal free from the metal surface.

The crystal size of the seed material chosen was ideal for this experiment. The 0-2 μm diamond crystals were applied dry to the metal surface and then the surface was wetted with DI water followed by application of 5-8 μm diamond crystals. Crystals smaller than 10 μm are overcome with electrostatic forces causing them to clump which prevents uniform distribution even when suspended in the liquids mentioned in section 5.3.[20] The corners of smaller crystals pierced the surface of the DI and sank, proving them unsuitable for use in a fluidized bed which requires them to float. However, this challenge was eventually overcome and the 0-2 μm diamond powder was successfully implemented.

Early experiments in the current work in scale-up of the HFCVD reactor indicated that the substrate must be covered with the filaments and the filament-to-filament spacing must be close to the filament-to-substrate distance.[21] Original substrate diameter was 6.48 cm and total filament horizontal coverage for nine wires was 3.63 cm. The substrate was redesigned for 5.08 cm and the wires redesigned maintaining the filament-to-filament spacing for 13 wires at 5.44 cm so that the substrate was completely covered. This increased average power density resulted in an increase in convective, radiative, and conductive heat transfer. An internal and external cooling system was installed to prevent overheating of the substrate and to protect the external components of the reactor.

Carburization of the tungsten filaments was necessary to minimize tungsten contamination in the final product. Tungsten evaporation rates are much higher than that of tungsten carbide (WC or $WC_2$) and require carburization to avoid contamination during diamond growth.[22] Care must be taken to avoid over carburization as graphitization of the tungsten surface, cannot easily be reversed and will prevent the bond disassociation of the inlet gas. Over-carburization was prevented by limiting carburization to 30 minutes, thus preventing complete conversion from $W_2C$ to WC.

# 3. A BRIEF HISTORY OF DIAMOND GROWTH

HFCVD was chosen for producing large diamond films utilizing the reactor design and the operating conditions used in previous work as a starting point. The design and operating parameters were then altered to facilitate the scale-up needed to achieve large scale growth.

In determining the feed gas ratio for the CVD reaction required to produce diamond, results reported by Angus in 1993 and Bachmann in 1991 were reviewed.[23, 24] Bachmann's investigations of several CVD systems yielded the requisite gas mixture, noting that the only requirement for success was the correct ratio of elemental carbon, hydrogen, and oxygen. Different gas concentrations and compositions yield different growth orientations.[23, 25, 26] Initial ratios chosen for carbon, hydrogen and oxygen were optimized on the CO line as reported on the ternary diagram but produced oxygen contamination in the final crystal. In this work, only one-fifth of the expected amount of oxygen was required, and the reaction produced less oxygen contamination in the diamond matrix than using the CO line.

The nucleation stage is the most important step of growth, regardless of crystal orientation.[27] This step determines the rate, organization, orientation, and overall condition of the film produced. Spitsyn studied epitaxial growth, morphology, and growth kinetics in an attempt to optimize growth rate and concluded that multiple gas phase activation methods could be plotted as a function of deposition rate versus reciprocal absolute temperature.[26] This work was utilized to determine the optimal

nucleation conditions. Researchers for Oak Ridge National Laboratory concluded that adding oxygen to the carbon and hydrogen gas mixture lowered the required substrate and filament temperature requirements.[28] Asmussen concluded that the addition of oxygen during the nucleation phase can interfere with nucleation density.[29] Therefore, during experimentation, oxygen was added only after the nucleation stage. Chao demonstrated that, under certain conditions, smooth diamond films can be created using heteroepitaxial growth.[30] While heteroepitaxial growth was attempted on silicon and metals such as copper, platinum, titanium, and molybdenum, polycrystalline growth was always the result.[31-35]

Micron-sized diamond powder can be used to electrophoretically distribute diamond seed crystals, as proven by Lee, which may then be consolidated through growth via HFCVD.[20] For this work, acetone was used to suspend 5 μm crystals to obtain a monolayer of seeds using a similar electrophoretic distribution technique. Growth was consistent with original orientation but large area growth, by Lee's definition, did not result.

Nucleation and metastable growth was revisited in 1999 to see if heteroepitaxial growth could yield single-crystal growth.[36] Although the mechanisms for growth in several methods were exhaustively researched and outlined, this research did not provide a means to achieve single crystal growth. Kwon attempted to determine if the flow distribution of the starting gas could be more evenly distributed via micro channel

over the surface of the substrate.[37] This was initially attempted in the current work and led to the current nozzle design.

It has been proposed that growth rate of diamond via HFCVD has been too slow to be practical for commercial purposes.[38] In the current work, this slow growth rate is used as an advantage to allow for auto-alignment of the diamond seed. Yan and researchers in 2002 reported growth rates as high as 150 μm/hour using microwave plasma assisted CVD (MPCVD).[39] In 2002, Asmussen discussed the advances of the prior decade regarding reaction mechanics in hot filament reactions.[29] His book discussed numerous deposition/termination methods based primarily on the 4.5 eV bond disassociation of hydrogen.[29] The primary ion that contributes to the active deposition phase was identified as $CH_3^-$, providing a significant and well-confirmed result whose importance is linked to calculation of the growth rate based on ionic species concentration.[29, 38] Homogeneous nucleation mechanics were discussed in detail outlining the possibility of a large structure utilizing scale-up techniques from smaller structures and intermediate carbide materials on homogeneous substrates have been shown to be the true medium for growth in certain circumstances.[29] This carbide formation was observed in the current work during this investigation. Deposition chemistry conditions chosen for nucleation are not necessarily the optimal conditions for subsequent growth, with pressures as low as 2-10 torr being best for nucleation and pressures of 20-40 torr being best for post-nucleation growth. The addition of oxygen

increases nucleation density at reduced substrate (below 900 C) temperatures due to the lower binding energy of OH to C at 3.68 eV versus CH to C at 4.63 eV.

Other disadvantages of HFCVD include the bypass of carbon containing compounds; restrictions of substrate-to-filament distance; distance of filament-to-filament; and the need for filament carburization prior to use. HFCVD requires the use of carburized filaments that cause bond disassociation, and therefore convert carbon sources to ionic $CH_3^-$.[29] Substrate-to-filament distances must not exceed 8 mm due to recombination of participating species of methyl and hydrogen ions.[29] The filament-to-filament distance should approximate the filament-to-substrate distance during scale-up to promote temperature uniformity of heating and greatest decomposition of the inlet species to their corresponding ions.[29] Carburization of the filaments prior to use is essential and allow for clean growth.[40] In tungsten, the final product on the filament surface should be tungsten carbide (WC and $WC_2$).

In 2004, study of single-crystal growth mechanics revealed which growth plane and orientation were favored at specific substrate temperatures, gas inlet concentrations, and etching pretreatment.[41] Diamond was reportedly grown on tungsten carbide, which is consistent with the statements made by Asmussen.[29] Silicon substrates were re-examined in 2007 with advanced slurry substrate pre-treatment utilizing diamond and zirconium with improved results.[42]

The limitations for diamond growth via all CVD processes are that they can only produce a diamond of equivalent surface area to the substrate. Microwave plasma is

believed by some researchers to be the only method of producing high quality single crystal diamond.[12] To overcome limitations in horizontal growth in MPACVD in 2005, researchers attempted to use a repeating method to grow diamond vertically in multiple steps leading to a single crystal vertical growth of 1 cm.[43] Crystal horizontal dimensions were 5 x 5 mm.

For Microwave CVD, excellent quality diamond can be grown via homoepitaxial growth as long as the starting material is well-prepared.[44, 45] The challenge lies in separating the growth from the starting material. Ion implantation has been used to commercially grow consistent quality single crystal diamond utilizing the lift-off method.[46, 47] This provides a method to theoretically reproduce the surface area of any starting crystal. However, a new mosaic technique is gaining ground to increase the surface area of the final product while using smaller starting materials placed in proximity during growth.[13, 19]

Creating custom substrates via ink jet application of nano-diamond suspension was successfully accomplished.[48] While single-crystal diamond was not the intended result, CVD was implemented to lattice the nano-diamond powder. Other strategies previously employed to align nano-crystal diamond include the use of a solvent such as n-hexane on a copper substrate. Interaction between the diamond, copper, and solvent created an electrostatic effect that allowed for the self-alignment of the crystals.[32] Subsequent nucleation and growth produced polycrystalline results. Very recent advances in DC Ark Plasma techniques show promise for producing large, single crystal

growth.[17] Even though this method produces high growth rates, it also produces contamination resulting in non-homogeneity in the final film.

Regardless of which low pressure, high temperature method is employed, the objective remains constant: Upon contact of the incoming gas with hot filaments, the bonds of the diatomic molecules (hydrogen and oxygen) and one of the hydrogen bonds in the methane molecule disassociate, resulting in free radicals of hydrogen, oxygen, and the methane radical, $CH_3^{\cdot}$.[49] First, hydrogen etches the surface of the diamond seed and terminates the carbon bonds with hydrogen. Loosely connected, the hydrogen bonds are then periodically replaced by the methane radical, carbon-side down. This replacement extends the $sp^3$ bonded carbon and again terminates with hydrogen bonds, awaiting the next methane radical. Termination structure of the carbon atoms are determined by the starting structure. For example, a (111) diamond will produce more (111) oriented diamond growth.

Based on the research stated above, one method that showed promise for large-area diamond films was HFCVD with homoepitaxial growth and seed crystal alignment. The seed crystal alignment proved challenging, requiring a multi-step procedure discussed in section 5.3. The slow growth rate of HFCVD can be used as an advantage. Overcoming the balance between hydrogen etching and growth will provide very slow growth rates. This low growth rate (0.1-0.9 μm/hour) may allow for alignment via bias of the seeds and subsequent growth into a coalesced single crystal diamond surface.

# 4. DISCUSSION

## 4.1 Homoepitaxial growth

Heteroepitaxial growth was accomplished on metal substrates due to prior observations of the interaction between metal and diamond which created highly oriented films.[35, 50, 51] However, homoepitaxial growth was chosen because most heteroepitaxial growth methods do not show promise for large substrates due to bond angle dislocations between the substrate and growth.[52] Even with the recent advances in Ir/YSZ/Si (001) heteroepitaxial growth, the substrate pretreatment is complex and time consuming.[18] In addition, the smooth films that have been produced on iridium that minimize these dislocations are unsuitable for electronics applications.[18, 53] This challenge of bond dislocation is inherent in the nature of the materials. Therefore, its solutions afore mentioned must be a modification of the natural properties of the material such as doping, scratching, layering, and other pretreatment options. It would be less time consuming and less costly to start with a technique that is insensitive to submicron defects or create a technique that self corrects defects as the reaction proceeds.

## 4.2 Crystal seed stock

A final technique utilizing 0-2 µm (statistical size) diamond polishing powder was implemented. The clumping issue was overcome using a dry method to discharge the electrostatic buildup on the crystals before applying them to the substrate surface.

The desired crystal morphology should be in the orientation of interest because the orientation that is used is the orientation that will grow in the current reactor. Cuboid octahedral and randomly oriented crystals are available and have been used. The primary stock used is a combination of (111), (101), and (110). Crystals are distributed but not aligned on their faces prior to insertion into the reactor. Faces are auto-aligned during the experiment allowing for single crystal growth.

### 4.3 Scale-up

Research in scale-up on HFCVD reactors indicate that the substrate must be covered with the filaments and the filament to filament spacing must be close to the filament to substrate distance. The substrate is designed for 2" (5.08 cm) and the wires maintain the filament-to-filament spacing so that the substrate was completely covered. Increased power density increased convection, radiation, and conductive heat transfer. To compensate, an internal and external cooling system was employed. Maximum internal cooling system heat removal rate is 400 watts. The external cooling system heat removal rate is 1000 watts.

### 4.4 Hot filament pretreatment

Tungsten evaporation rates are much higher than tungsten carbide (WC or $WC_2$). Without carburization, contamination of the diamond growth is inevitable. Graphitization of the tungsten surface (over carburization) cannot be reversed and will prevent the bond disassociation of the inlet gas. Although graphite is both thermally

and electrically conductive, experiments conducted with over graphitized filaments show surface temperature of the wire reduced by over 150 degrees Celsius.

### 4.5 Copper as a substrate holder

Some authors report growing diamond on copper.[54] Initially, it was thought copper could be used as a fluidized bed during the reaction by melting the copper during growth. This proved to be challenging as copper exhibits a 0.5 ppm vapor pressure at 20 torr and 900 C. This pressure was sufficient to interfere with diamond growth.

# 5. EXPERIMENTAL EQUIPMENT DESIGN

An overview of the equipment inside of the reactor is shown in figure 1. The reactor is an 18” inner diameter, 30” tall vessel equipped with a calcium fluoride crystal site glass, pressure sensor, two internal temperature sensors, support stand and a cooling system for the substrate. The stand provides a support for the once-thru cooling coils under the substrate holder. A boron nitride substrate holder, with a 5.1 cm diameter hole drilled 3 mm into the block, provides a thermal barrier to protect the copper cooling block from overheating. It is necessary to use a material between the thermal mass and the substrate in order to align the crystals. The thermal mass is used to regulate the temperature changes between the substrate cooling system and the filaments. Upon a change in temperature either from the cooling system or the filaments, the thermal mass (boron nitride block) increases the time it takes for the temperature to change on either side of the block. This reduces thermal stress on the substrate and simplifies temperature adjustments through gradual changes.

This material, consisting of diamond, copper, titanium, stainless steel, silicon, or other materials, was placed directly in the recess in the substrate holder with the align diamond crystals on top as seen in figure 2. The filaments, constructed of 0.019” diameter tungsten wire were suspended between two copper bars and supported by boron nitride plates. Direct current power was applied across the bars and through the tungsten. The tungsten has a lower electrical conductivity and therefore much higher electrical resistance than copper.

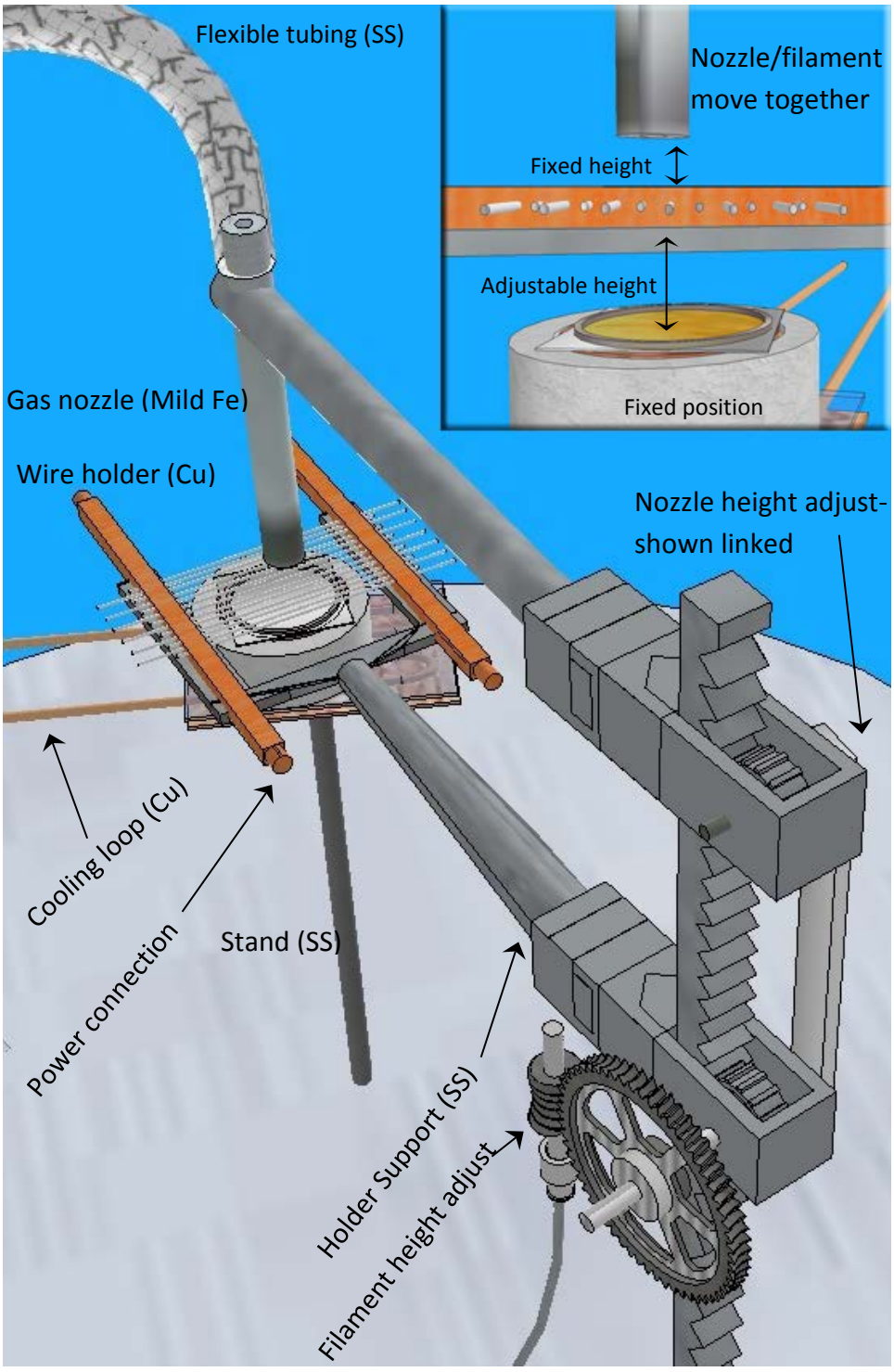


Figure 1: Overall CVD reactor system design

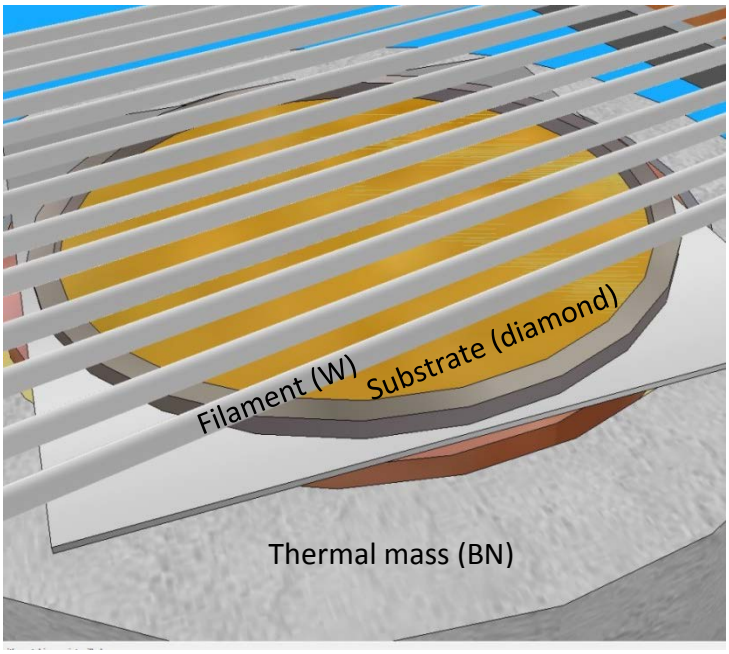

Figure 2: Substrate design

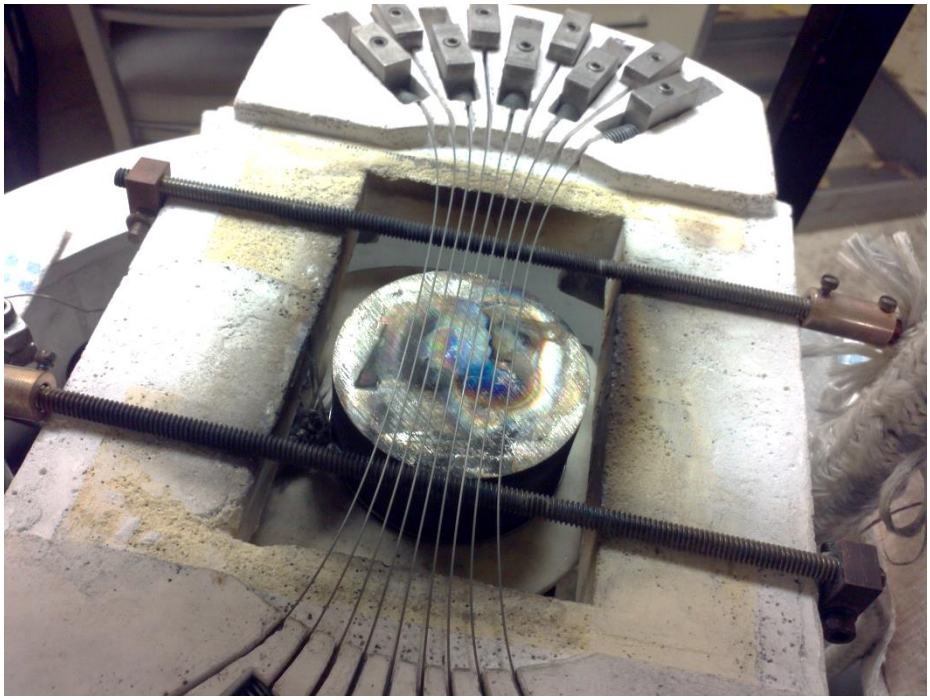
Figure 3: Original filament holder design

The resistances to current caused the tungsten wires to heat and eventually glow; providing the necessary energy for the experiment. The gas for the CVD was distributed through a ¼" outer diameter Swagelok® tube with a reduced inner diameter to 0.1080". The combined flow rates of the hydrogen, oxygen, and methane are 202.25 standard cubic centimeters per minute (SCCM). This produced a flow of 1.87 feet per second (laminar flow) at the nozzle. The ideal nozzle-to-filament spacing for 202.25 SCCM is 0.9065". The power supply for the filaments is two HP 6682A in auto-parallel with a capacity of 21 volts and 480 amps for a total power capacity of 10 kW. Flow of ultra-high purity grade methane, oxygen, and hydrogen is controlled by a MKS 100 series flow controller fed into a MKS type 247D readout. The positive bias for the substrate is applied via a custom designed high voltage/low amps (0-600 V. 0-250 mA) power supply. Filament temperature measurements are conducted externally via Mikron Pyrometer model M90. Tungsten filaments were provided by Midwest Tungsten Service, Inc.

## 5.1 Original filament holder design

The original filament holder was an alumina design in which wires were held into place via aluminum blocks threaded through by the filament with a set screw tensioned with a spring as shown in figure 3. Tension bars served to make electrical contact were placed at 90 degree angels to the wire and held into place via the threads of the wire.

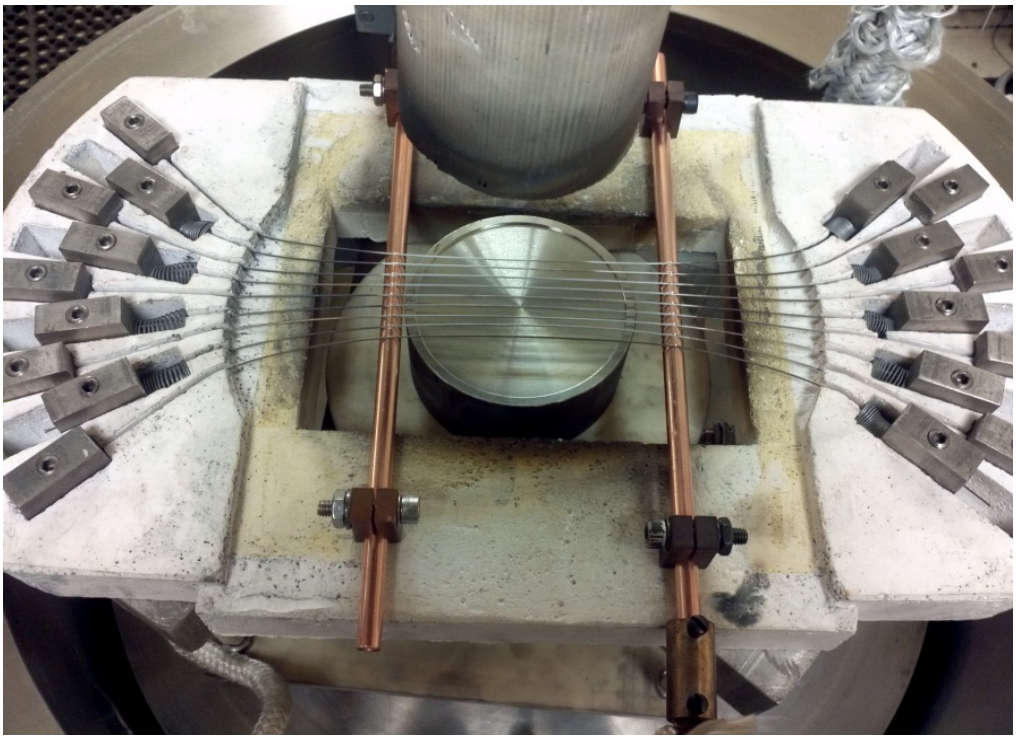

Figure 4: Modified original filament holder design

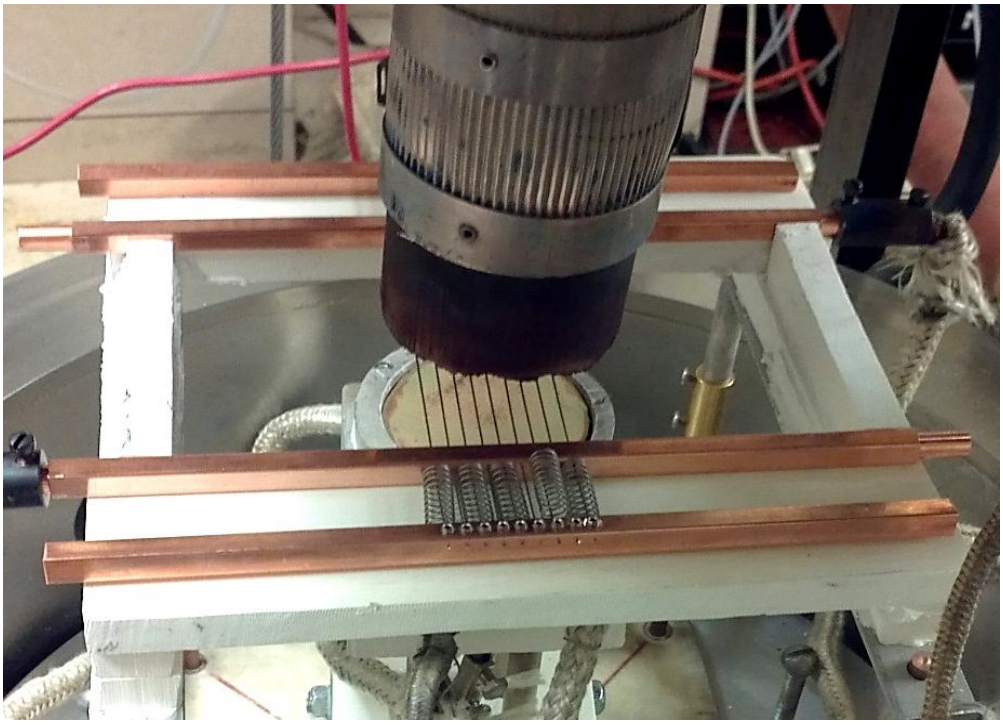

Figure 5: Intermediate filament holder design

This design requires tension to ensure good contact with the threads, with higher tension on the outside wires as opposed to reduced tension at the inside. This inequality and high tension utilizing stainless steel tension bars allowed for only 1-2 hours of operation before wire break. The temperature variation across the wires was over 100 degrees C. Initially, the threaded rods were replaced with copper as shown in figure 4 to increase heat transfer efficiency (the SS rods glowed and ultimately limited their lifetime). The copper rods with recesses provided better heat transfer but only increased the life of the wires to three hours. High tension requirements in the wire made them subject to embrittlement. Without the high tension, contact was intermittent and arcing was common. It was decided to redesign the filament holder. Optimal design should allow for variation in the tension such that the distance between the electrically conducting rods could be varied. Also, the most effective design will be with all wires equally spaced with equal tension.

## 5.2 Intermediate and final filament holder design

The initial redesign consisted of two parallel copper bars separated by springs. Set screws on the outside wire maintained the desired tension on the wires. Consistent tension between the wire and copper appear to have improved contact resulting in increased wire longevity, as shown in figure 5. Wire diameter is 0.019", and hole diameter is 0.025". When the first runs occurred, some wire contacts were not as good as others. This caused the wire to glow on the lateral surface of the inside wire, resulting in undesired thermal variations in the temperature in that filament. Uptake of

carbon by the filaments (through carburization) caused the filaments to increase in diameter occlude this hole until eventually this problem is eliminated usually within the first 1-2 hours. The wires could then be used for multiple runs each lasting approximately 72 hours. Wire life has been improved from 1-2 hours to over 500 hours.

This intermittent contact issue was resolved with the latest design. It was found that tension is not required. Only one side of the set screws was tightened allowing for good contact as shown in figure 6. The other side was allowed to act as a sliding contact inside the copper hole during heating and expansion. To test how much expansion

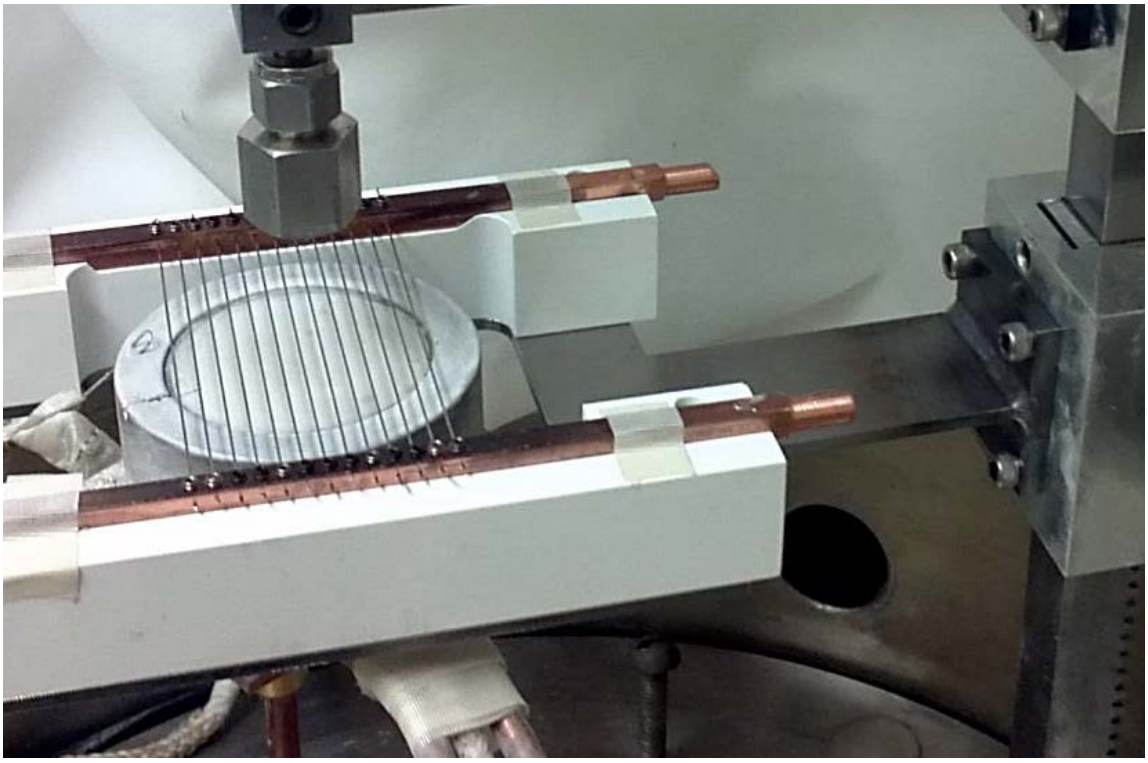

Figure 6: Final filament holder design

occurs, the outside wire was tensioned on both sides. The wire subsequently expanded and deformed during heating, and cracked on cooling. All other wires remained parallel

and intact. Temperature variations were less than 20 degrees Celsius for any wire.

Supports for the copper rods are composed of boron nitride which is electrically insulative and thermally conductive. Total wire length needed per experiment from original design has been reduced from 350 cm to 110 cm. The wire number has been increased from 9 to 13 to cover the entire surface of the substrate.

## 5.3 Substrate pretreatment

### 5.3.1 Introduction to alignment methods- A case study

As in microwave chamber experimental design, the growth of large area crystals in commercial HFCVD reactors relies on heteroepitaxial growth. However, the current design relies upon distribution, orientation, and alignment of small diamond crystals to provide a framework on which to coalesce a single-diamond wafer. Homoepitaxial growth of single crystal diamond using diamond seed crystals has been previously unsuccessful, which has been attributed to misalignment of the smaller diamond with the new growth. As with large area MPACVD, HFCVD growth with misaligned crystals produces polycrystalline growth. Several methods have been attempted for homoepitaxial growth including diamond suspended crystals using inkjet printers and micro-etching of surfaces for diamond to deposit using lasers.[55] Heteroepitaxial methods including mechanical etching and laser etching have been attempted to minimize the lattice defect in substrates (mismatch offset). What follows is a case study

demonstrating one alignment technique in the current work that has been successfully applied. Procedures for applying these methods are shown in appendix C.

### 5.3.2 Experimental method for alignment

Creating a substrate of aligned diamond seed stock requires an inventory of diamond crystals that can be mobilized (organized) microscopically on a macroscopic scale. The tedious technique of placing individual crystals one at a time, attempted in the past, failed because the space between the crystals was proportional to the crystal size. This spacing made coalescence unlikely and, in the event of coalescence, made the resultant product polycrystalline. The goal is to place the crystals side by side with void space (aside from the void space that forms as a result of the geometry) on the average of less than 5% of the diameter of the crystals. Experiments with this configuration yielded highly oriented diamond. If the space between crystals is minimized, the packing fraction increases.

For the configuration chosen, the maximum packing fraction is near 100% due to the triangular shape of the crystals. An increase in packing fraction requires less diamond growth for neighboring crystals to connect and thereby increases the probability of coalescence into a single crystal. Several dozen natural and synthetic diamond seed stock materials were chosen between 40-2500 mesh. The ideal size, based on mobility, gravitational effect versus electrostatic potential, and mechanical distribution capability, is 270-2500 mesh natural or synthetic. It is possible to create uniformly distributed crystals within this range. [56]

There are several ways to mobilize the crystals. One method used mechanical alignment through agitation. The crystals were place on a durable surface and vibrated until a uniform layer was created. During one of the runs using this method, a highly oriented diamond was created. The alignment of the crystals was serendipitous and as yet not been reproduced. Subsequent attempts using the same technique created layers that were poorly aligned and several seed crystals thick, suggesting that mechanical alignment is not predictable.

Fluidizing the crystals with ethanol was more successful because friction was reduced, allowing for greater mobility during agitation. However, since the density of diamond is much higher than ethanol and ethanol's surface tension is low, the seed crystals sank quickly, although they could still be mobilized through agitation. The addition of another liquid, such as water, did not increase surface tension. Different binary solution concentrations yielded inverse relationships between surface tension and adhesion, none of which were acceptable for developing a cohesive mobile floating film.

Crystal alignment was attempted during several experiments by creating a fluidized bed of molten copper and silver directly below the crystals. The lower density of diamond compared with the metals will allow them to float. The metals chosen had melting points at or near the required substrate temperature (1084.62 Celsius for copper and 961.78 Celsius for silver). It is not possible to melt these metals because their heat transfer restrictions prevent solid/liquid phase transitions at the desired

temperatures. In addition, the vapor pressure of the metals interferes with diamond growth. However, there has been some success in molten metal-diamond substrates such as nickel.[35]

Another alignment method involved using surface tension and electrostatics. Canola oil was chosen so that the crystals would float on the surface. Canola oil was an interesting choice with sufficient surface tension and no electrical conductivity, which allowed the crystals to move freely on the surface of the oil while isolating the charge to each crystal during electrostatic treatment. A 1000-volt potential was applied to the surface, electrostatically charging the crystals. Electrostatic alignment of small crystals can be accomplished because diamond can act as dialectic in strong electrical fields. Under the right conditions, this produces an image current making it responsive to electrostatic and magnetic fields.[57] If the diamonds are small enough, the image current will be strong enough to overcome gravitation and friction forces for the diamond to move. In the case of 50 μm seed crystals, the image current generated from a 1 kV commercial ionizer (estimated via stated 4 watt power consumption and estimated 4 mA current) corona wire is more than sufficient to allow for the motion of the crystals. Since the oil functions as an insulator, it was not affected by the field. As crystals came into contact with each other, they clung together via electrostatics and formed a uniformly distributed coating a single crystal thick. While this procedure was useful in determining the nature of charge collection on diamond, the oil is a poor choice due to

contamination of the substrate with a long chain hydrocarbon. However, this did elucidate that a fluidized bed was possible.

The final method utilized a fluidized bed composed of de-ionized water with natural diamond crystals 0-2 μm, 5.5-8 μm, 35 μm, 50 μm and mixtures of several of these sizes. The surface tension of water is higher than the oils used and is compatible with the CVD reaction. Polished copper or a platinum/iridium alloy was wetted with DI water and the diamond crystals were gently applied via sieving. A film developed on the surface of the solution and then a glass burette was injected into the film to remove the water. Water does not readily adhere to the metals used; causing the film to quickly retract from the surface. The contact angle between the liquid and metal was measured at approximately 90 degrees for copper.

Based on these results, it became clear that it was necessary to find a material that would not interfere with the surface tension and, more importantly, would increase the adhesion of the fluid to the metal. Nanocrystalline natural diamond powder was the solution. It was applied as a surface coating to the metal prior to wetting the surface. The coating was then removed with ethanol to verify the wetting technique was not micro abrasion during the application. Rewetting the surface without the micro diamond caused retraction of the DI. A new coating was applied. The water and diamond coating did not retract during extraction of the DI; forming a contact angle of less than 2 degrees. As the extraction progressed, the film came to rest in place forming an aligned layer a single crystal thick and 5 cm in diameter. The metal surface still

contained some DI as well as the crystal layer. Placing the sample into the reactor and applying the vacuum removes the remainder of the water. The nanodiamond and DI do not interfere with the CVD reaction.

To test the alignment procedure to determine if single crystal diamond would result from this procedure, a custom designed HFCVD reactor was used. The ultimate goal is to investigate the creation of a 5 cm diameter single crystal diamond wafer. The substrate stage is cooled and stationary and utilizes a boron nitride ring placed directly on top of the substrate to alter the flow characteristics of the feed gas exiting the 0.25 cm diameter nozzle directly above the stage. The target growth mechanism is homoepitaxial growth with a positively biased substrate. The wire holder and nozzle can be moved during growth but is primarily used to move the filaments and nozzle into place after insertion of the sample. Without pre-alignment techniques in place, polycrystalline growth always occurs with this equipment. The final result of this method is shown in appendix C.

### 5.3.3 Theory of alignment method

Diamond seed crystals have been aligned with Lorentz forces generated though a 3-D electrostatic and pulsing magnetic field. Preferentially textured films have been produced using this method.[57] Through the use of a mosaic of properly oriented diamond seed crystals, it is possible to create single crystal films. The process requires an initial inventory of diamond seed crystals carefully sorted for the proper orientation [001, 011, or 111] and appropriate size (0.1 μm to 1000 μm). It is possible to create

uniformly distributed crystals within this range.[56] It has been proven that highly oriented diamond films can be created through seeding.[58, 59]

The size of the seed crystals must be large enough to survive the initial evaporation, which occurs in the CVD process while conditions equalize. Once on the surface of the substrate and prior to use in the reactor, the crystals are exposed to electrostatic and electromagnetic fields. Since diamond crystals are dielectrics, it has been proven that the interaction of these fields will create surface charge distributions on the diamond seeds. The surface charging mechanism will be different for different seed crystal morphologies. The substrate is placed in a 3D electrostatic field, which will cause the crystals to move via the Lorentz force to spatially distribute the crystals uniformly on the surface and to axially align each crystal.[60] When subjected to a medium containing active free radicals of carbon and hydrogen, diamond will grow on the oriented seed crystals and, since the seeds are uniformly oriented, the CVD diamond growth will coalesce into a smooth, large area, single crystal surface. Growth conditions are chosen which favor the desired crystal orientation.

This seeding and orientation method can be used only on certain noble metals since the method requires noninterference of the metal with the growth zone, a highly polished surface, and may depend upon the lattice parameters of the substrate. The coalesced surface will be allowed to continue to grow at a rate of 0.1-0.9 μm/hour.

### 5.3.4 Results and discussion of alignment method

Electronic grade copper was pretreated by applying a thin coating of 0-2 µm natural diamond powder. Excess material was removed via polishing cloth. DI water was applied to the surface of the copper. DI was not allowed to touch the outside edge of the metal as seen in figure 7.

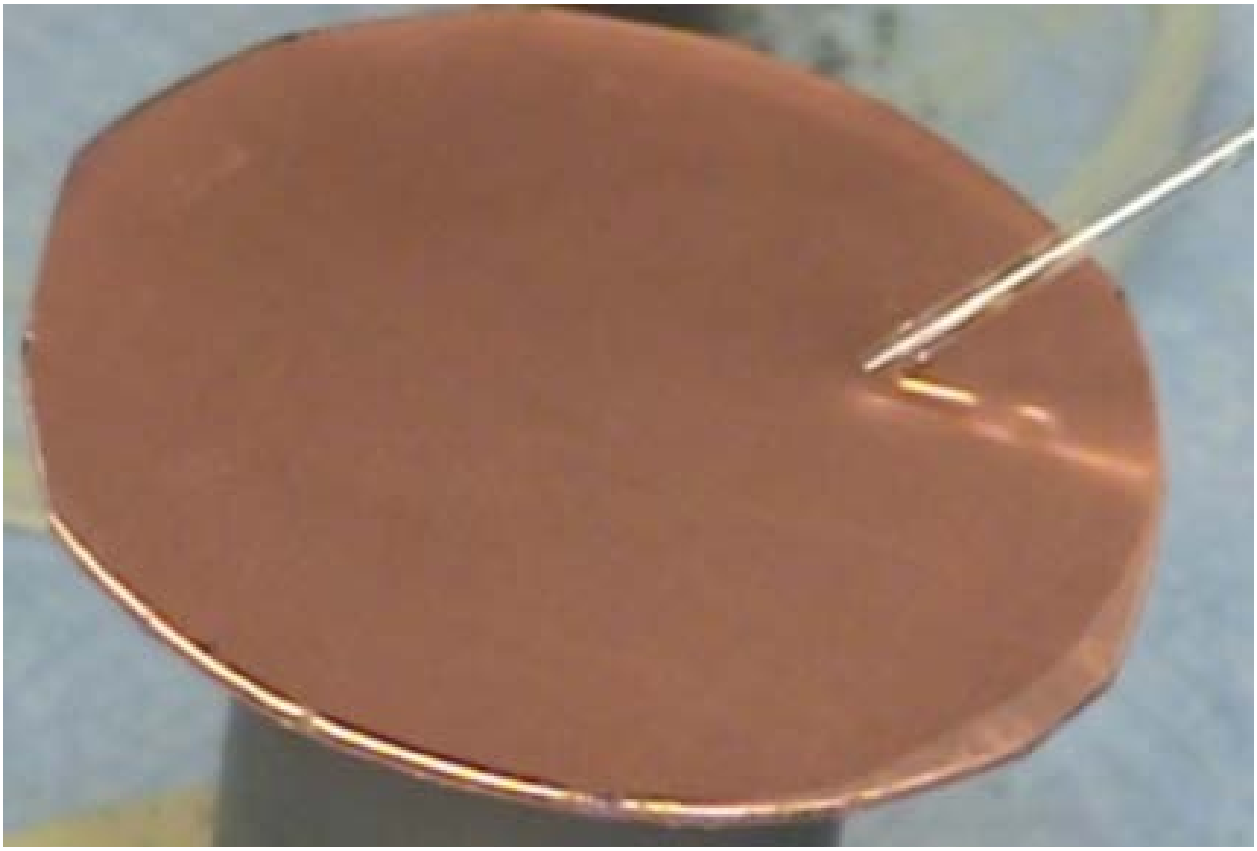

Figure 7: After pretreatment of the copper surface with nano-diamond, contact angle is nearly 0 degrees. This process is reversible by removing the coating with any organic solvent

35 µm +/- 10% seed crystals were applied to the surface of the DI via 35 µm sieve. Overlapping of the crystals was avoided. Once the fluid surface was covered, the surface was exposed to the 1 kV, 4 mA DC corona wire at 2 mm; charging the surface. Diamond movement was visible during this phase. A one Hertz pulsed, 50 gauss

electromagnet was applied 2 mm from the diamond/liquid surface for several minutes. A pulsed magnet was used to encourage relaxation of the crystals which appears to create the most orderly arrangement followed by visible movement of the crystal. The electromagnetic force was terminated when movement of the crystals cease which varied from 2-5 minutes. A glass pipette was used to pierce the diamond film near the interface between the copper and diamond/liquid. The DI was slowly removed; allowing the crystals to come to rest on the copper surface. A small layer of water was left to be evaporated in the reactor. A HFCVD run was initiated for growth.

An optical microscope image was taken before the substrate was placed into the reactor as seen in figure 8.

Figure 8: Aligned diamond crystals before HFCVD run. Open area was determined using Adobe Photoshop® analysis package. Calculated open area is shown as black. Magnification is 400x.

The image was later edited in Photoshop® CC with the analysis package. Crystal edges were identified using the high pass/overlay technique which is common in post image processing. Total pixel count for the crystals and spaces were measured. A saturation layer was applied to identify dark areas of the image (spaces). A select by color range identified the dark areas. Using the histogram data, the total pixel count was 166578 +/-60.17 whereas the spaces were measured as 6461 +/- 29.39. This yields an open area of 3.88% +/- 0.45%. A HFCVD run was performed on the substrate. The run was terminated prior to complete coalescence of the diamond film so that the film did not interfere with the image process calculations. After the HFCVD run was complete utilizing the optical image and histogram data from Photoshop®, the total pixel count was 152036 +/-64.09 whereas the spaces were measured as 11972 +/- 39.78. This yields an open area of 7.87% +/- 0.31%. The processed image is shown in figure 9.

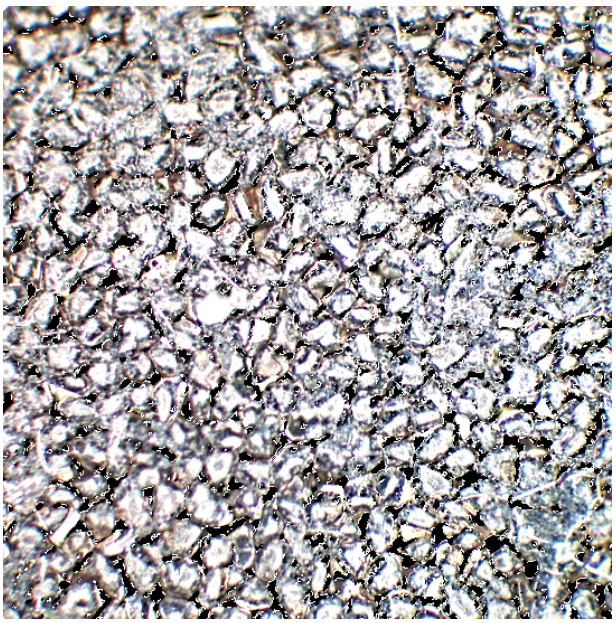

Figure 9: Aligned diamond crystals after HFCVD run. Open area was determined using Adobe Photoshop® analysis package. Calculated open area is shown as black. Magnification is 300x.

Glassy, non-textured, large-area diamond growth for the area of interest on the bottom of the film was confirmed via micro Raman and SEM EDS. The above open area procedure is detailed fully in appendix D.

### 5.3.5 Conclusion of alignment method

The open area doubled after the HFCVD run. Analysis of the average seed crystal size before and after the run indicated this was due to hydrogen etching and movement of the seeds during growth. Seed size decreased approximately 10% on average due to the high temperature of the nucleation phase. Glassy, non-textured, large-area diamond formed between the seed crystals during this run and was counted as open area. Prior runs where open areas were greater than 10% always yielded polycrystalline growth. The objective of the alignment procedure was not to maintain the open area but to allow crystals in close proximity to coalesce despite reduction due to etching. Smaller diameter seed stock yields less contamination in the growth with fewer defects.

## 5.4 Choosing the CVD materials

For CVD to occur, an energy source is required to break the incoming stable gas molecules and produce the ions necessary for vapor deposition. The ratio of starting gas molecules determines whether and in what arrangement diamond will form during the experiment. A significant amount of work has been conducted in this area to determine which atomic ratios are necessary for diamond growth. A ternary diagram

was examined for this purpose.[61] Based on this prior work, gases were selected for use in this work that would provide the greatest degree of control of atomic ratios: Methane, oxygen, and hydrogen. Using these three materials, the carbon-hydrogen-oxygen (C-H-O) ternary diagram can be used to determine the ideal growth environment for diamond. In most cases, this will be a C:O ratio of 1:1 with a less than 1% by atom carbon.

# 6. IDEAL GROWTH PARAMETERS

The objective is to use a HFCVD reactor to produce a large area single crystal diamond of the highest quality possible. An investigation into the optimization of parameters yields more of a range than a single value. Examining the parameters in table 1 will assist in designing equipment that can accomplish the objective. Moreover, it is important to have accurate measurement and control of those parameters.

Table 1: Ideal parameters for CVD operations

| | |
|---|---|
| Nozzle to filament distance | 2.54 cm |
| Filament to substrate distance | 6-8 mm |
| Filament holder design | Copper |
| Filament temperature | 1800-2200 C |
| Substrate temperature | 700-900 C |
| Substrate Seed diameter | 0-2 (statistical) μm |
| Substrate holder material | Diamond with Platinum/iridium |
| Thermal mass material | Boron nitride |
| Substrate holder depth | 1 mm |
| Seed crystal pretreatment | Nano-diamond fluidized bed alignment |
| Substrate bias (positive) | 100(+)volts for 1 hr., off after |
| Substrate holder cooling | Once through water |
| Vessel cooling | Once through water |

# 7. OPERATION OF THE REACTOR

Prior to operation of the filaments, equilibrium inlet gas flow and composition must be balanced by gas removal via vacuum pump. The composition of the gas must be set prior to operation of the filaments due to the size of the chamber. The residence time of the chamber is approximately eight hours to reach the correct values for oxygen and methane if the correct value is not initially correct.

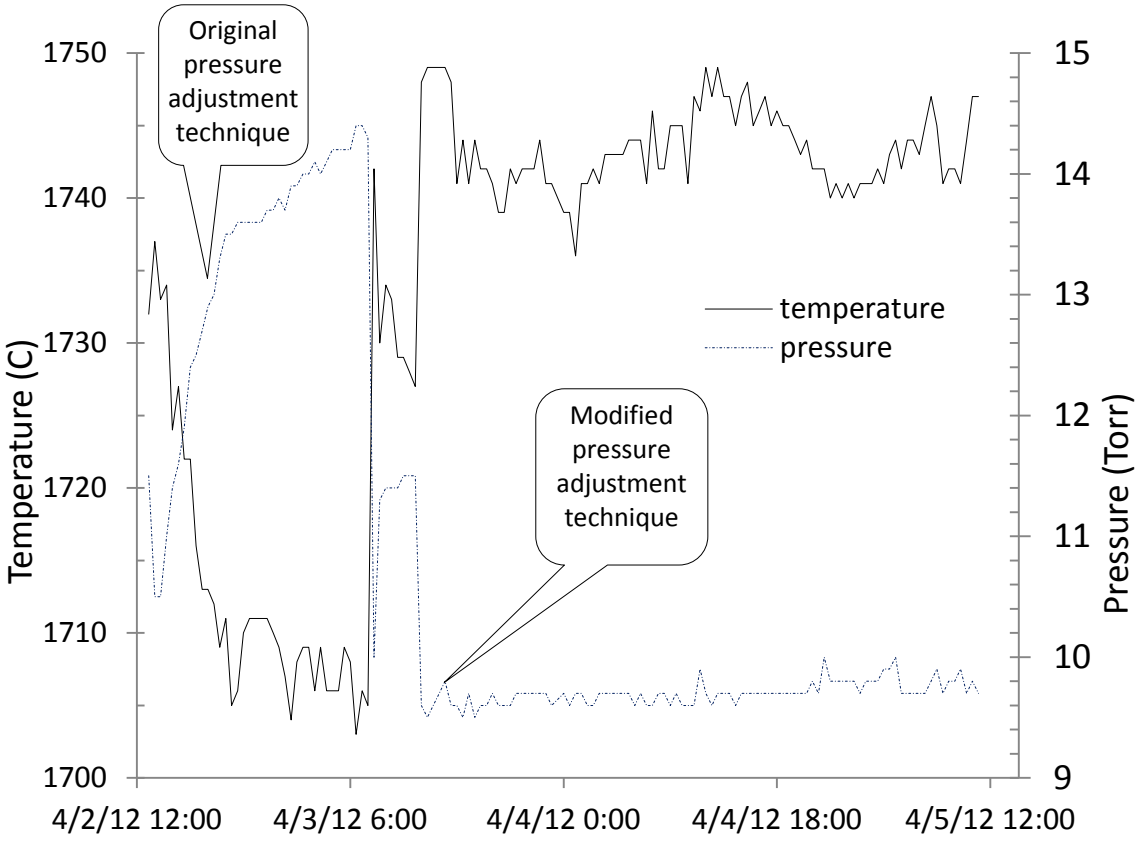


Figure 10: Run 12- Temperature/pressure data: pressure is adjusted, temperature responds automatically and inversely.

Once the appropriate pressure is reached with the correct composition, power can be applied to the filaments. Once filament power is set appropriately, fine tuning of

the substrate temperature can be accomplished with the substrate cooling system. Runs 1-11 used a manual pressure/temperature adjustment. A steady-state balance was determined using a temperature/pressure adjustment technique as shown in figure 10. Ultimately, a highly sensitive vacuum throttling value was installed that allowed the system to stabilize in both temperature and pressure with minimal adjustment without electronic control. Full instructions on system startup and operation are located in appendix B.

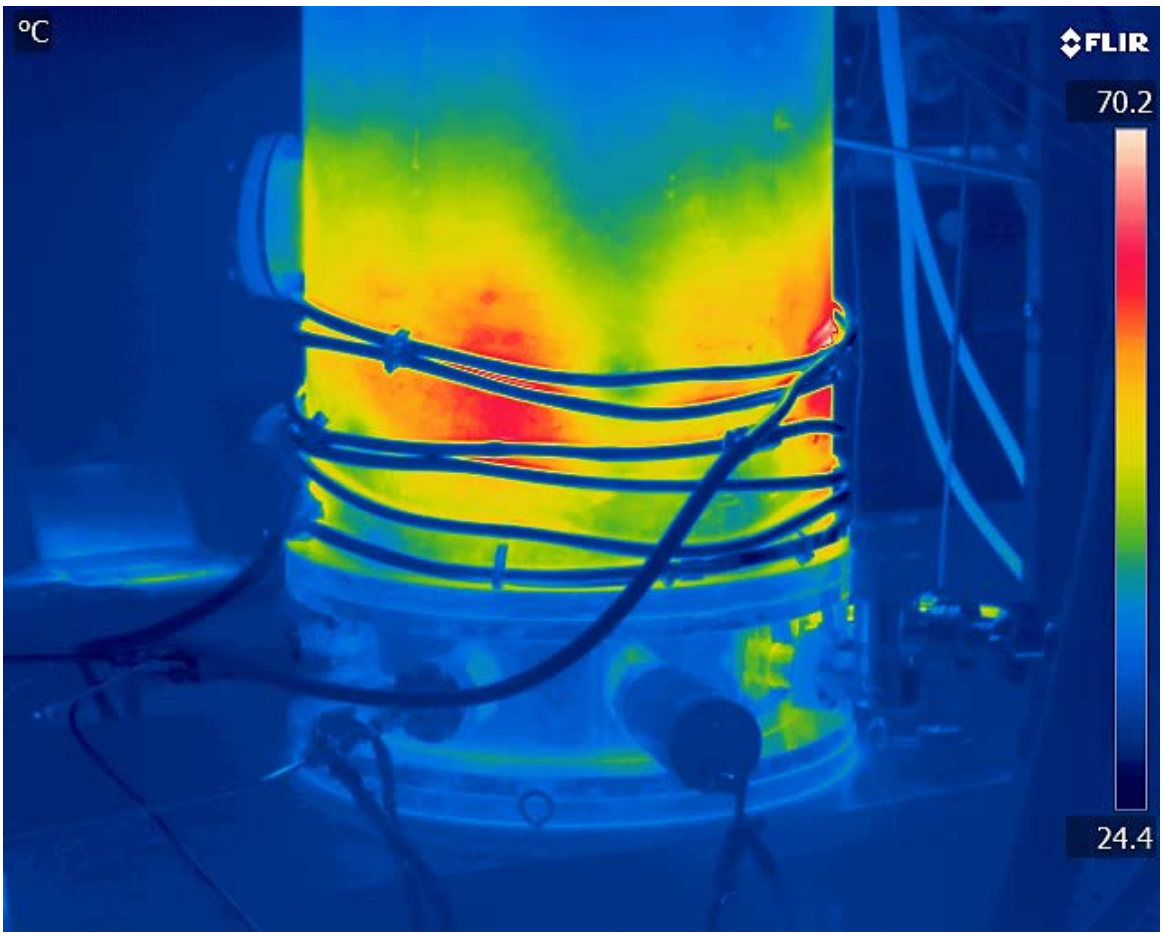

Figure 11: External thermal image of the reactor in operation.

# 8. EXPERIMENTAL RESULTS

The definition of a single crystal is *a crystal, usually grown artificially, in which all parts have the same crystallographic orientation*. This definition was taken from McGraw-Hill Dictionary of Scientific & Technical Terms©, 6E but does not adequately describe the tools necessary to characterize a crystal. It is generally understood in crystallography that single crystals give rise to a characteristic X-Ray pattern through diffraction of the beam. There are companies that use X-Ray diffraction, Raman and light spectroscopy as well as other methods to guarantee the quality of a specimen, but the costs of using these companies' services is prohibitively expensive in the current context. In the absence of a formal definition, as opposed to a narrative description of a single crystal diamond, the following table is presented and used as a measuring tool to evaluate the results of the following experiments. The values and descriptions were taken from the references listed in the bibliography for the report of single crystal diamond growth.[62]

Table 2: Single crystal diamond characterization

| **Instrument** | **Randomly oriented** | **Poorly oriented** | **Oriented** | **Highly oriented** | **Single crystal** |
|---|---|---|---|---|---|
| **XRD-homogenous sample** | FWHM>1 multiple peaks | | 1 strong peak, 1 weak | | FWHM<.15 single peak |
| **Raman= 1332 $cm^{-1}$** | FWHM >12 | phonon shift | FWHM 10-12 | FWHM 6-10 | FWHM 2-6 |
| **FESEM/SEM** | Crystallites visible | | Crystallites | Crystallites | No visible morphology |
| **Optical microscope** | Crystallites visible | Grains visible | May not see grains | | Translucent-"glass like" |

Results from runs 1-3 were conducted with the alumina wire support utilized in the work conducted by Kwon.[37] This design features 9 parallel wires, 4 mm apart kept in tension via springs held by aluminum blocks with a set screw as seen in figure 3. Although the wires are parallel across the substrate, their span increases as the distance increases away from the substrate. This is necessary to allow sufficient space for the aluminum blocks as they require approximately 4 mm per side. Lengths of the runs were limited to three hours due to thermal breakdown of the wires held at excess tension. Optical microscope and Micro Raman analysis confirms the nucleation of diamond on the diamond substrate. The sample was too small for collection to conduct SEM imaging.


Figure 12: Run 4a. Optical microscope image of diamond film growth on copper. Holes that appear in the image are a result of 50 µm seed crystals that came off during reactor shut down.

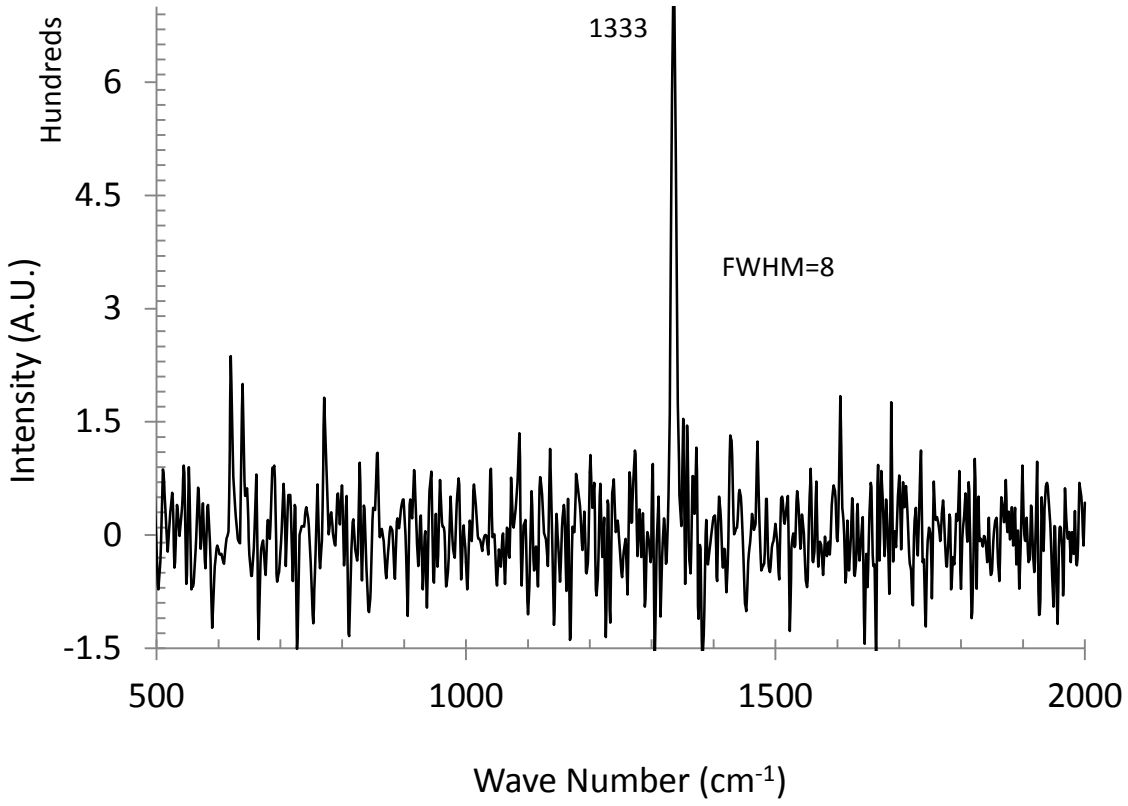


Figure 13: Run 4a. Micro Raman spectrograph of diamond film. Low intensity diamond peak and high signal noise is indicative of small crystal size (less than 5 µm).

Runs 4-5 were used as diagnostic tools in the development of a new wire holder shown in figure 5. A new wire holder design was necessary to allow the experiment to proceed past three hours. A 0.019" wire threaded through the copper rod provides constant contact. Wires are parallel the entire distance of the assembly. Longer experiment times were necessary based on the diamond growth rate observed during the first few runs. The first diamond film using this equipment was created during run 4a as seen in figure 12. As the copper surface contracted after the run, the 50 µm seeds used during

the run were compressed by the film; causing them to pop off the surface of the copper.

Micro Raman analysis confirms the existence of diamond shown in figure 13.

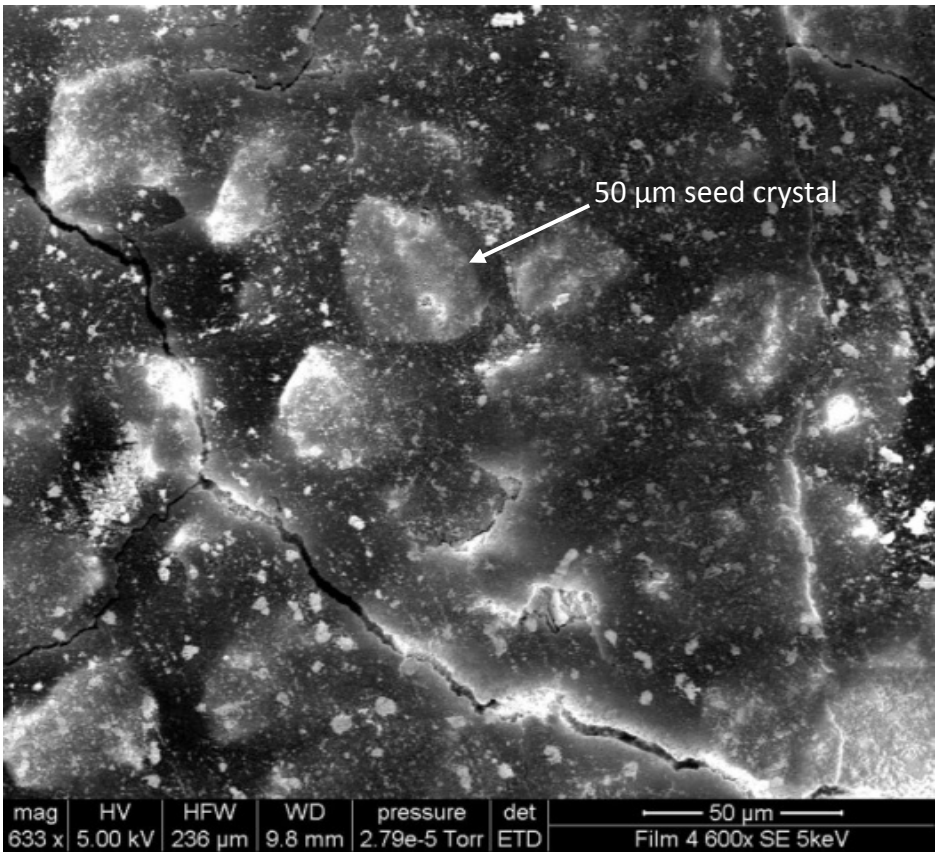


Figure 14: SEM analysis of run 6. Diamond film which appears translucent by artifacts of charge collection on the 50 µm seed crystals seen below.

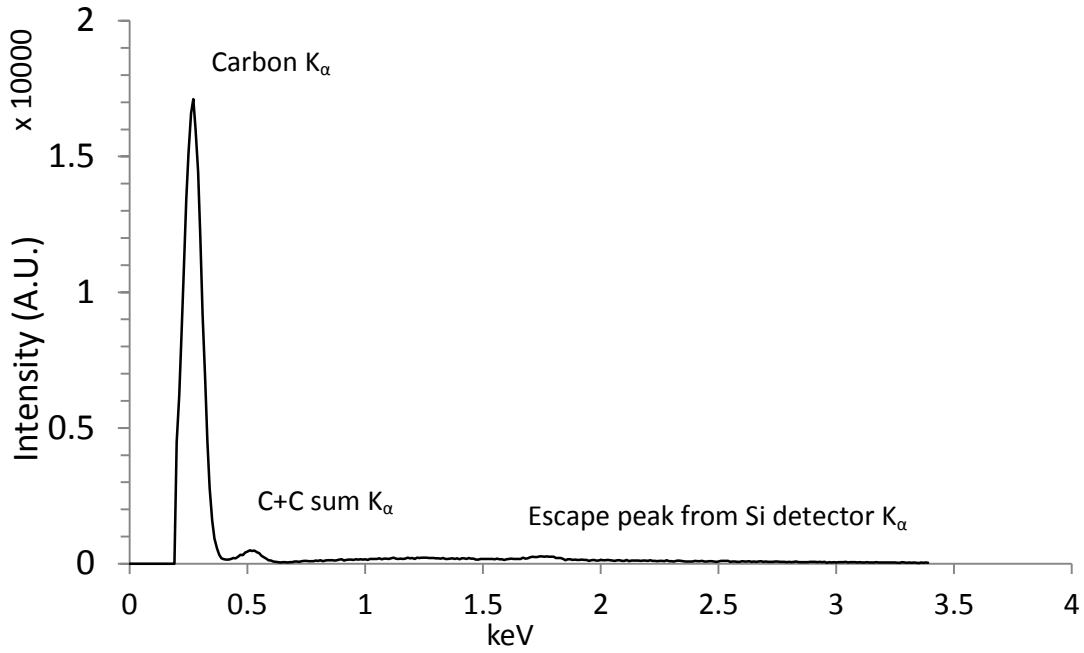

Figure 15: SEM/EDS characteristic energy of diamond growth during run 6.

A diamond peak was recorded via micro Raman at 1333 $cm^{-1}$. The shift from 1332 $cm^{-1}$ is due to stress on the $sp^3$ bonds in the crystal due to dopant(s) or other imperfections during growth. Growth rate for run 4a was estimated at 1 µm per hour. To construct a film 100 µm µm thick would therefore require at least four days continuous operation.

Run 6 was conducted with the new wire holder design that utilized two copper bars per side separated by springs with 0.025" holes drilled 4 mm apart as shown in figure 6.

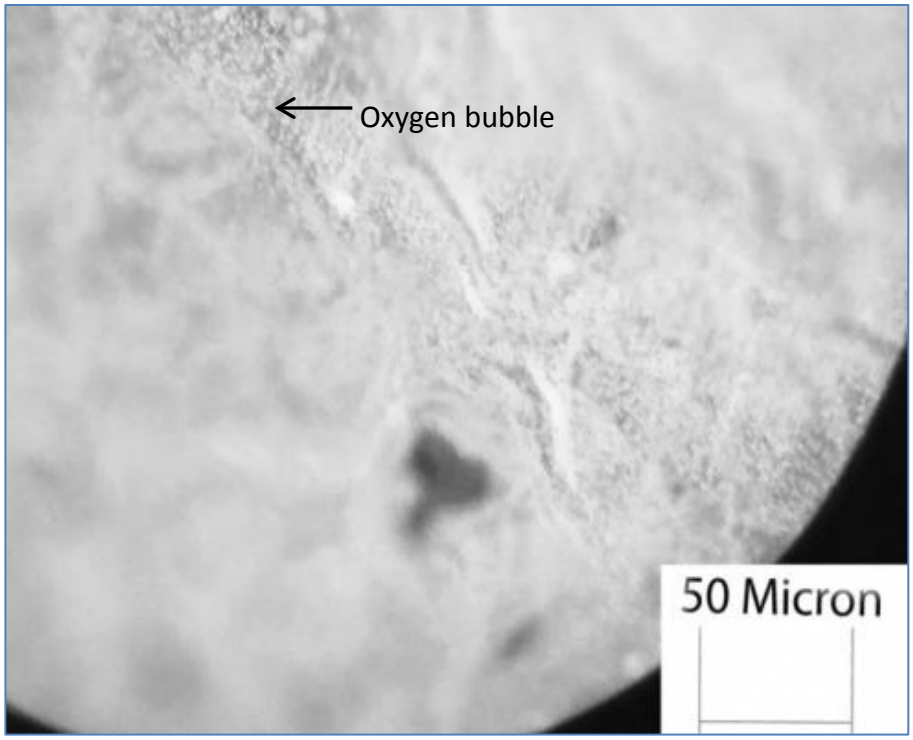


Figure 16: Run 6 optical microscope image of diamond film showing spherical anomalies. Confirmed by SEM EDS analysis, the anomalies were identified as 98% oxygen.

Results from this run confirmed with Scanning Electron Microscope (SEM) Energy Dispersive X-Ray Spectrometer (EDS), optical microscope, and Micro Raman confirm the creation of a diamond film 1.5 cm by 1 cm. Small circles on the optical microscope image are bubbles in the crystal as seen in figure 16. EDS analysis shows these bubbles to be 98% oxygen, indicating an excess of oxygen in the reactant gas. Even though a bias was not applied, the seed crystals showed excellent alignment and are responsible for the favorable results.

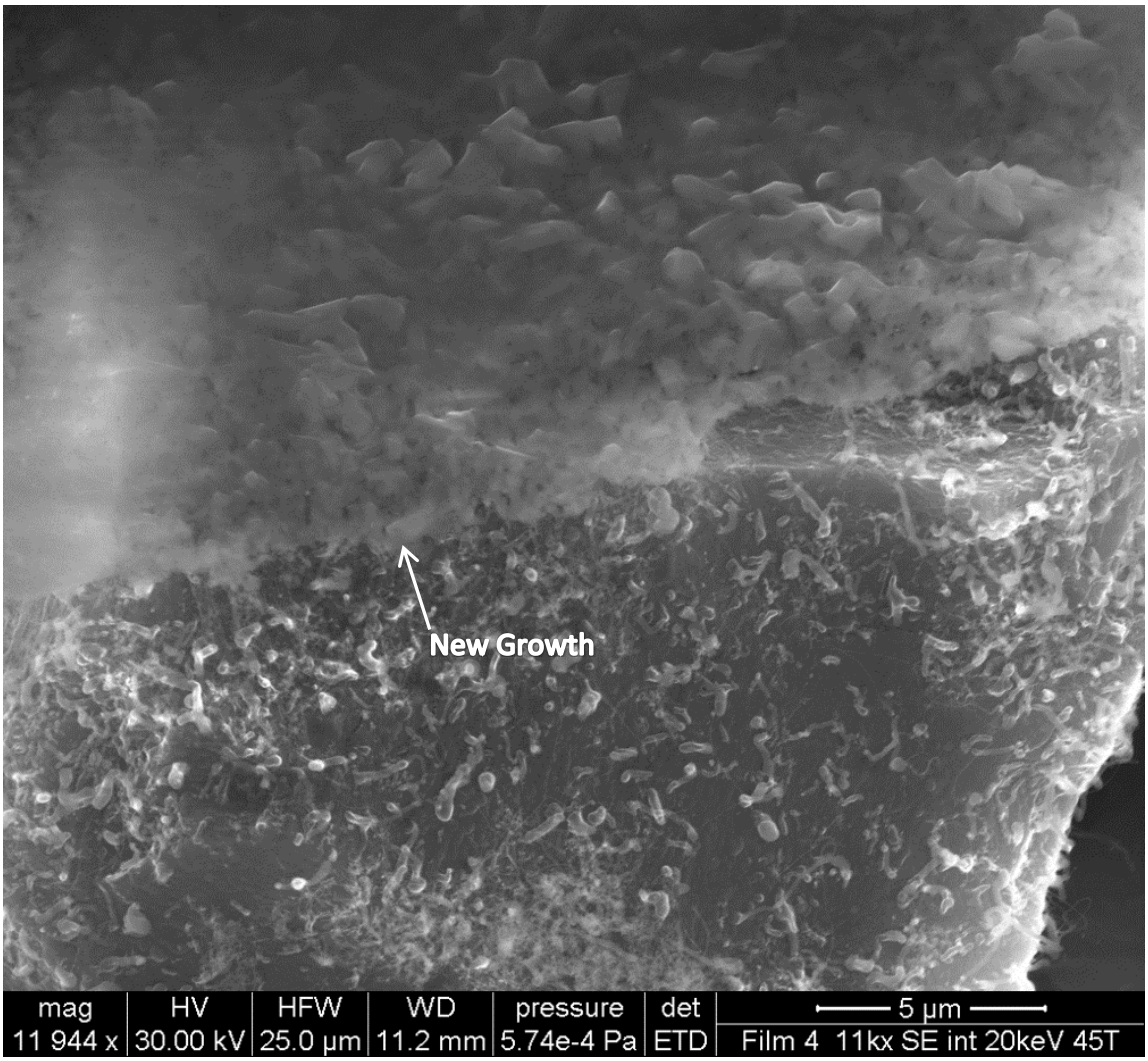


Figure 17: Run 6. Close-up of a single 50 µm seed crystal shown from the side. Top portion of the crystal is new growth.

Interlacing structures found between the diamond seeds and the new growth was identified as magnesium oxalate and tungsten carbide. It is believed that this interleaving structure is responsible for creating the bridge between the seed crystals which provided the platform on which the diamond grew.[63] As seen in figure 20, "white" cross hashing structures on the larger structure (50 µm crystal) developed

during the run and act to bind neighboring crystals together. The false white color is charge collecting on the surface of the sample.

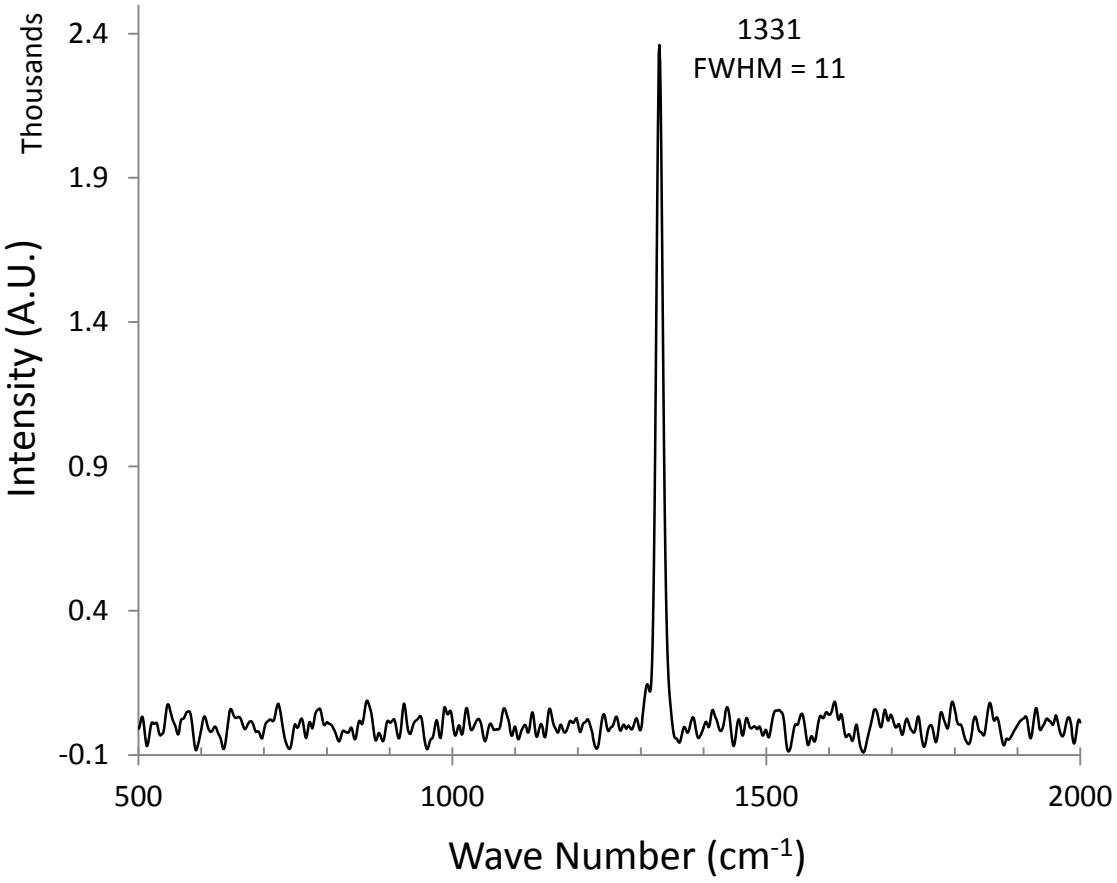


Figure 18: Run 6. Micro Raman spectrograph of the diamond film shown in figure 16.

At beam energies at 5 keV and lower, the film is visible as seen in figure 14. The small white dots are oxygen bubbles trapped during diamond growth. The film grew on a curved portion of the copper holder and sample. During cooling, the difference between the coefficient of expansion of copper and diamond caused the film to be released from the copper. However, the stress during cooling was sufficient enough to cause the film to crack.

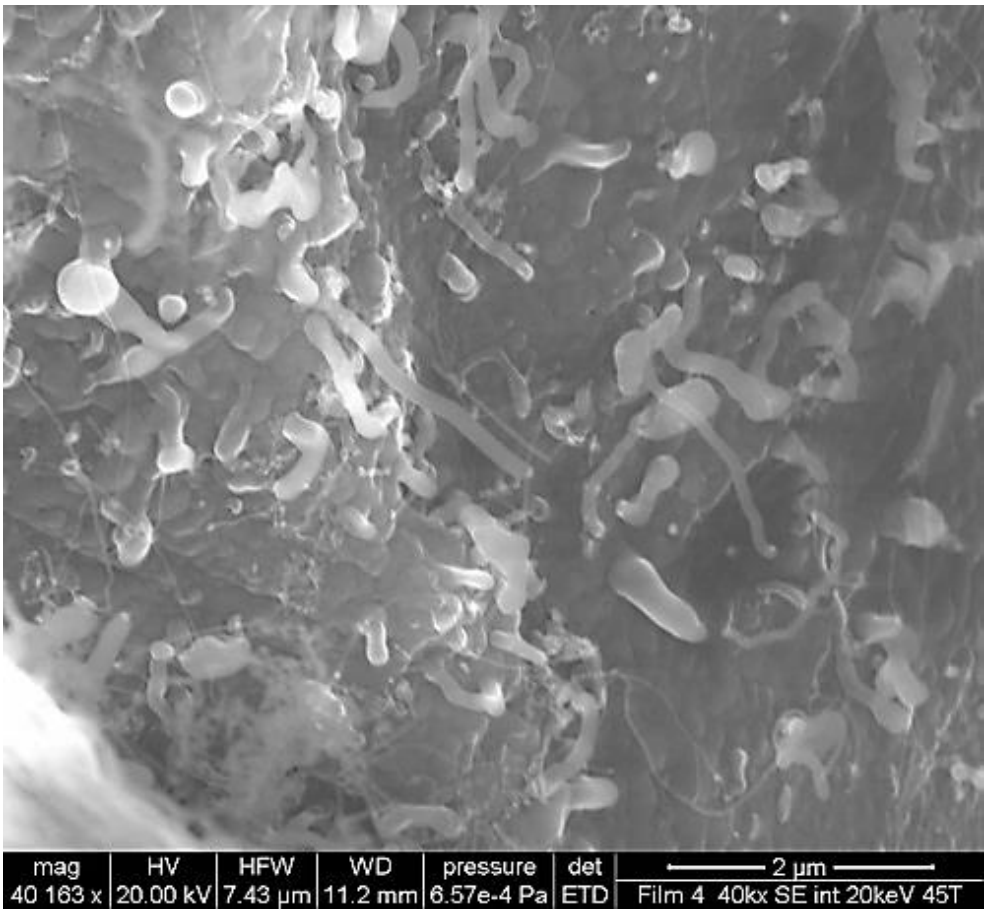


Figure 19: Run 6. Higher magnification of the seed crystal showing diamond tendrils which are believed to be responsible for horizontal diamond growth.

The source of magnesium is a contaminate identified on its certificate of analysis for the tungsten wire. The diamond was exposed to long wave (365 nm) ultraviolet waves. This caused the sample to fluoresce dark blue. Small tendril nanostructures developing laterally faster than vertically as seen in figure 19. In contrast to figure 17 and 19 which shows diamond growing horizontally and vertically at different rates and mechanisms, diamond has only been reported to develop isotropically.

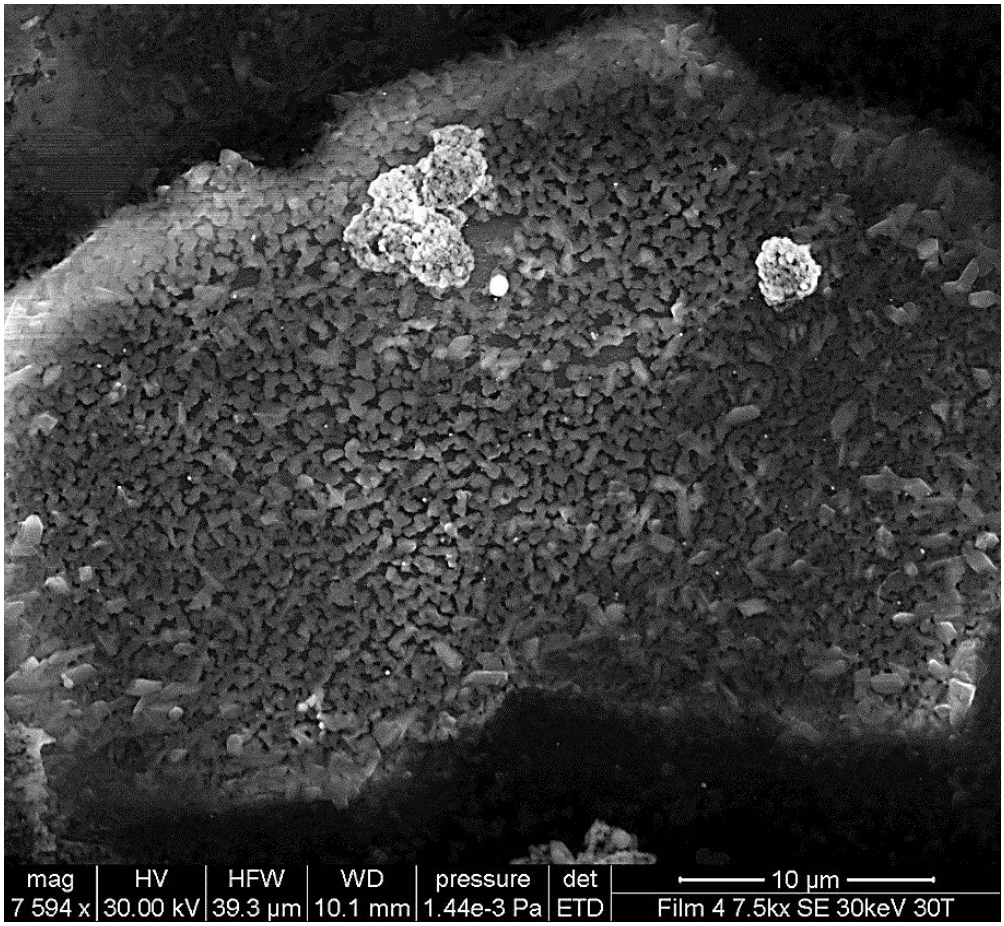


Figure 20: A 50 µm seed crystal shown with new growth for run 6. Errors in growth (white spot in the middle top of the image) are an indication that growth occurred too quickly in this region to allow for ordered growth.

Runs 7-17 were an attempt to repeat the success of run 6 while eliminating the imperfections found. Imperfections found were oxygen bubbles, curved growing surface, and imperfect surface topography as seen in figure 20. The copper substrate holder was removed to see if copper assists or interferes with growth. In all but one run, diamond did not form without the copper. Run 7 was remarkable in that diamond grew directly onto the stainless steel as seen in figure 21.

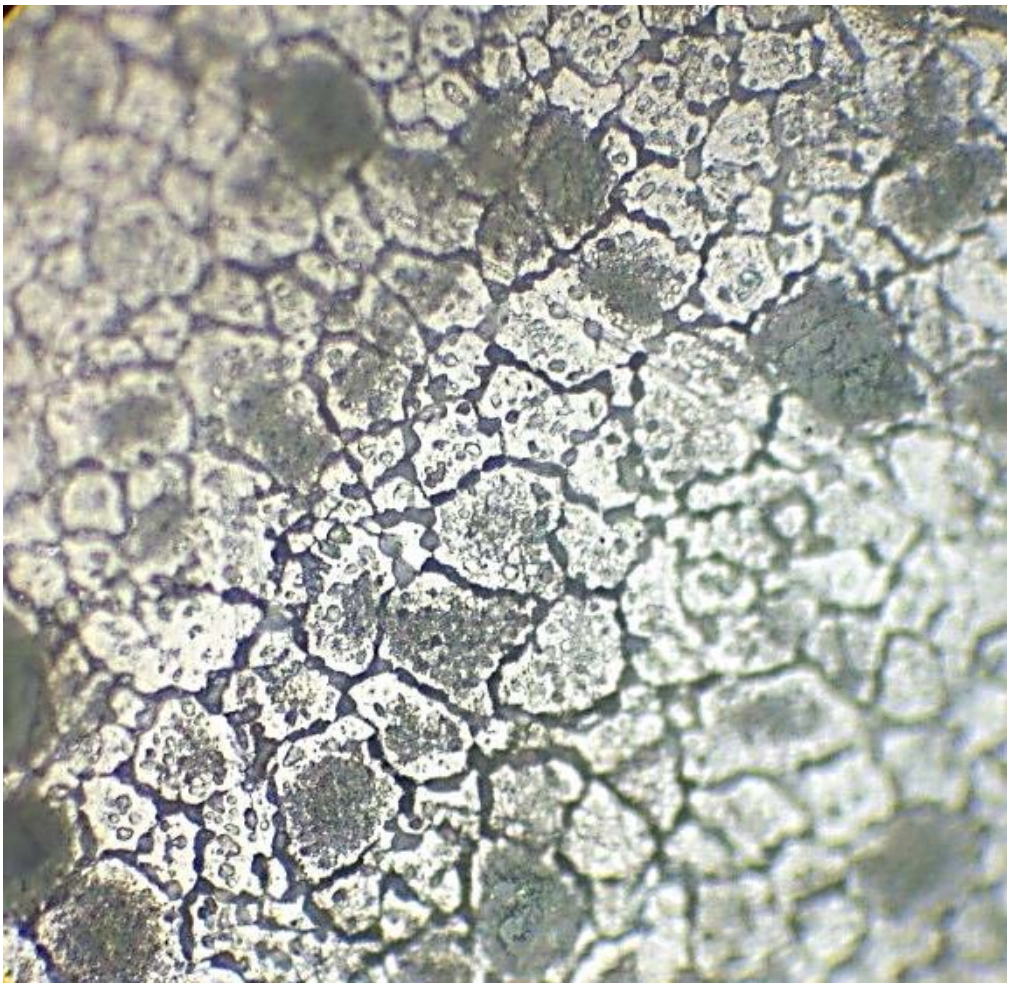

Figure 21: Run 7. Diamond mosaic grown on stainless steel. 200x magnification

A mosaic of diamond structures grew directly on the surface of the stainless steel. As the steel contracted during cooling, the disconnected films moved closer to one another but did not overlap. The structure remained intact and did not come away from the surface.

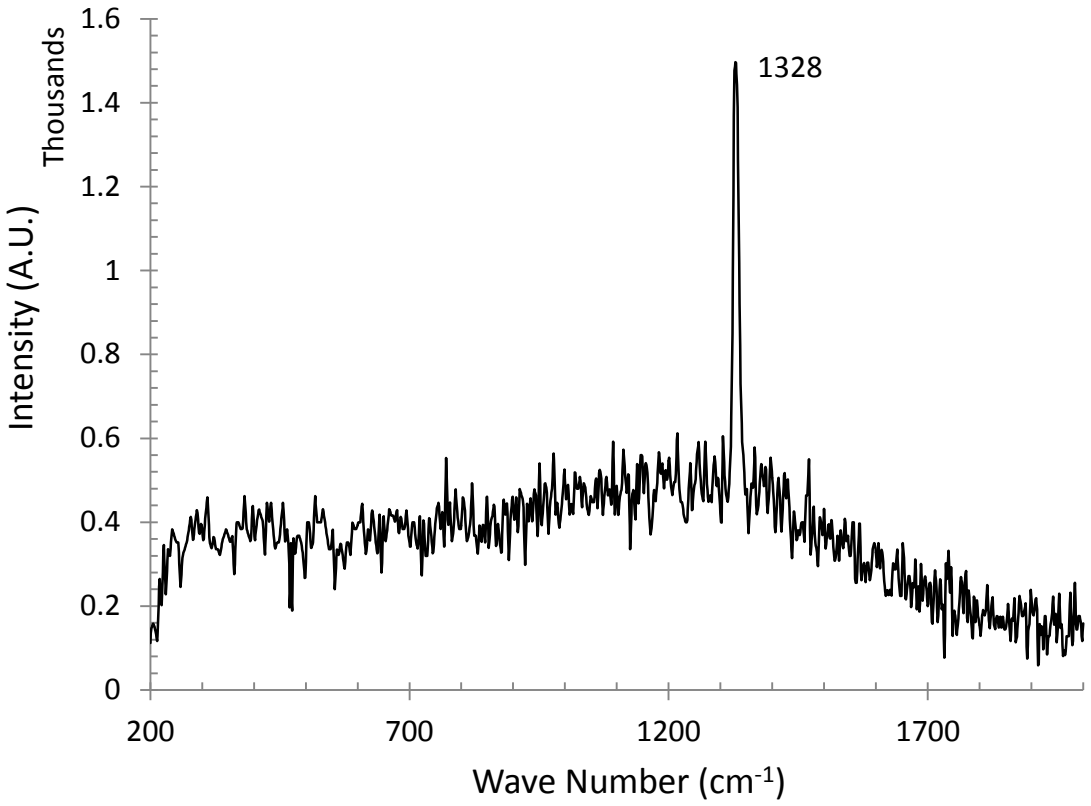


Figure 22: Run 7. Micro Raman spectrograph of diamond coating grown on stainless steel.

Runs 18-26 were performed on silicon wafers in the attempt to demonstrate the reactor can form diamond on traditional substrates. Some diamond films developed during these runs. In some of the runs, a translucent diamond film was created. Run 24 shown in figure 23 showed the formation of a film growing horizontally across the surface of the silicon similar to the growth mechanism of run 6. The diamond film originated at the interface between the diamond seeds on the surface of the silicon substrate and the silicon. Diamond grew on silicon where diamond was not present but rather "migrated" horizontally away from the seed crystals. The silicon substrate holder material has electrical and heat properties that differ significantly from copper.

However, the result is the same: horizontal growth plane of diamond near the seed crystal surface across the substrate holder material. This was seen in runs 6 on copper, run 7 on stainless steel, run 24 on silicon, and runs 53-56 on platinum/iridium.

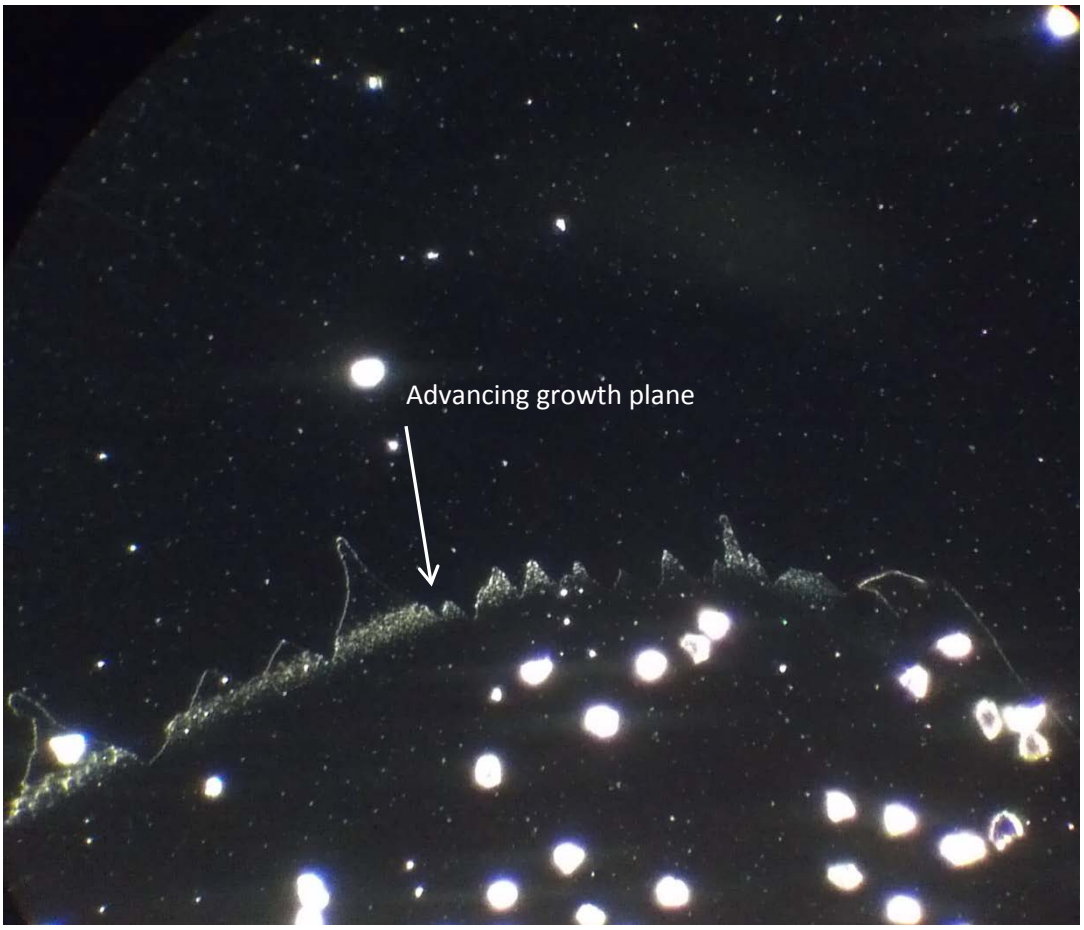

Figure 23: Run 24. Diamond grown horizontally on silicon. 200x magnification.

Runs 27-30 were an attempt to dope existing diamond crystals with cobalt while creating new diamond growth on 50 µm seed crystals. The color of diamond shifted from clear to a subtle blue. Ultrasonic and acid cleaning was performed to ensure the coloration was not superficial.

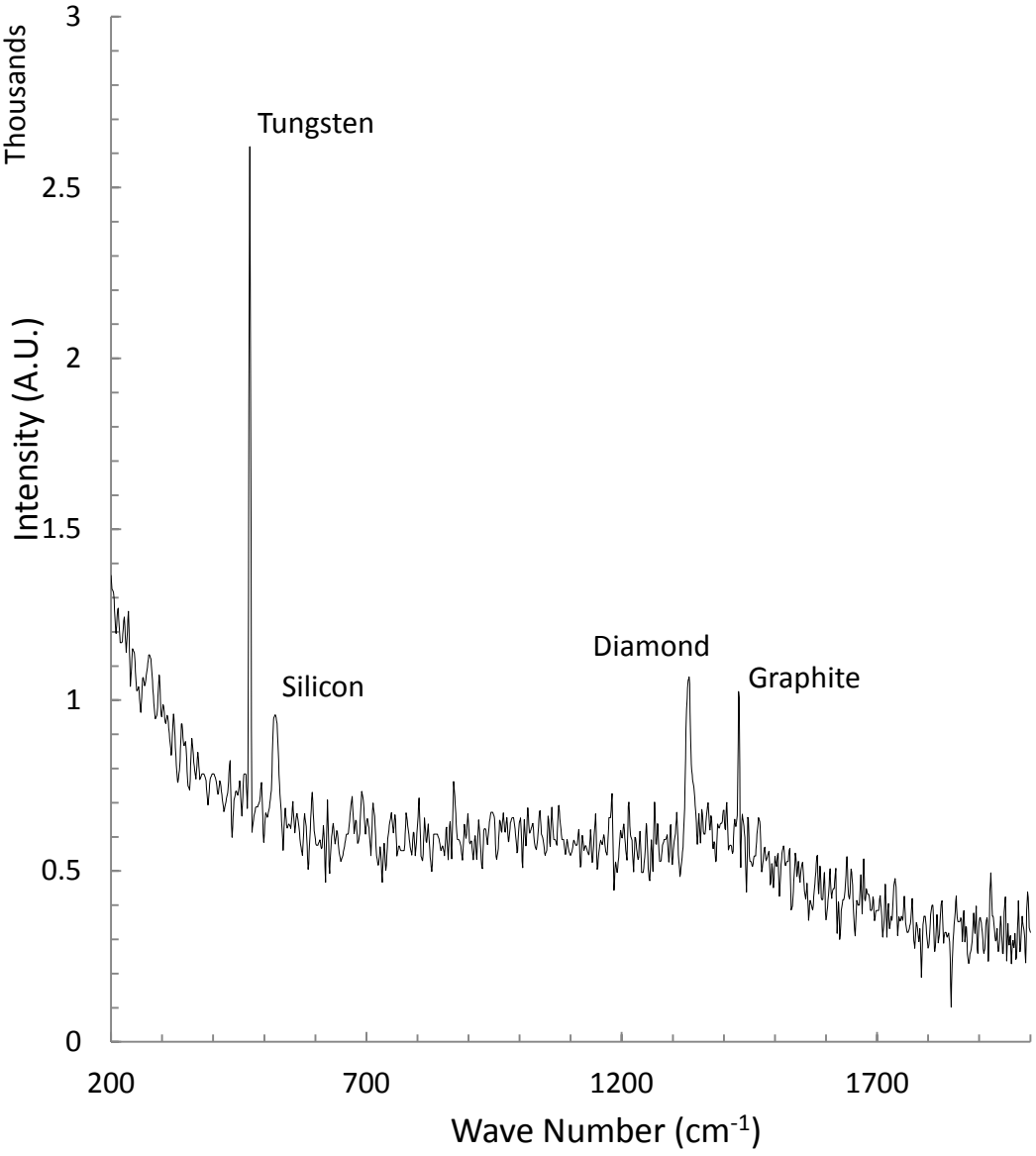


Figure 24: Run 24. Micro Raman spectrograph of film shown in figure 23.

At 200x magnification, run 27 and 29 demonstrate the 50 µm diamond sample doped with cobalt by the pale blue color after the run.

Figure 25: Run 27 before and after cobalt doping. It was not possible to track each crystal. The two crystals shown are indicative of the before and after color.

Due to the size of the crystals, it was not possible to photograph one crystal before and after treatment on run 27. Therefore, in run 29, 0.25 carat diamond chips were used to track individual crystals. The diamond chips were cleaned using ultrasonic and acid cleaning. It was verified optically in run 29 that diamond was doped with cobalt.

Figure 26: Run 29. 0.25 carat diamond doped with cobalt (before treatment to the left and after to the right).

Runs 31-43 are investigations into how the inability to control specific mechanical parameters affects growth. This investigation included changes in pressure, temperature, coverage area of the substrate by the filament, parallelism of all surfaces, and filament holder design.

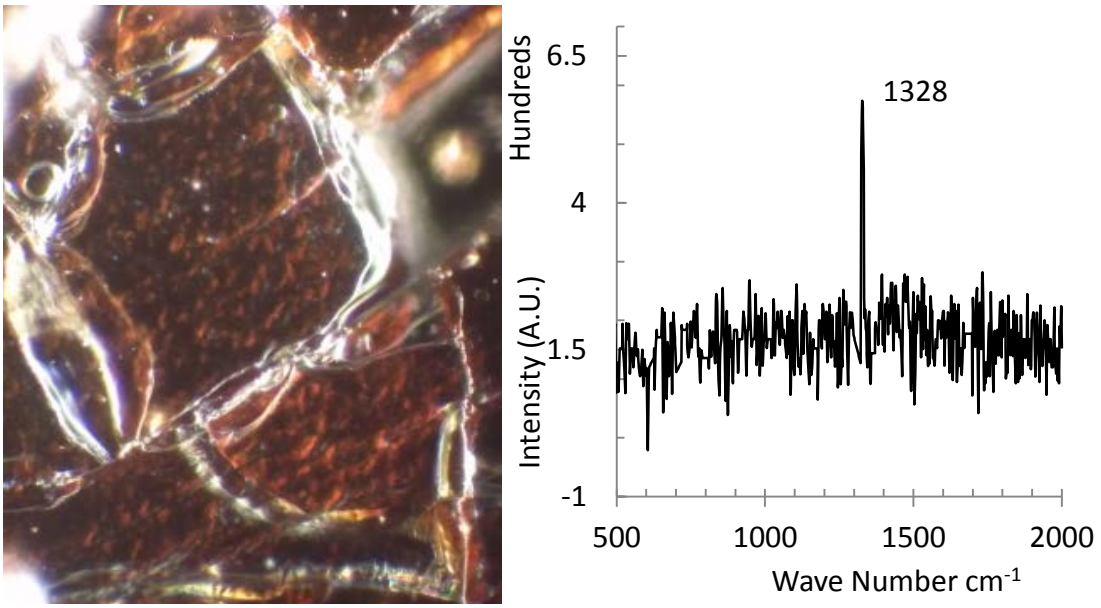


Figure 27: Run 31. Semitransparent diamond plate that was grown on stainless steel that cracked during reactor cool down phase. Brown structures shown below the crystal is ferrous oxide. 200x magnification.

During this investigation, a 1” thick stainless steel plate was used to test the heat transfer away from the substrate by measuring reactor coolant flow temperatures. In addition to the thermal information collected during run 31, a semitransparent diamond film was grown along the edge of the plate.

Runs 44 and 45 investigated the theory that diamond grows horizontally in the reactor designed. An area in the center of the copper was not seeded with diamond. Examination after the experiment of the unseeded area did contain a grown diamond film. This led to run 46 where the copper was seeded with 0-2 μm powder spaced microns apart. If the diamond film grows horizontally, then the seed stock should coalesce into a single film horizontally faster than vertically. This is what was observed in run 46. However, the film was brittle and shattered upon thermal contraction of the copper holder. Run 47 was allowed to run for 168 hours (as opposed to run 46 for 70.5 hours) to thicken the film. Run 47 was pre-treated the same as the prior run. The film on this run coalesced and did not crack. However, the coating produced was atomically bonded to the copper and could not be removed. The greyish film over the surface in figure 28 was originally classified as disordered (D) band graphite and diamond. A scratch test was performed on the surface with a stainless steel scalpel. The surface was also exposed to a 12-hour diamond powder polishing cycle.

Figure 28: Run 47. Diamond Like Carbon (DLC)/diamond (111) growth bonded to copper. The film cannot be scratched (even with diamond) or removed from the copper.

The copper backing was polished but had no effect on the diamond coated surface. The coating could not be scratched or polished and was therefore reclassified from D-band graphite to Diamond Like Carbon **(**DLC). Raman analysis yielded a sharp peak at 1357 $cm^{-1}$ and 1332 $cm^{-1}$ for the area shown in figure 30. This sharp peak is unusual for diamond like coatings that contain both $sp^2$ and $sp^3$ bonded carbon. The peaks for DLC are usually surrounded by gradual "humps" that rise and fall indicating a high degree of disorder.

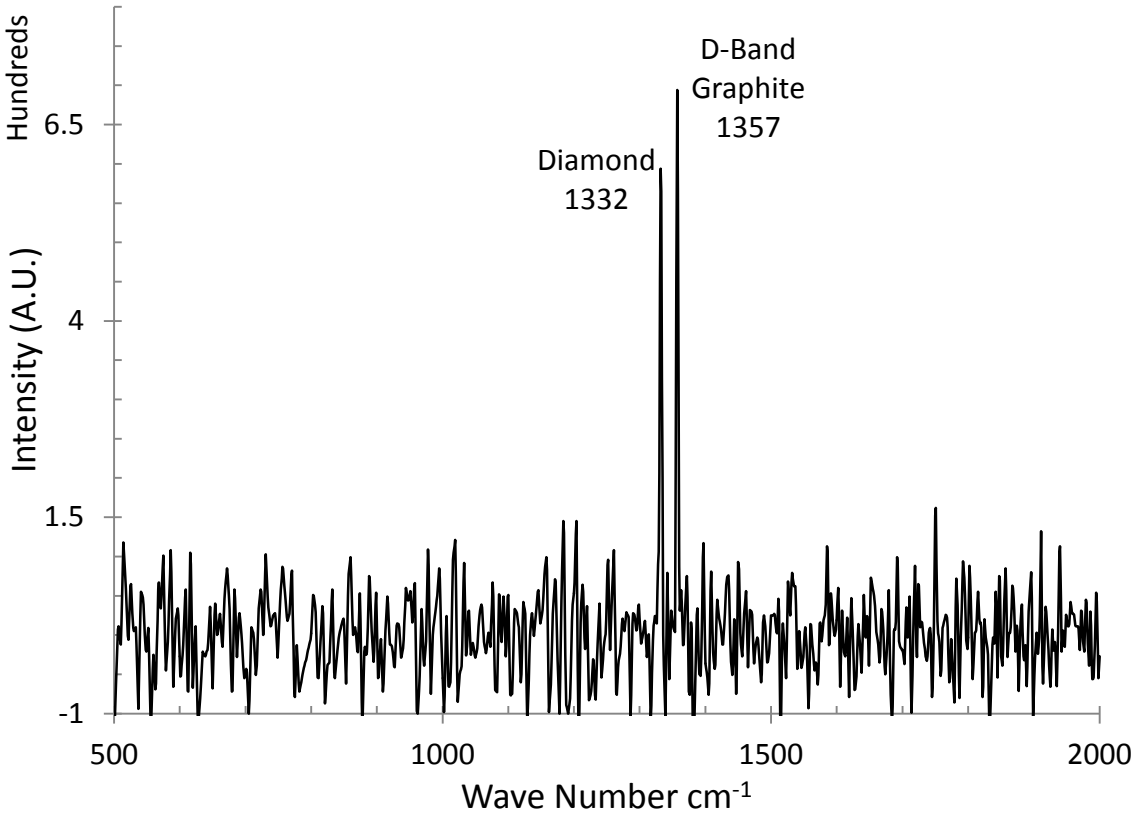


Figure 29: Run 47 Raman spectrograph for the DLC film.

In addition, DLC typically has an overlapping broad peak at diamond, D, and G bands of graphite. G band graphite is not shown in figure 29. This coating only has sharp peaks indicating a strong degree of order in the structure. The hardness of the film is likely attributed to the ratio of diamond to DLC. The ordered arrangement of (111) shaped peaks in the film are not characteristic of typical DLC films. Within this same sample is a region where only the graphite band can be found as shown in figure 31 whose structure is consistent with DLC films of its type.

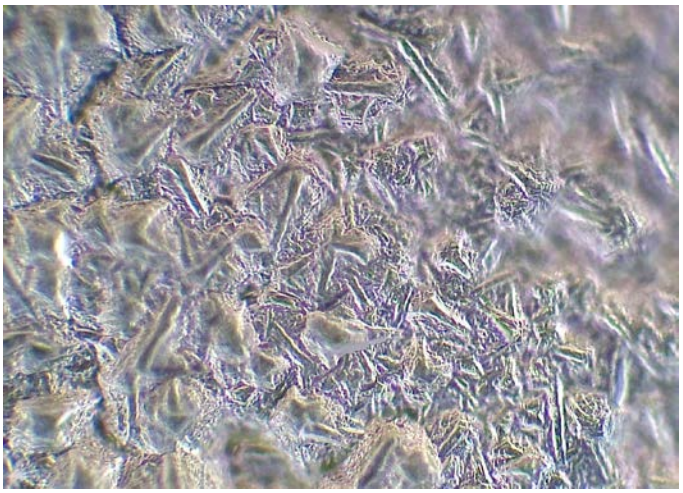
Figure 30: Run 47- (111) diamond/DLC growth. Magnification is 400x.

Runs 44-61 incorporate the new rack and pinion filament holder and gas distribution header design. The showerhead design was replaced due to contamination of the alumina by metals vaporized during heating. This contamination is likely due to the proximity of the showerhead to the filaments.

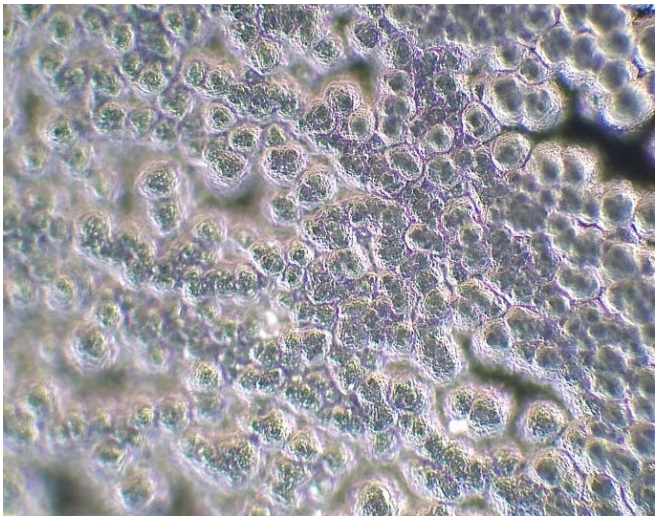
Figure 31: Run 47- DLC growth only on a different portion of the same film as above. Magnification is 300x.

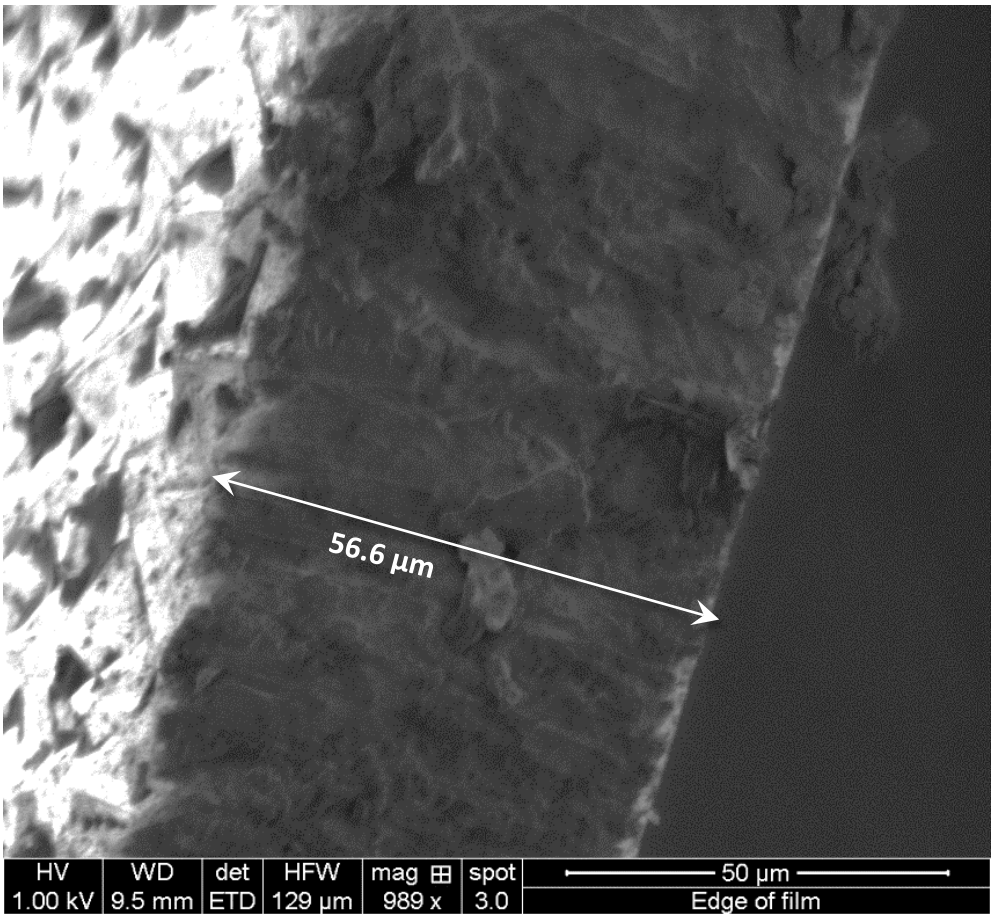

Figure 32: Run 49 on Pt/Ir foil shown in figure 33. SEM image shows the 56.6 µm thick edge of the diamond film.

The new nozzle ideal height was determined by conducting a series of flow studies designed to identify the ideal height from the filaments by changing the distance from the filaments to the nozzle such that the gas interacted with the filaments lowering the temperature of all filaments uniformly. The ideal distance is just less than one inch which during operation at 600 SCCM produces a 40 degree Celsius temperature drop in all filaments.

Run 49 utilized a new holder material: a 90%/10% platinum/iridium non-eutectic alloy that was thought to be more durable than copper based on lower partial pressure of the metal at the substrate temperatures of interest.

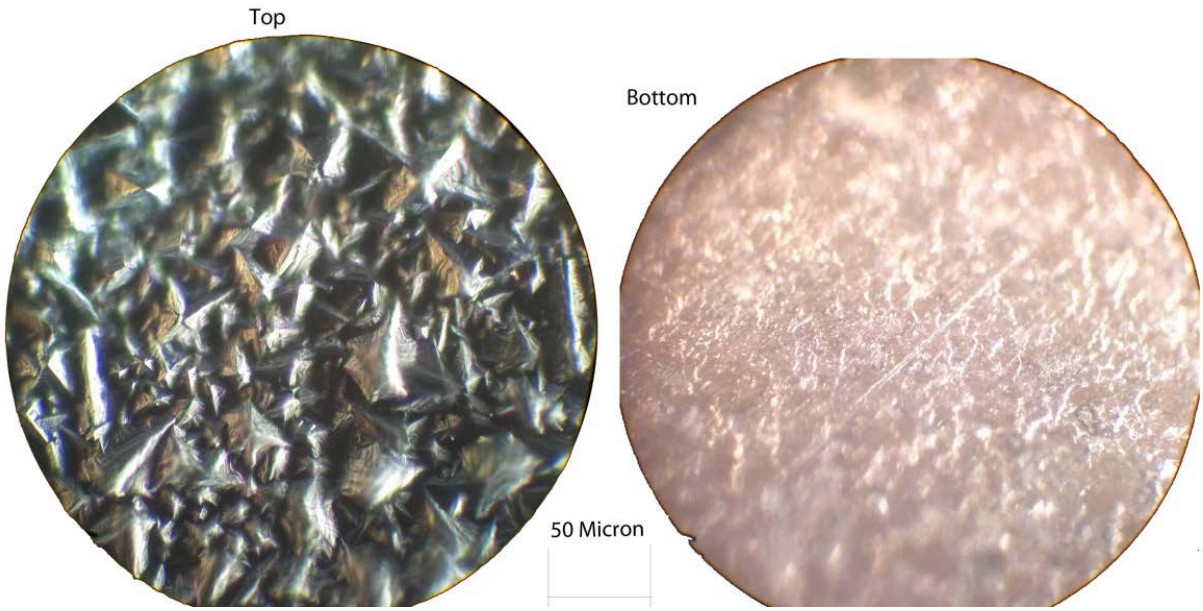


Figure 33: Run 49 images of the diamond film. The bottom of the film does not exhibit morphology and is translucent. Morphology on the top of the film is (111).

There was also some work conducted that demonstrated diamond can be grown on platinum.[33] Platinum and copper are face centered cubic (FCC). A FCC metal is malleable and soft and was likely to be available polished. Platinum has an atomic radius of 1.38 Å which is closer to diamond (1.54 Å) than copper. Platinum/iridium foil was 50 mm x 50 mm by 50 µm µm thick. Zero to two µm seed crystals were utilized in run 49 and produced a translucent diamond film approximately 2 mm in length and 56.6 µm thick.

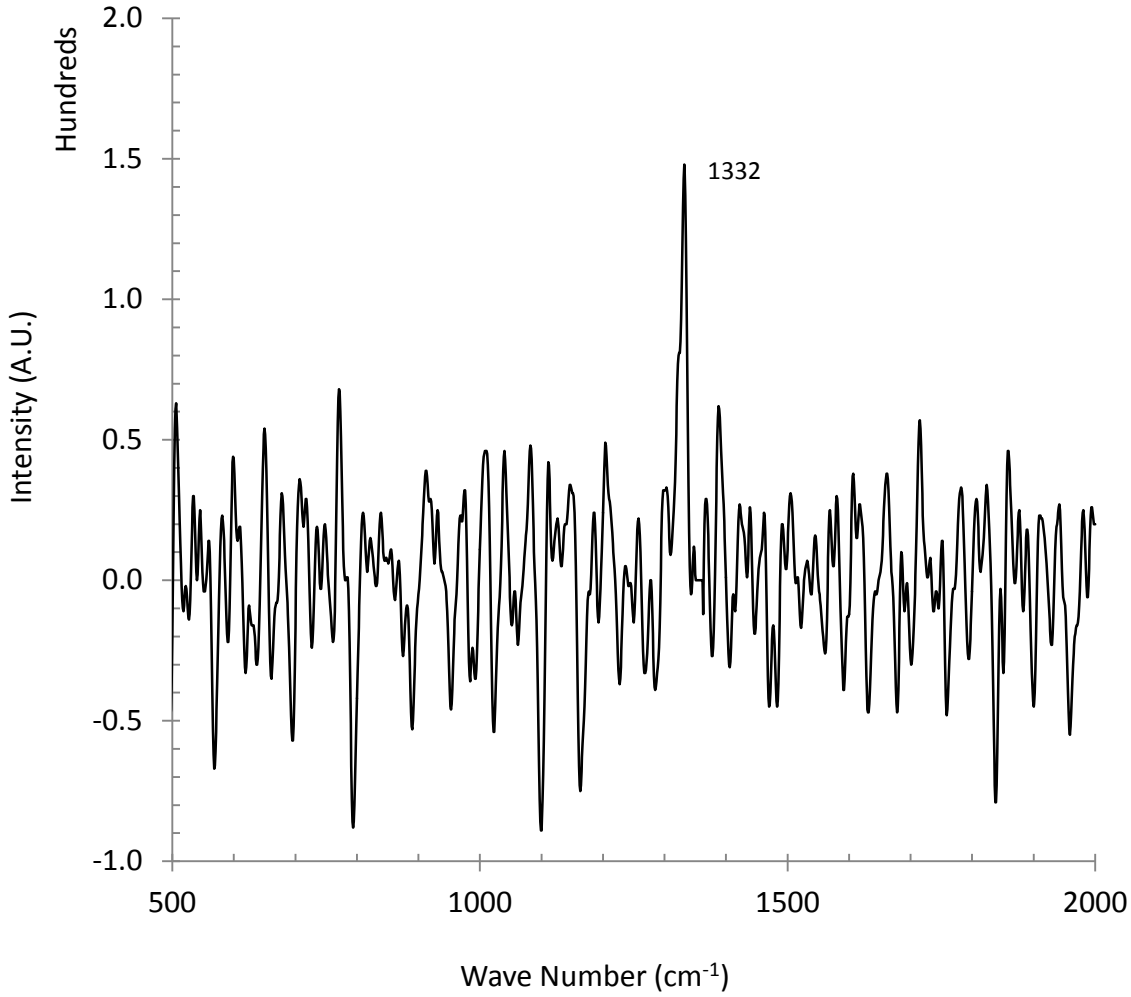


Figure 34: Raman spectrograph for run 49. Peak 1332 is diamond.

Runs 50-54 utilized similar conditions to run 49 but with a 2 inch diameter foil 100 µm thick. Less than 100 µm thick metal foils curl under thermal stress of heating.

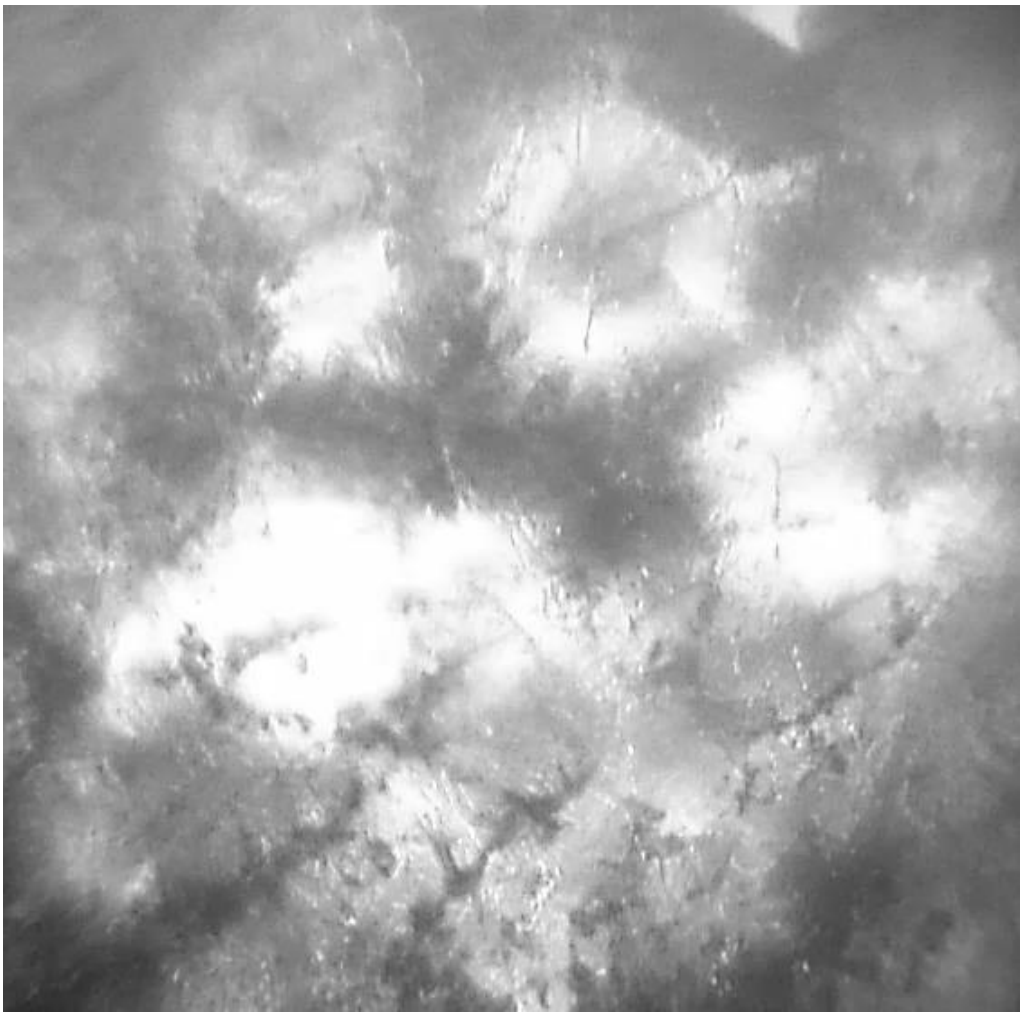

Figure 35: Run 54 optical image at 400x magnification. Glassy, transparent surface allows light to pass through showing the polycrystalline structure underneath.

Run 54 was terminated at 121 hours due to a visible growth plane that was visible through the site glass. It was speculated at the time that this growth was only polycrystalline in nature. During analysis, this was found to be only partially true. The polycrystalline surface had a single crystal diamond backing approximately 20 μm thick. Figure 35 shows an optical image of the film as seen from the side closest to the substrate holder (underside of the film). The translucency of the film makes it possible to see part of the structures on the other side of the film.

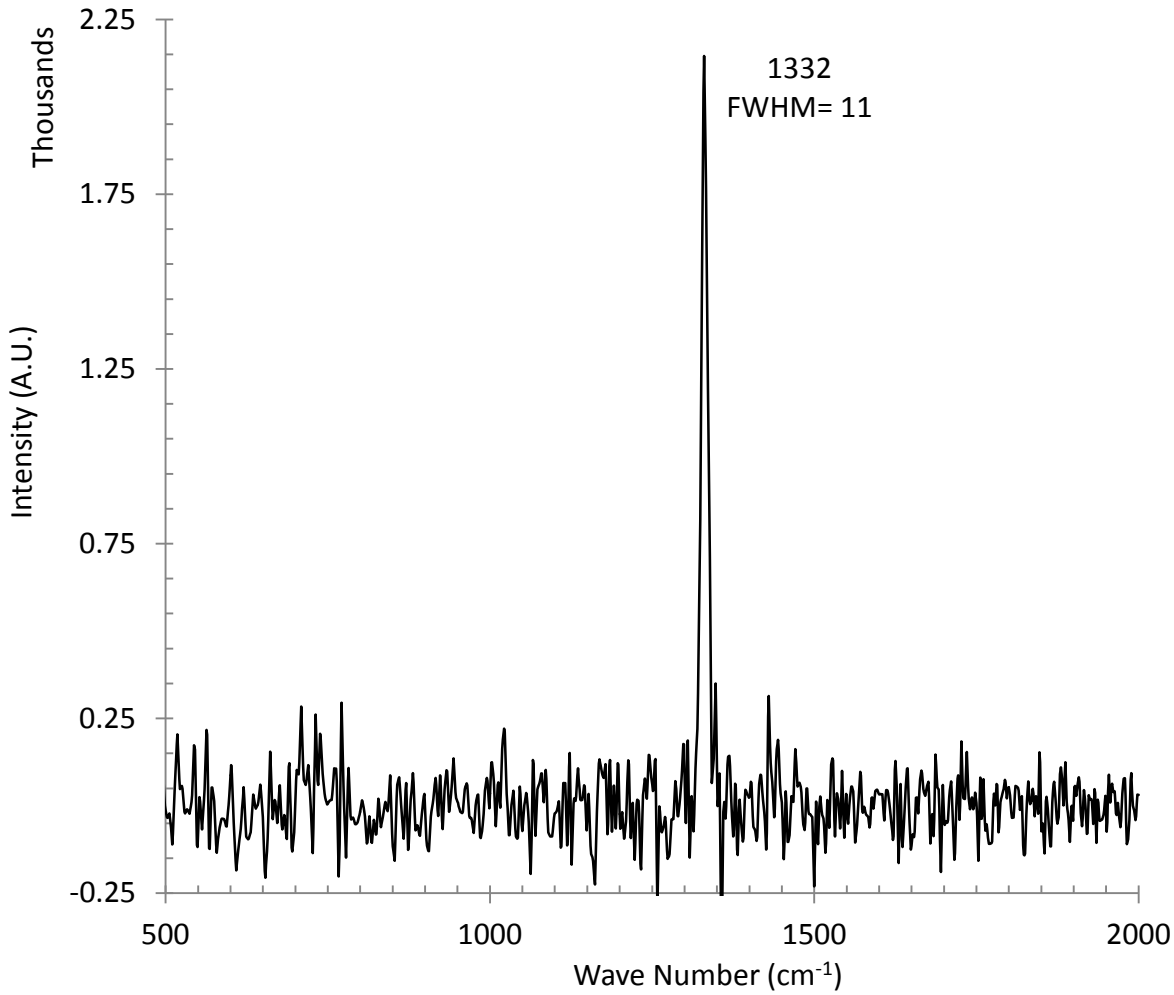


Figure 36: Run 54. Micro Raman (785 nm wavelength) result of 1332 $cm^{-1}$

Figure 36 shows a strong diamond peak at 1332 $cm^{-1}$. The full width half maximum (FWHM) is wider than expected for a film of this quality and is most likely due to platinum contamination transferred from the substrate holder.

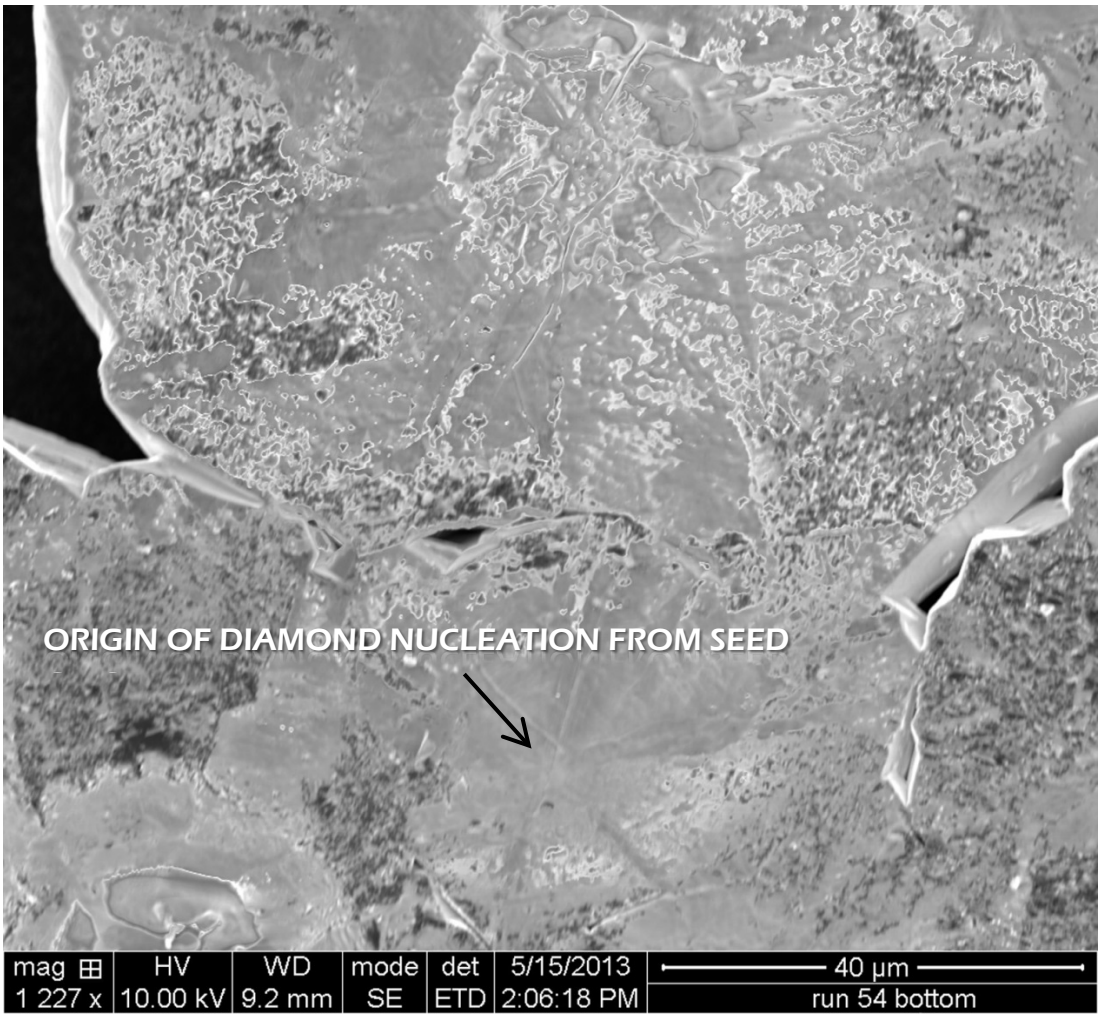

Figure 37: Bottom portion of the film in run 54.

Figure 37 shows macro nucleation from single diamond seed crystals. These macro structures coalesced into a single diamond structure. Although topographical features are present, morphology cannot be seen. X-Ray diffraction was used to assess the film. A strong (111) peak for diamond was found with a weak platinum (220) peak as well as a diamond (220) peak. Scattering from platinum contamination on the surface of the film caused dislocations of the (111) diamond face during growth. Since the XRD beam penetrates the surface of the film by approximately 100 µm, the spectrograph shows

the strong single crystal diamond (111) below the thin layer of platinum contamination as well as the (220) for diamond and platinum in the this surface layer.

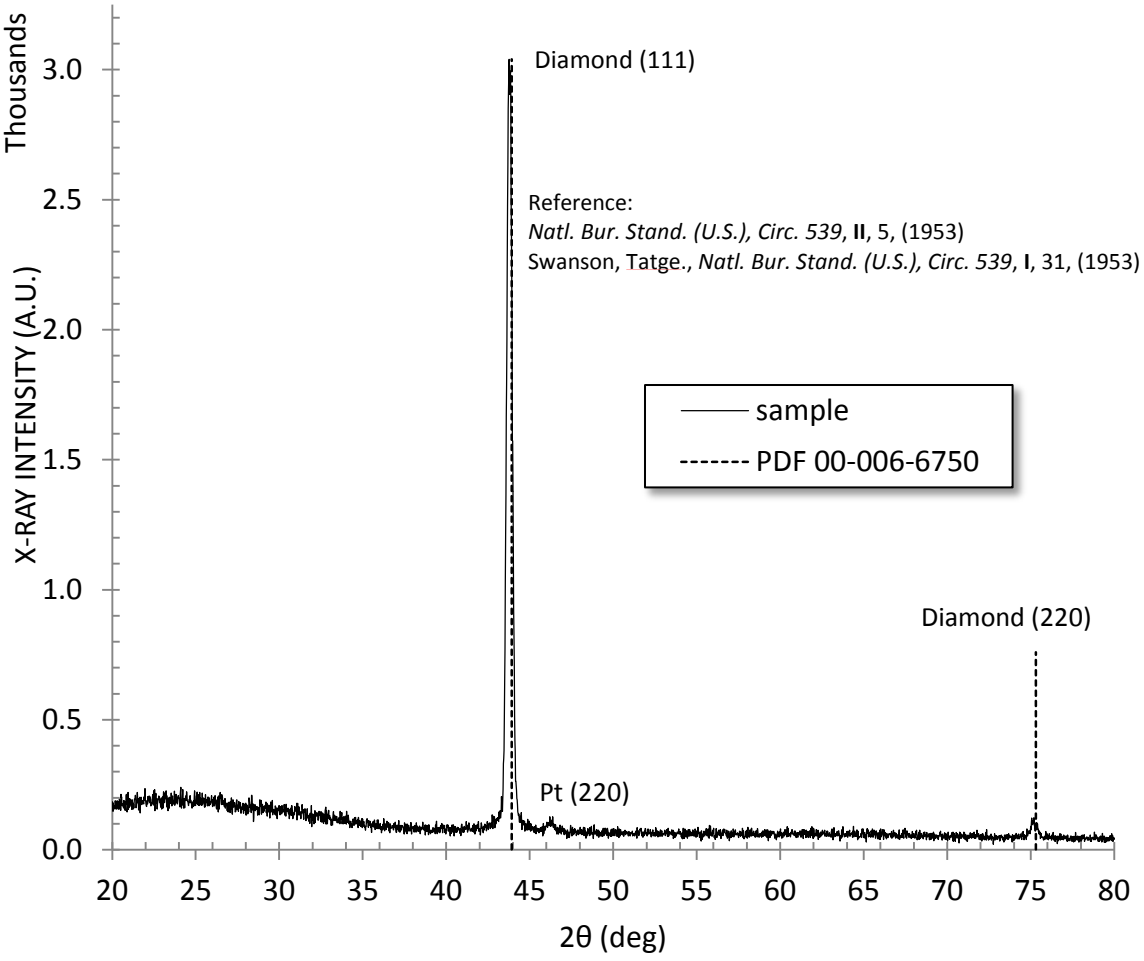


Figure 38: Run 54. X-Ray diffraction with 1 $cm^2$ window of the bottom of the single crystal diamond film.

If texturing were visible in the SEM images, the conclusion would have been that the diamond is strongly textured. However, in the absence of visible texturing and the possibility of twinning ruled out, it is concluded that the two (220) peaks are due to surface contamination. It is important to note that the surface was cleaned with near-

boiling aqua regia which is the only acid known to dissolve platinum. Therefore, the platinum seen in the SEM image is and XRD is an estimated 1-3 µm into the surface. This estimate was taken from the calculated scattering depth of the elections from the SEM beam at 10 keV in carbon.

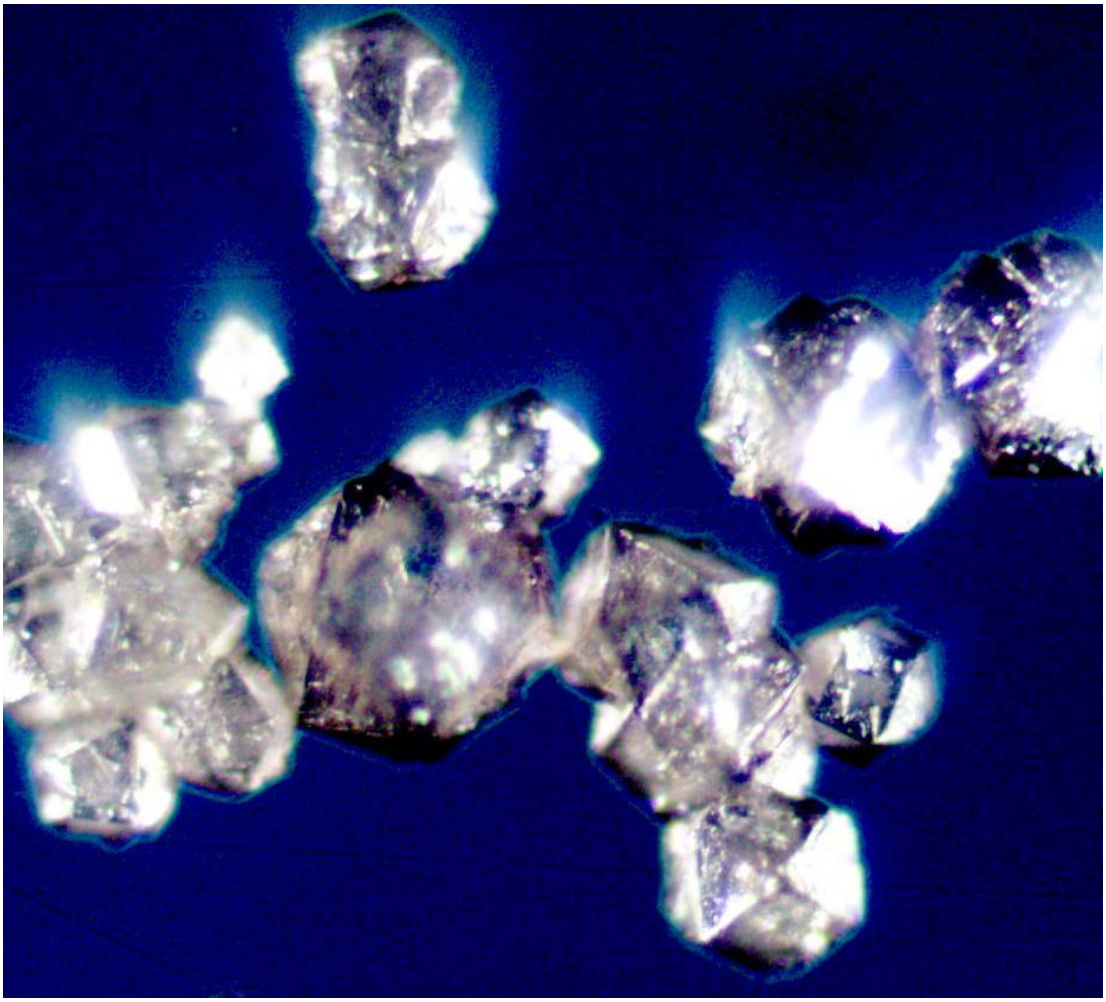

Figure 39: Diamond growth separate from the main diamond film. Magnification is 40x.

There was some diamond growth that did not coalesce as seen in figure 39. These diamonds appear to have formed isotropically and were located near the center

of the substrate. The largest structure shown in this figure 39 is over 600 µm in diameter. It is unusual to see such large structures in HFCVD growth systems.

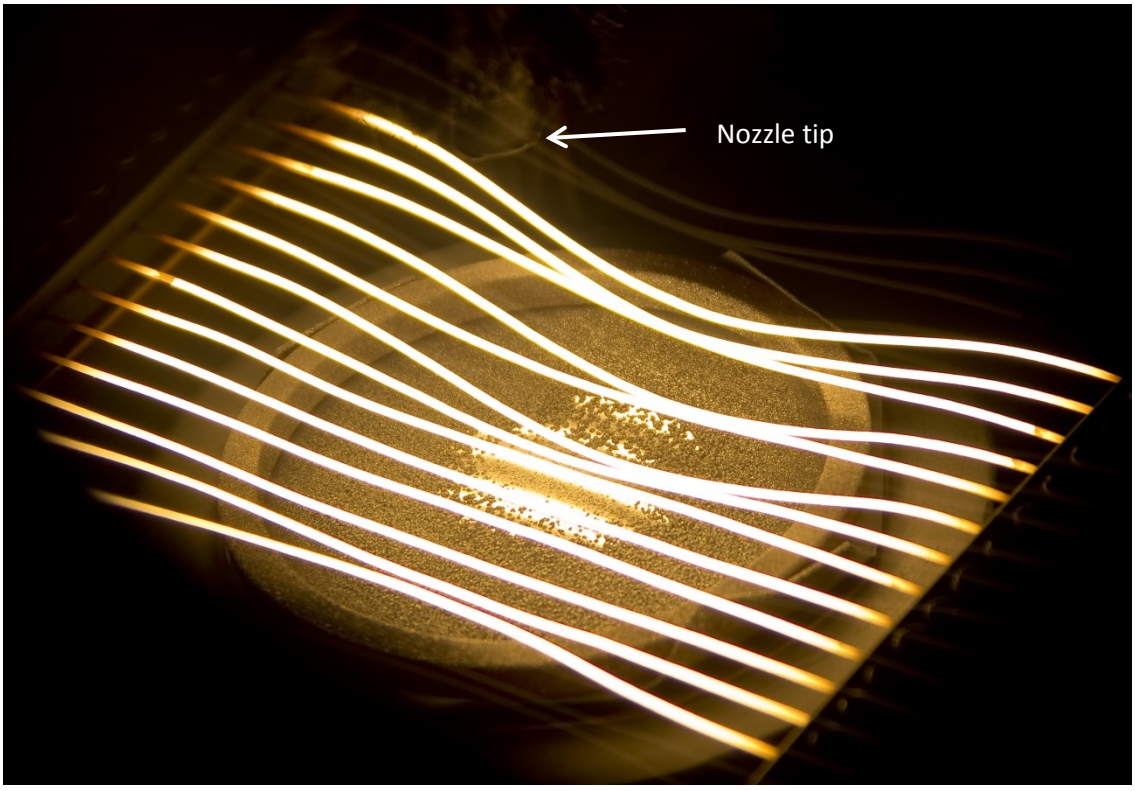


Figure 40: Run 55 on the last day of the run. Gas pressure supplied from the nozzle 0.9065" above the wires prevented closure of the film.

The diamond film created during run 55 shown in figure 41 is 4.4 cm in diameter and was grown using conditions similar to run 54 but allowed to proceed for 411 hours. The film grew from the outside of the hold-down ring toward the center. The nozzle that introduces the gas into the reactor is in the center of the substrate approximately 2.30 cm above the filaments. The inlet gas flow pressure at the center of the substrate prevented closure of the film. The image shown in figure 40 is 17 days into the run; one hour prior to shut down. This sample is 370 µm thick. As seen in

figure 43, the film is somewhat translucent and is smooth in appearance. This prompted the investigation and characterization that follows.

The growth region had no observable morphology and was created through coalesced homoepitaxial growth. An optical microscope image of the bottom portion of the film is shown in figure 43. If this were a textured diamond film at the magnification shown in the image, texturing would be visible unless it is an ultra-nanocrystalline diamond (UNCD) or nanocrystalline (NCD) film. If the diamond film is UNCD or NCD, X-ray Diffraction (XRD) could be used to confirm the quality of the film.[64-66]

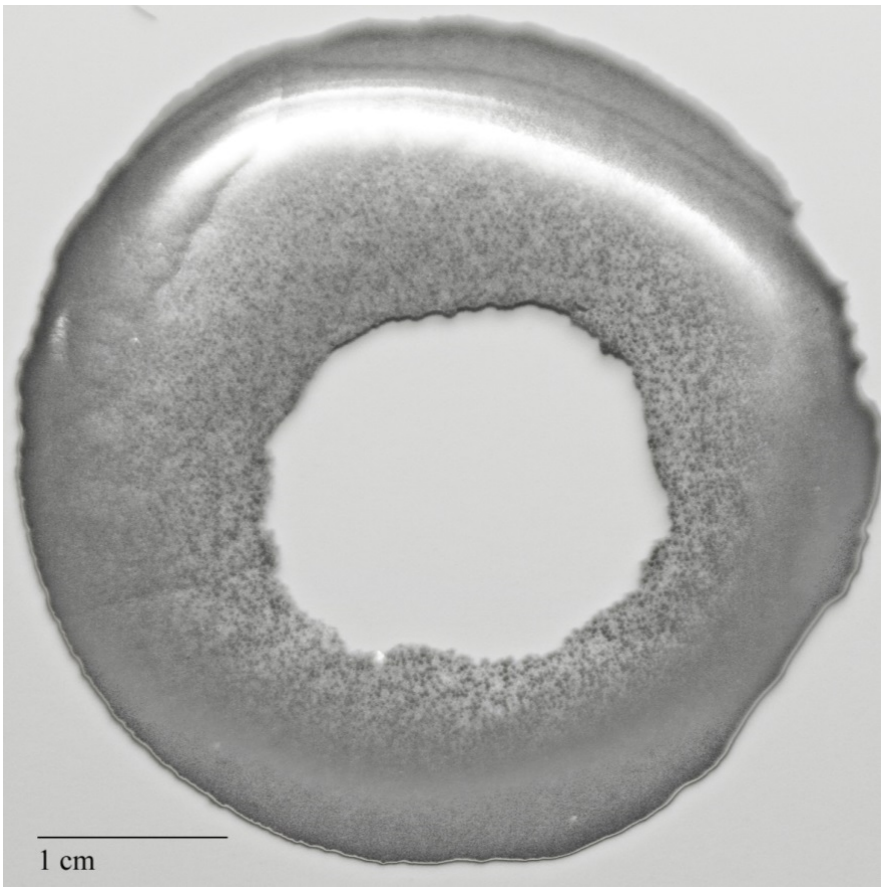


Figure 41: Run 55. 4.4 cm diameter single crystal. Side shown is the bottom of the film that grew closest to the platinum.

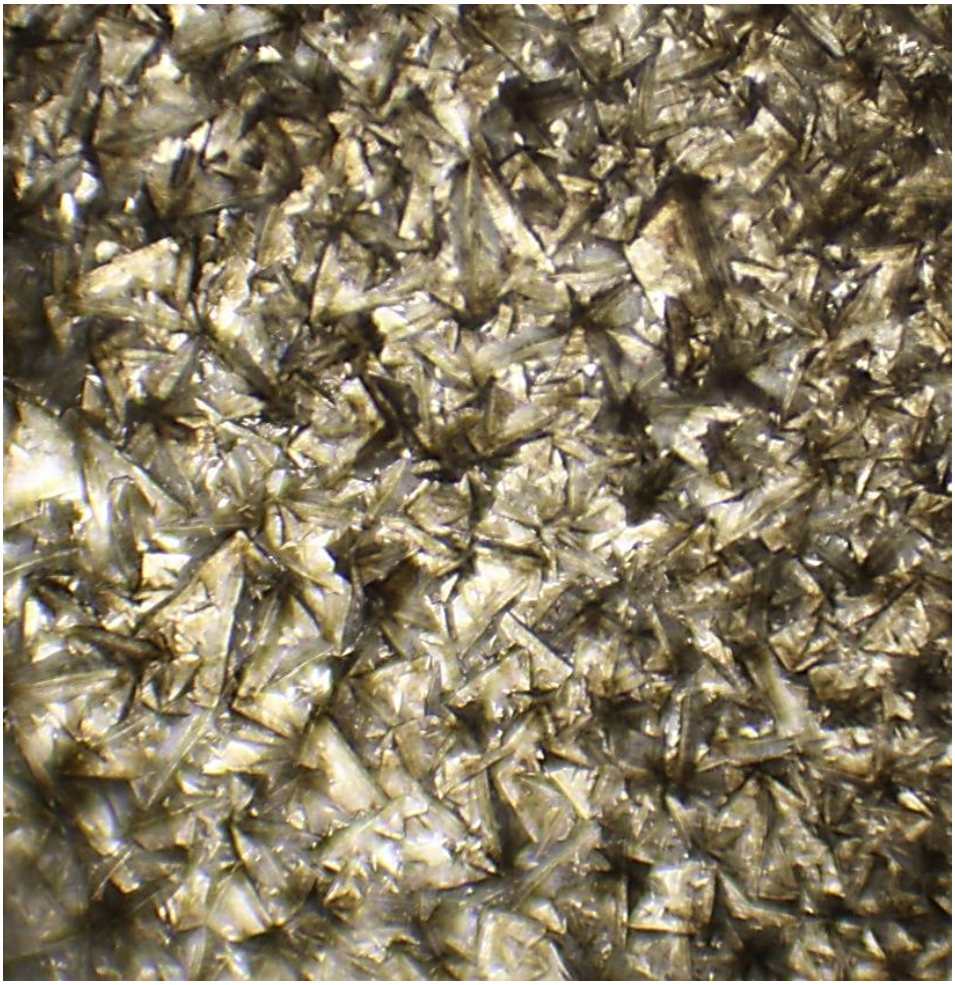

Figure 42: Top portion of the film for run 55. Triangle shaped diamond surface is (111). Magnification is 400x.

The film is layered vertically. The bottom portion of the film, which does not show morphology, is approximately 250 μm thick. The growth closest to the nozzle is shown in figure 42. (111) growth is clearly visible and shows some order in the growth.

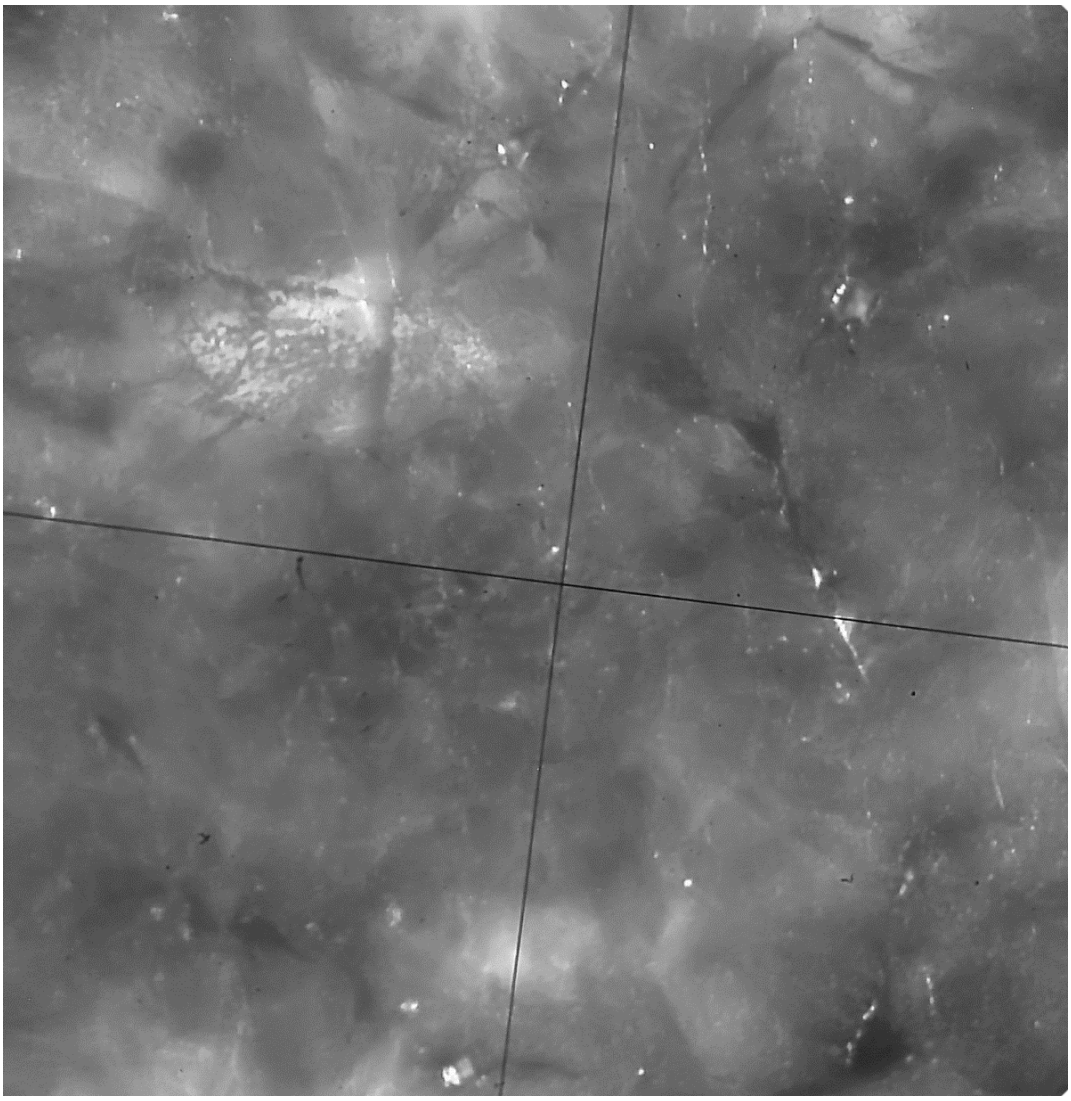

Figure 43: Run 55. Optical image of the diamond film. Side shown is the bottom of the film that grew closest to the platinum. Magnification is 400x.

The entire film is (1 1 1) with some (2 2 0) as seen in figures 46. XRD is designed for homogeneous samples. In the case of a layered film, multiple XRD methods are necessary to characterize the film. The structure of the film was determined using a high resolution Phillips X-Pert MRD X-Ray diffractometer (XRD) with a Cu $K\alpha_1$ radiation source (λ=1.54056 Å). The first XRD plot is a thin film scan that penetrates less than 20 μm into the sample. Three platinum growth planes are visible

as well as two diamond growth planes. Based on the ration of (111) to (220) growths, the thin film scan indicates a randomly oriented or contaminated crystal.

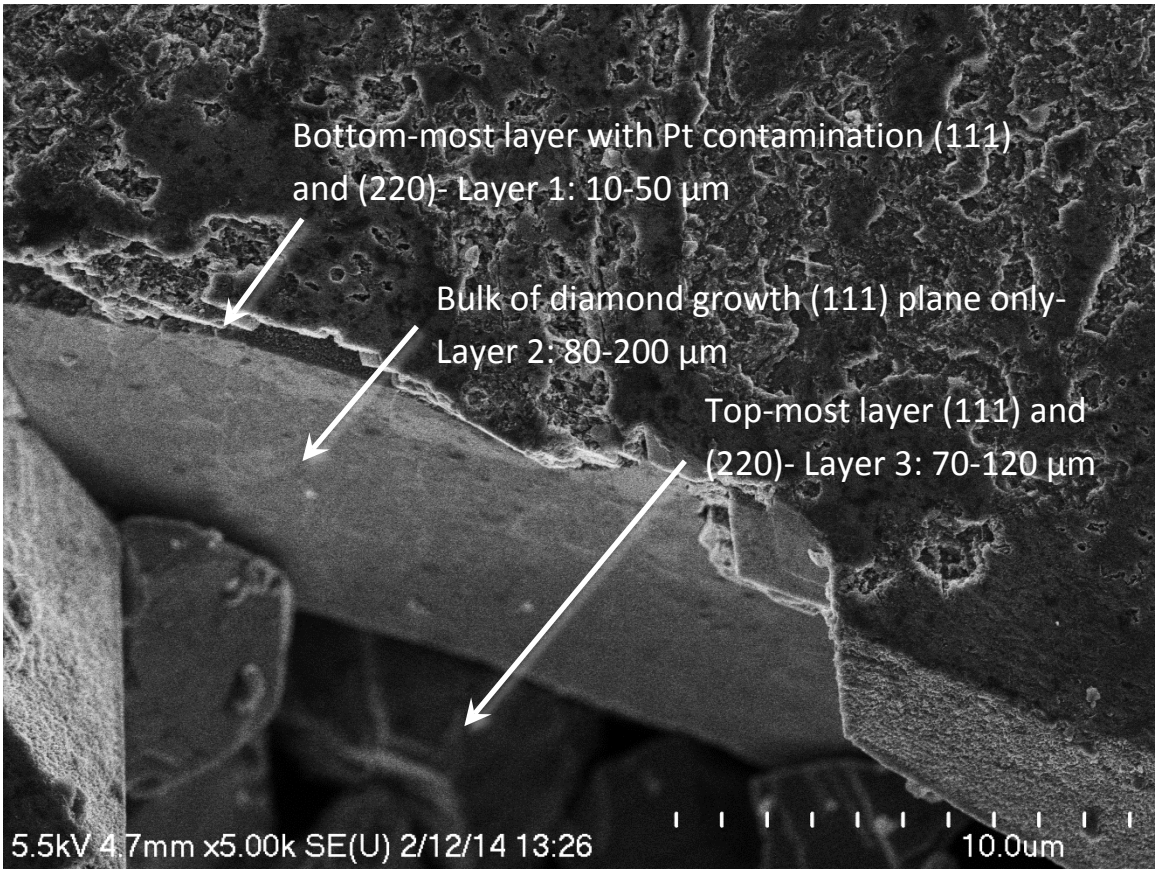


Figure 44: Field Emission SEM (FESEM) image of the film in run 55. Bottom most layer has platinum contamination causing disorder of the diamond film.

This random orientation is likely due to the bottom most layer of diamond being exposed and therefore contaminated with platinum. This layering is visible in figure 44. Figure 47 is a Gonio scan which is approximately 50-100 µm into the sample showing a reduction in the (220) peak.

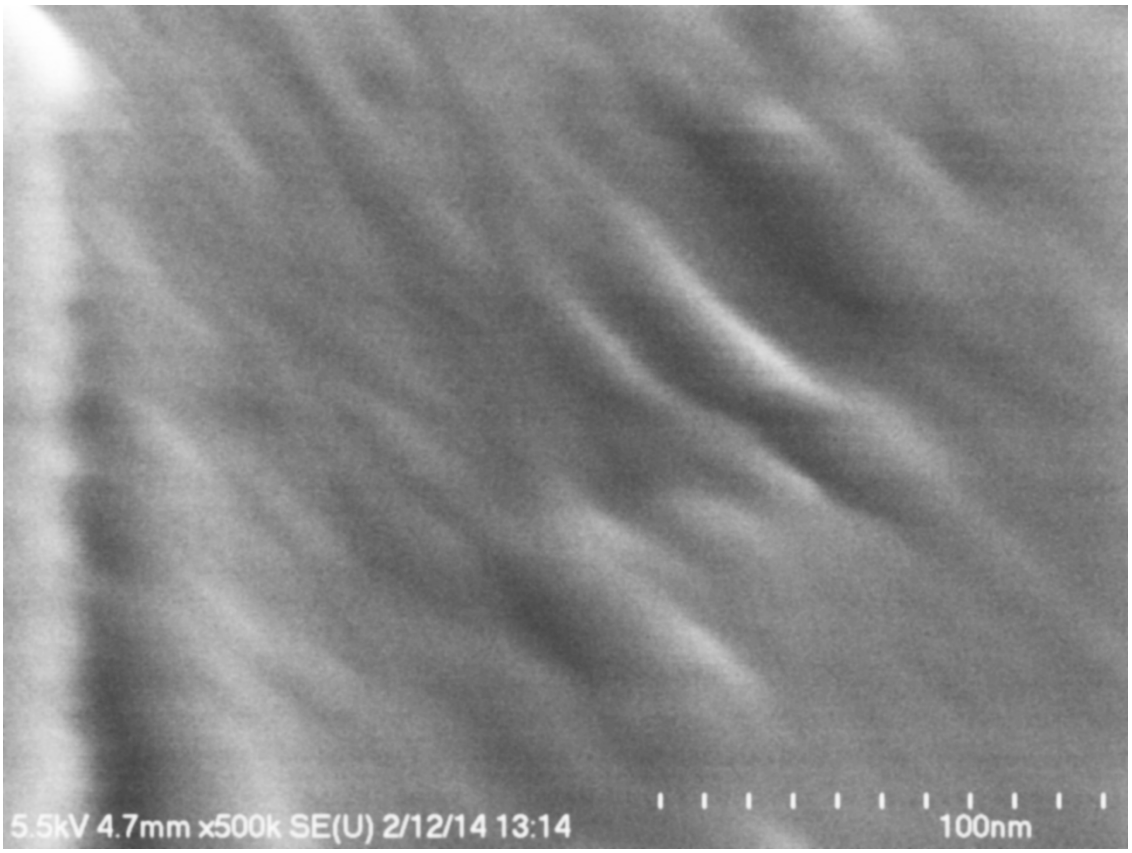

Figure 45: FESEM of bottom most layer of sample in run 55. No morphology can be seen.

Figure 45 is the highest resolution of the bottom most layer of the crystal that could be obtained. At a subdivision scale of 10 nm, no morphology could be seen. There are some topographical features indicative on the uneven surface of the platinum substrate holder.

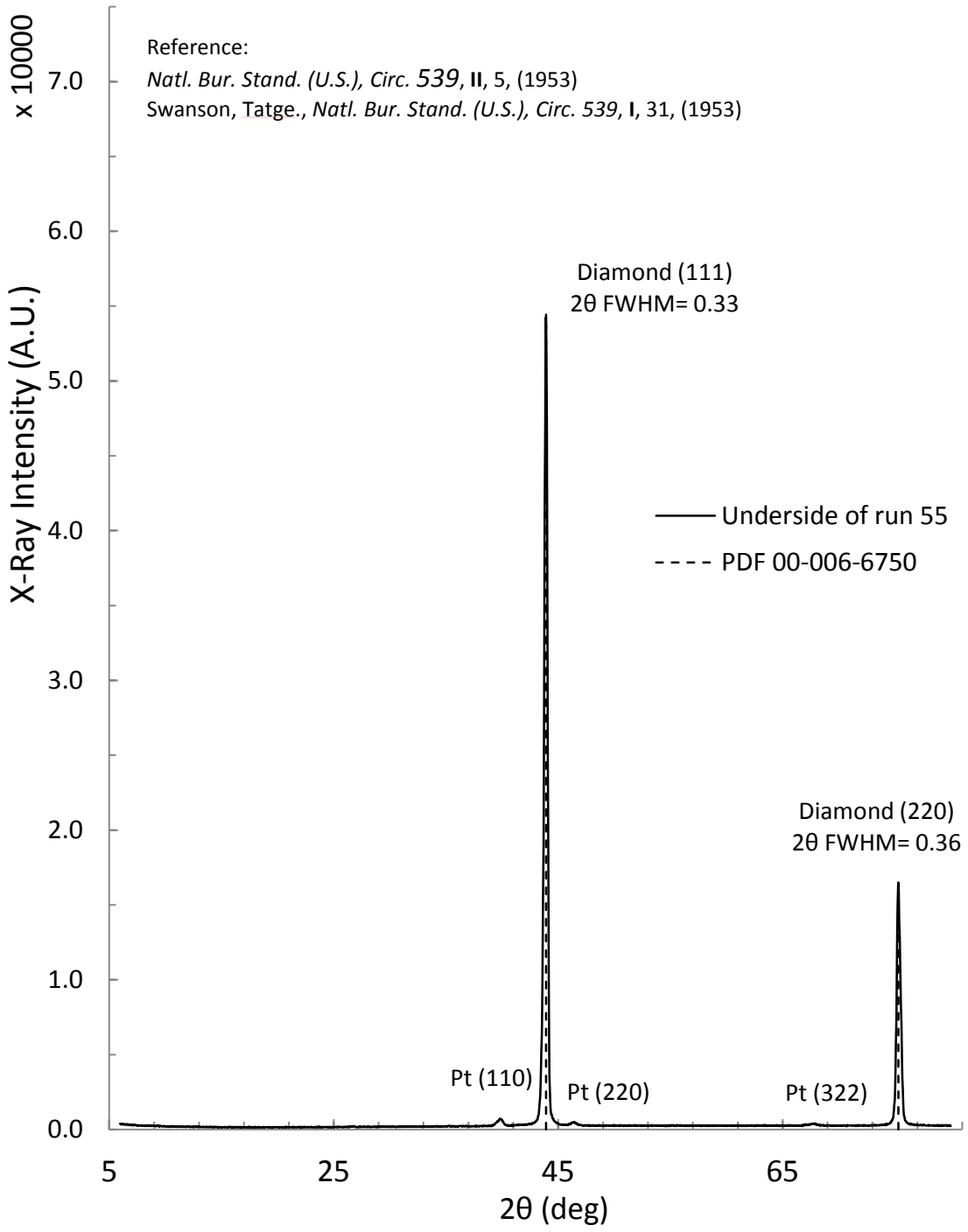


Figure 46: Thin film XRD of run 55 for the unpolished sample. (220) peak is from platinum contamination causing multiple growth patterns. Peak to signal broadening ratio is maintained. Platinum is more pronounced near the surface. Beam is ~10-20 µm into sample.

Instrumental broadening of the Phillips X-Pert MRD X-Ray diffractometer (XRD) was determined using NIST SRM 660a LaB6. Examination of sample peak broadening indicated no additional line broadening beyond instrumental broadening, indicating crystallite size is >200 nm. Twinning, mosaics, stacking faults, chemical heterogeneities, grain boundaries, crystallites, and micro stresses all cause peak broadening which is not present in the XRD.[67] Because texturing is not visible and a NCD film would produce peak broadening (which is not present in this sample), it was determined that the bulk of the diamond growth (second layer) is single crystal. The (110) peak and the (220) peak are from different layers of the same sample and not due to texturing. Ranges for thickness shown on figure 44 are from estimates constructed from the program Image J of SEM, FESEM, and optical images. The film thickness varies from one part of the sample to the other.

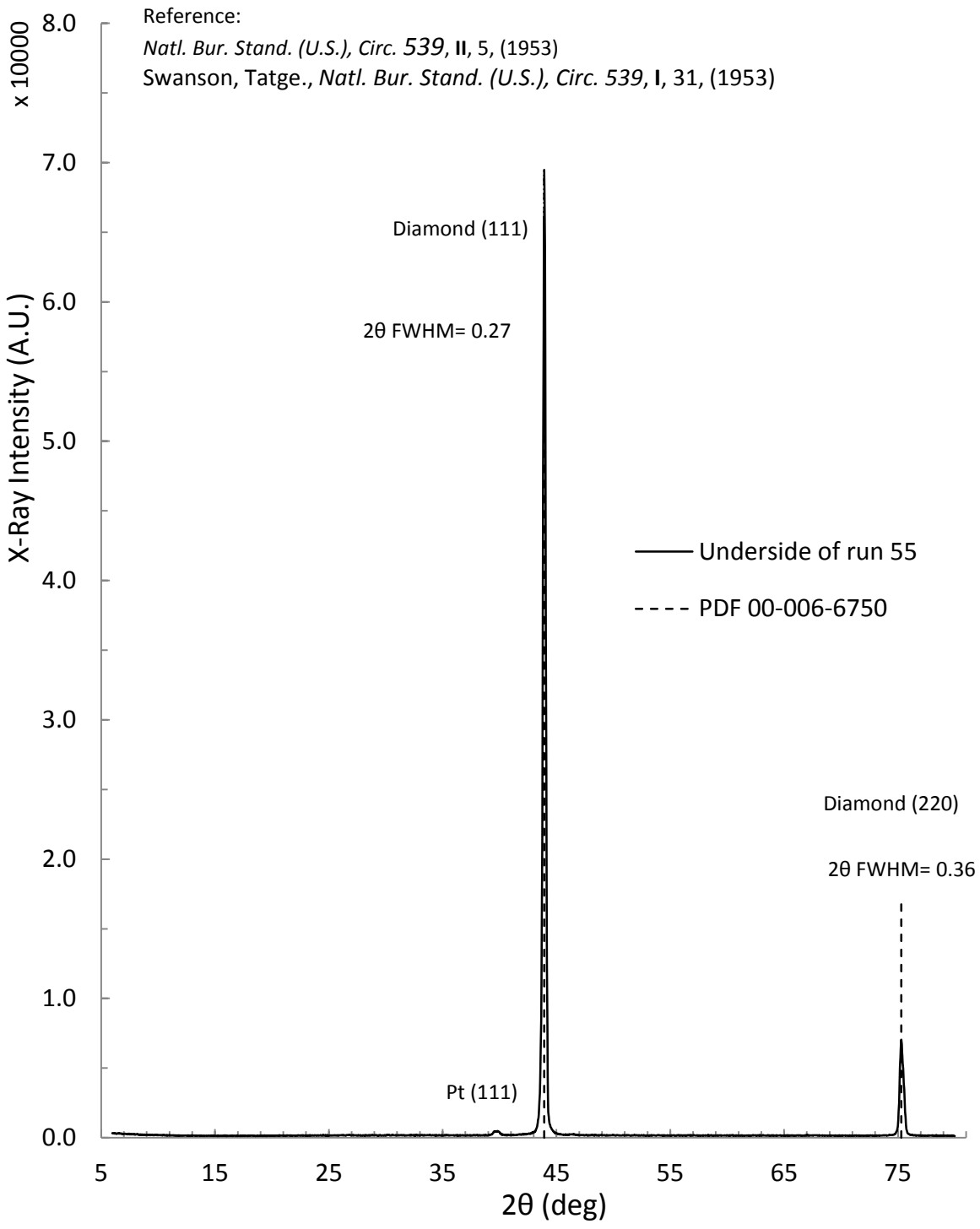


Figure 47: Gonio scan of run 55 X-Ray Diffraction for the single crystal (bottom of film) unpolished sample. (220) peak is from platinum contamination. Broader (220) peak likely indicates a separate plane from the main (111) crystal because instrument broadening should have maintained the same peak to signal broadening ratio. Beam is ~50-100 μm into sample.

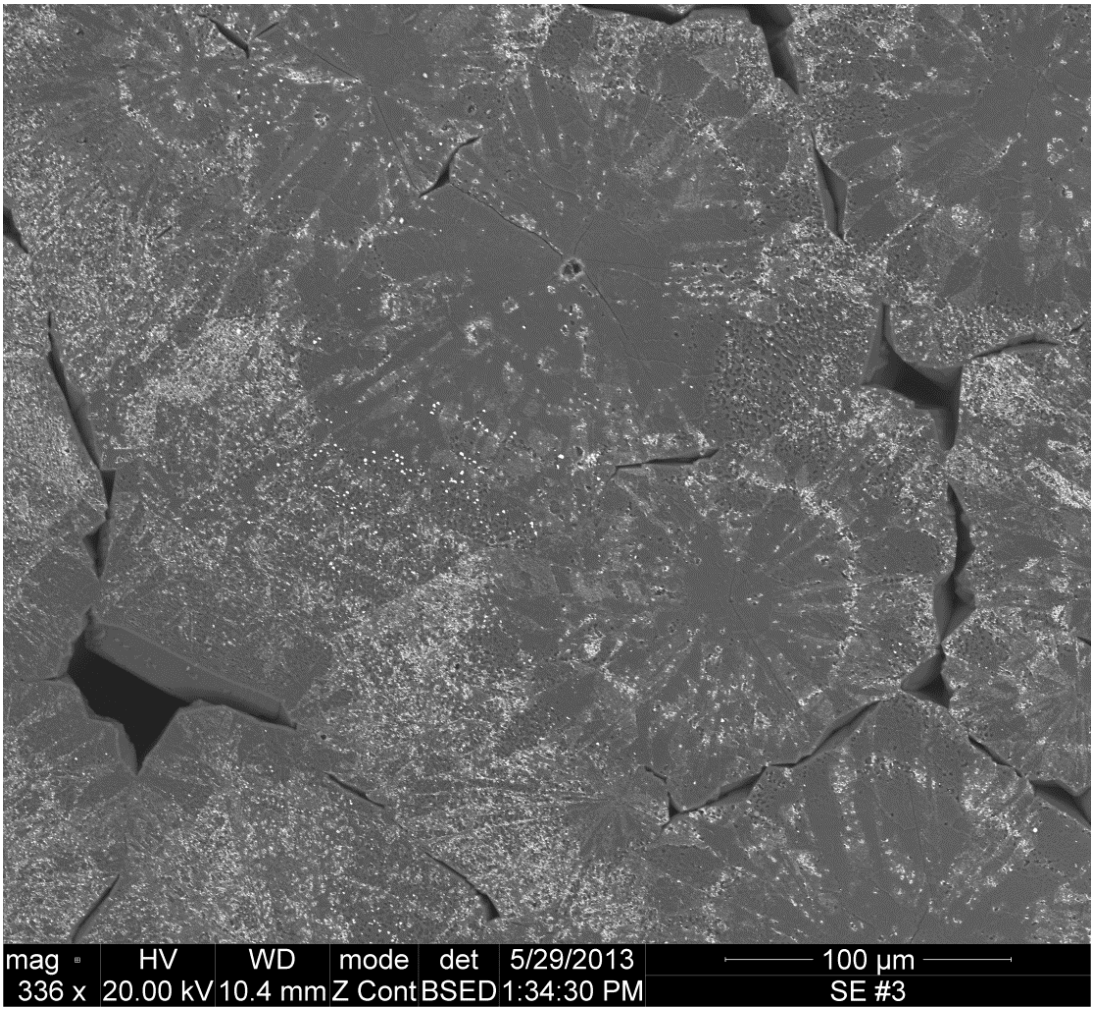

Figure 48: Unpolished run 55 with backscattering Z-contrast. Light color is platinum transfer from substrate holder.

XRD data provided strong evidence that there is platinum present in the bottom most portion of the film. This contamination should be present on a SEM with a backscattering detector image in Z-contrast mode. Figure 48 clearly indicates platinum contamination as present as lighter colored spots on the darker colored diamond surface. This image was taken at low magnification to reduce beam penetration into the sample so that a surface image could be obtained.

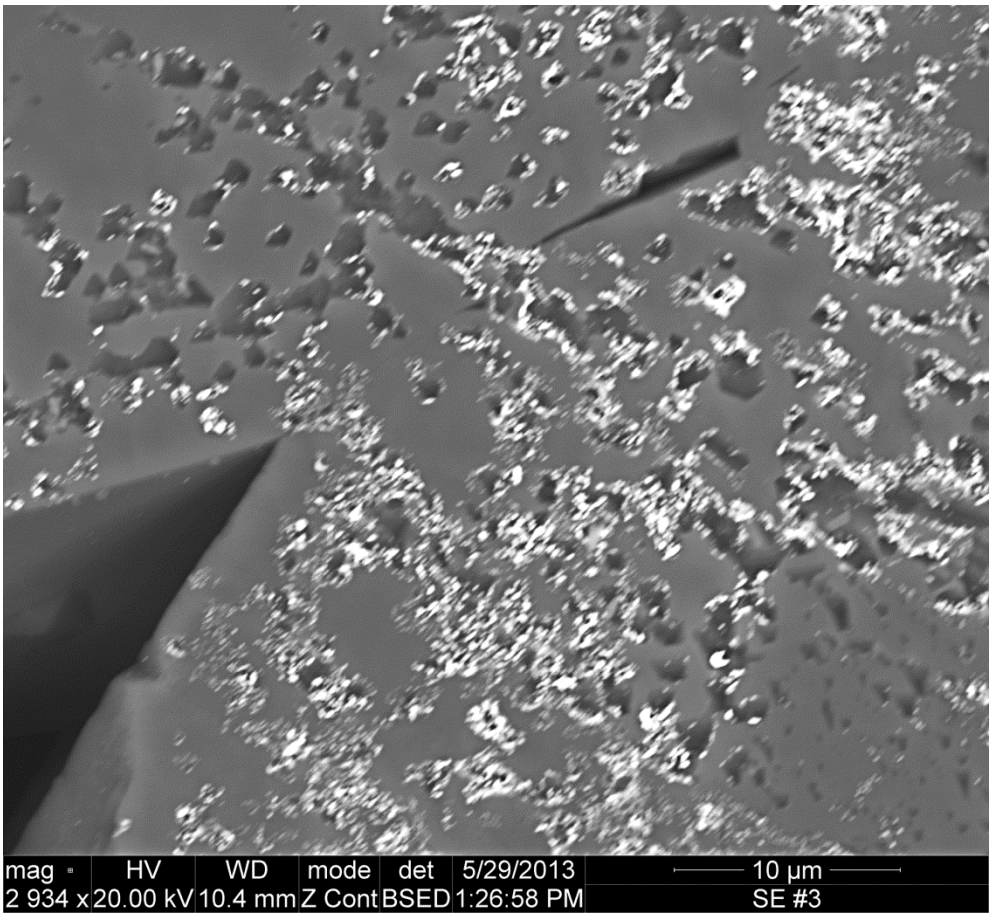

Figure 49: Run 55 with backscattering detector and Z-contrast. Light color is platinum transfer from substrate holder (higher magnification of previous image).

At a higher magnification of the same sample site, the BSED detector will show an image that is deeper into the sample as seen in figure 49. Again, lighter color indicates platinum contamination in the crystal but where contamination is not present, no morphology can be seen in the crystal. The “holes” that are seen in the image are caused by irregular growth from the platinum.

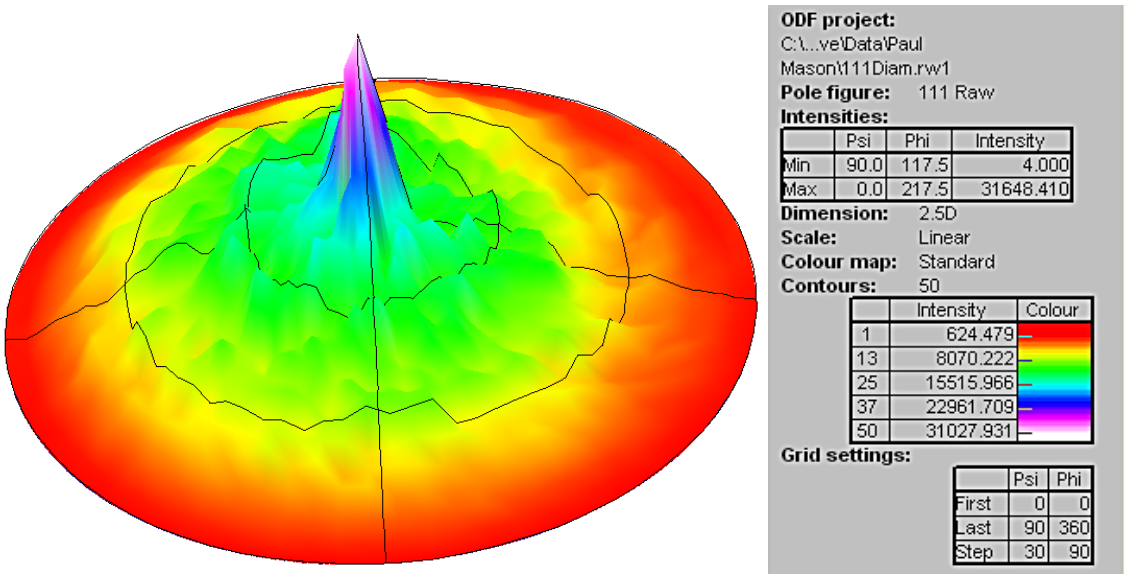


Figure 50: XRD pole figure of run 55 bottom of the film. Strong peak in the center of the (111) oriented film does not have a corresponding 220 map as expected for a strongly textured or contaminated film.

Figure 50 is a pole figure from the Phillips X-Pert MRD XRD. If the film were randomly oriented or contaminated (non-homogeneous), this is the pole figure one may expect. A strong peak is present in the (110) direction with scattering in the (220) direction. Since texturing is not visible and no peak broadening was recorded on the 2-theta plot, this pole figure shows that the sample is non-homogeneous on the surface. This is consistent with the FESEM image which shows the layering of the sample.

Prior the thermal imaging study, it was speculated that a hot spot had developed in the center of the substrate which prevented diamond growth in that region. Thermal imaging confirms consistent temperatures across the surface of the substrate. A flow study utilizing a helical nozzle design with a hollow cone gas projection allowed

for diamond growth at the center of the substrate. This confirms that gas flow pressure prevented closure of the film.

To study the growth of the film, a FLIR® 6703 infrared thermal imager was acquired. An example image of the study is shown in figure 51. Emissivity was set to obtain accurate measurements of the substrate. Substrate temperature was recorded at 703.3 +/- 7.2 C. Spectral data collected from the micro Raman indicates 1332 $cm^{-1}$ for all portions of the film. Two such spectra are shown in figures 52 and 53.

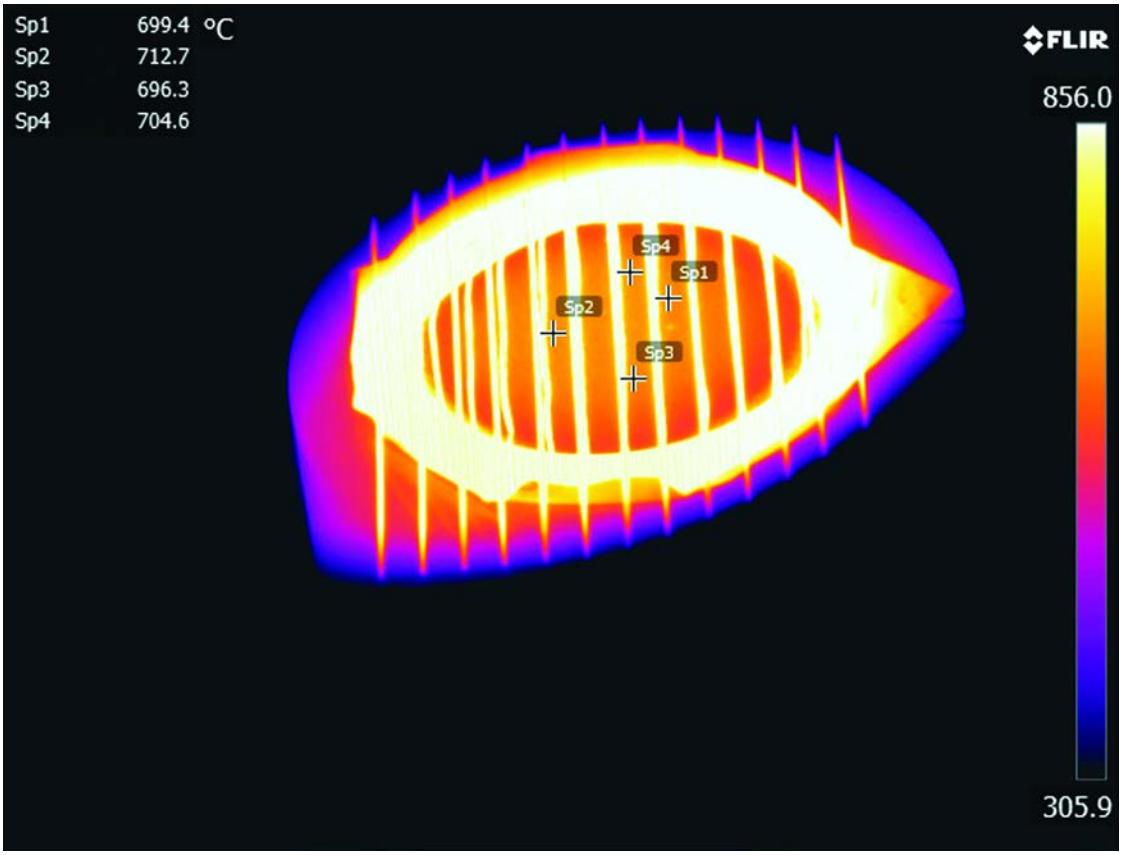

Figure 51: Thermal image of substrate during diamond growth

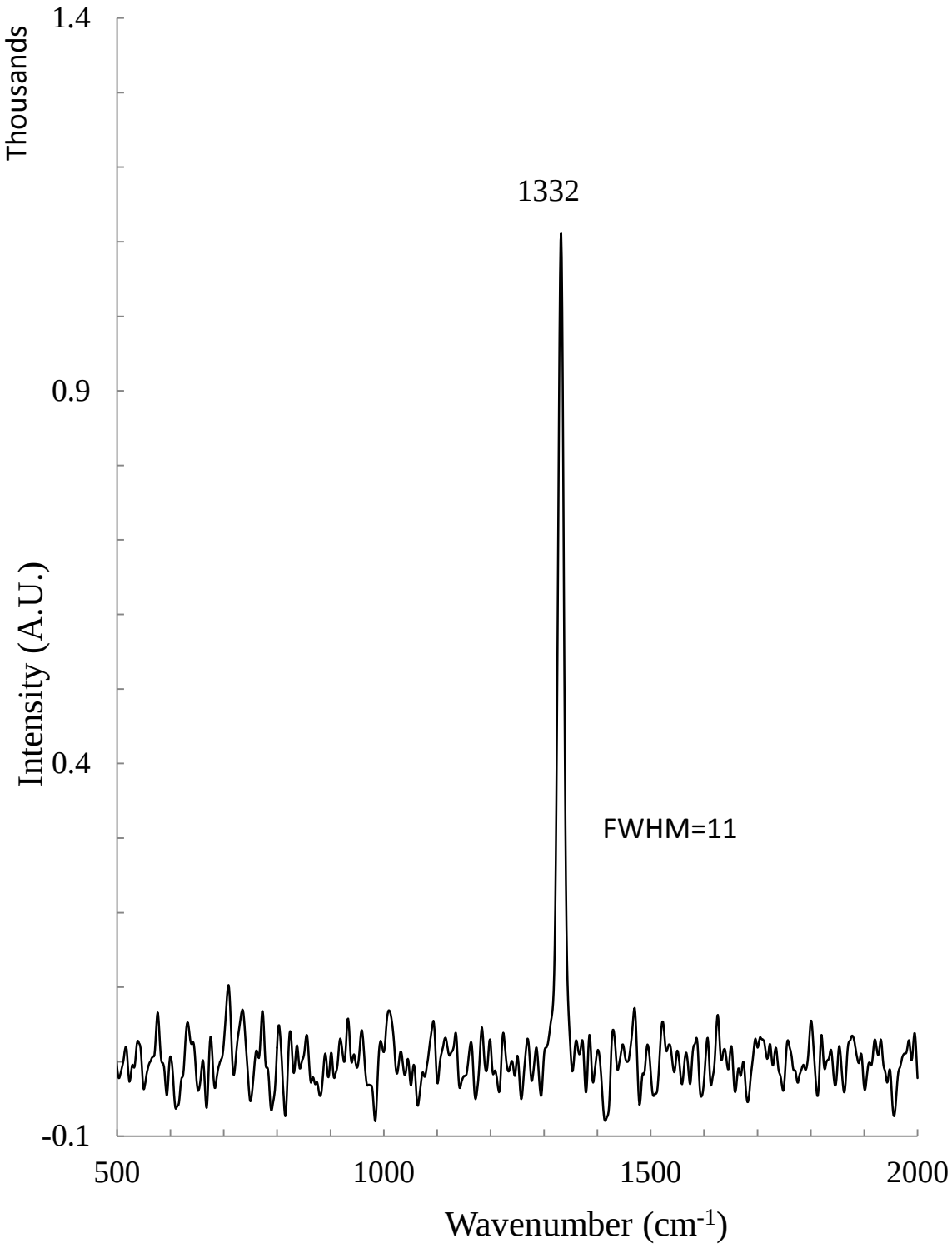


Figure 52: Run 55. Micro Raman (785 nm wavelength) result of 1332 $cm^{-1}$ from layer 1 in figure 44. Peak broadening is from platinum contamination of the outermost layer.

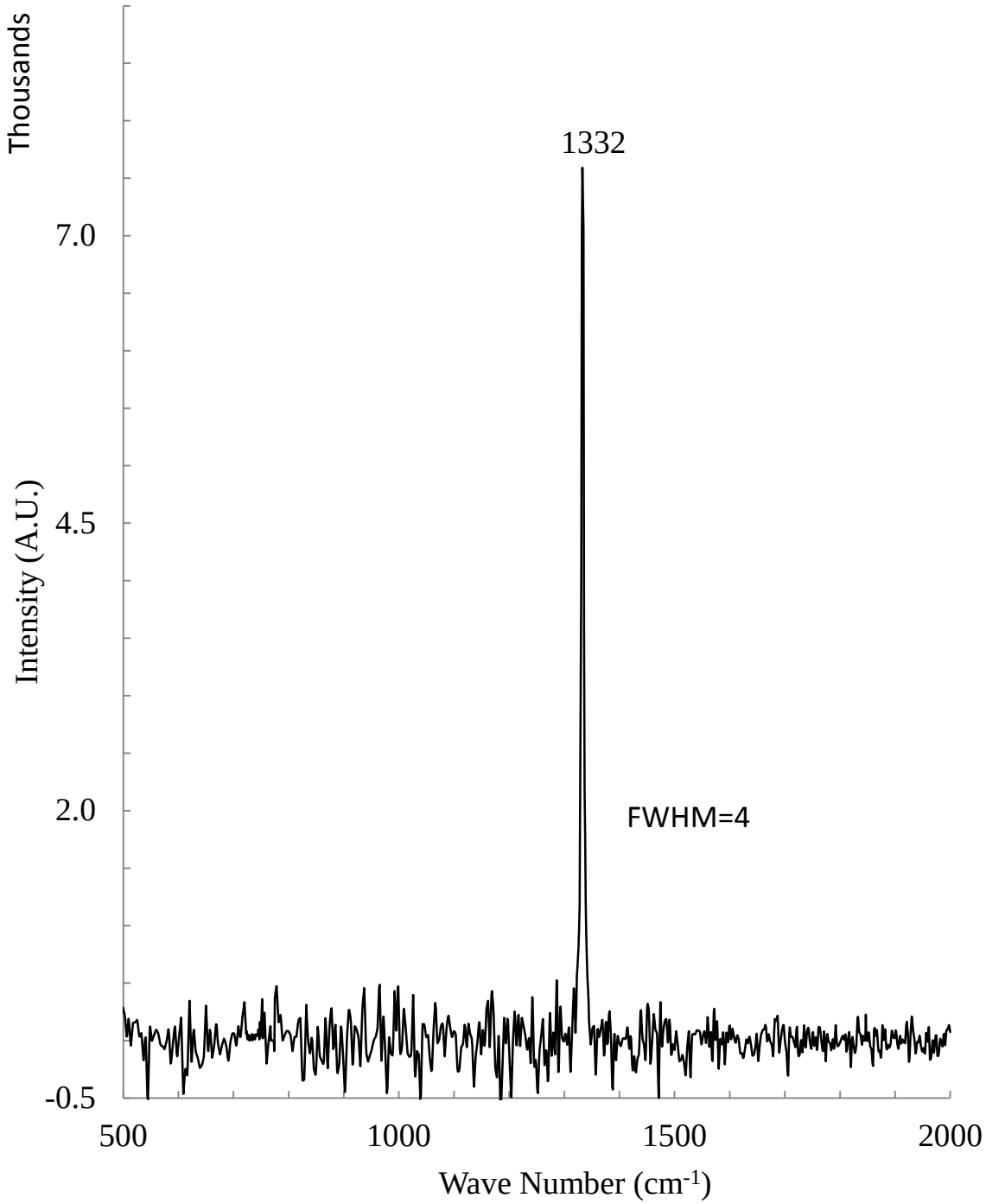


Figure 53: Run 55. Micro Raman (785 nm wavelength) result of 1332 $cm^{-1}$ from layer 2 in figure 44.

Peak broadening in the Raman spectrograph in figure 52 is due to platinum contamination in the outmost layer. In figure 53, broadening is instrument broadening and possible platinum scatter from layer 1. The scan in figure 53 was obtained while the sample was vertical and the beam was aimed at layer 2 in figure 44 (single-crystal). To compare this sample with a known single crystal diamond, an electronic grade single crystal diamond was purchased. The narrowest FWHM at 1332 $cm^{-1}$ that could be obtained was 5 $cm^{-1}$.

SEM analysis of diamond films is challenging due to charge collection that accumulates on the film and distorts the image. The film in run 55 was especially challenging to image as the single crystal portion is approximately half of the total thickness. Low voltage (less than 5 keV) imaging can produce a nearly defect free picture but only at low magnification. One such image is shown in figure 54.

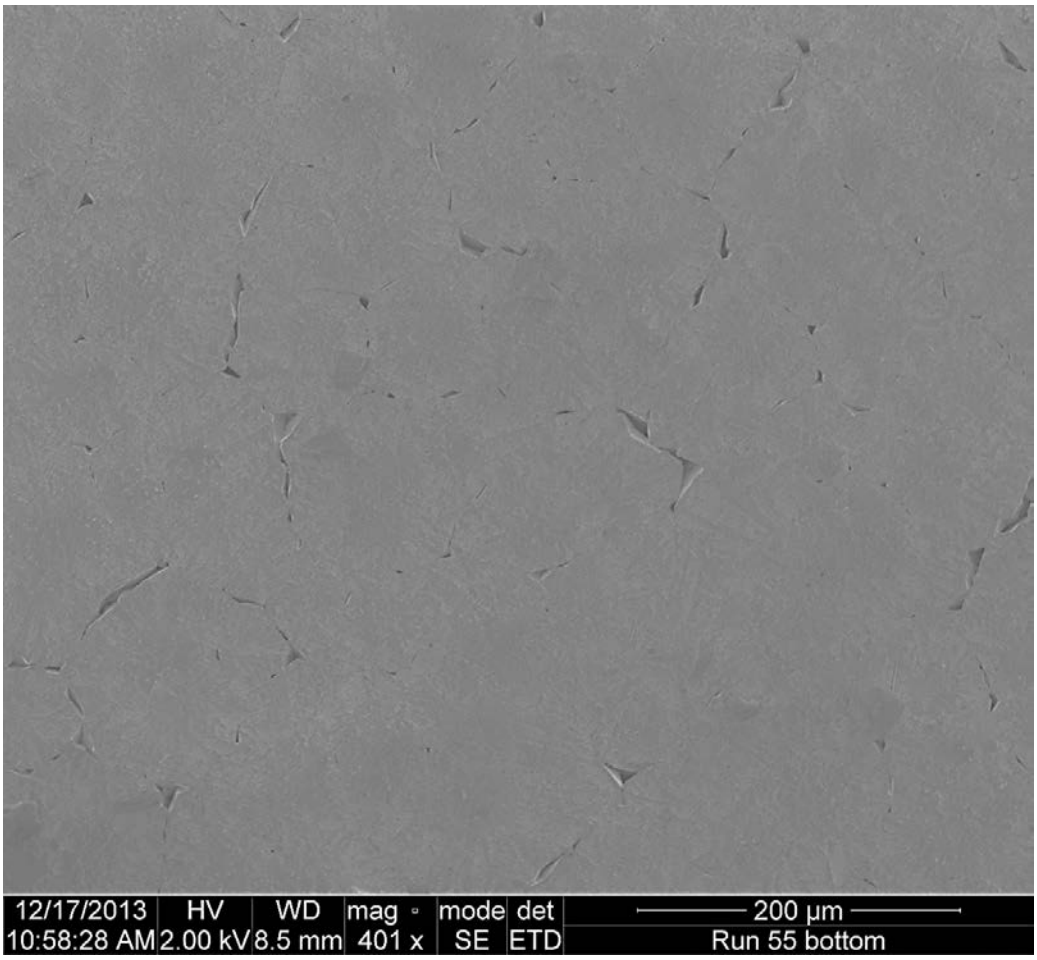

Figure 54: Run 55 Scanning Electron Microscope image taken at low energy and magnification to minimize charging. Crowded 200-400 µm nucleation sites merge into a single crystal.

Energy-dispersive X-ray spectroscopy (EDS) analysis was also performed while using the SEM. The film was identified as carbon with trace amounts of platinum.

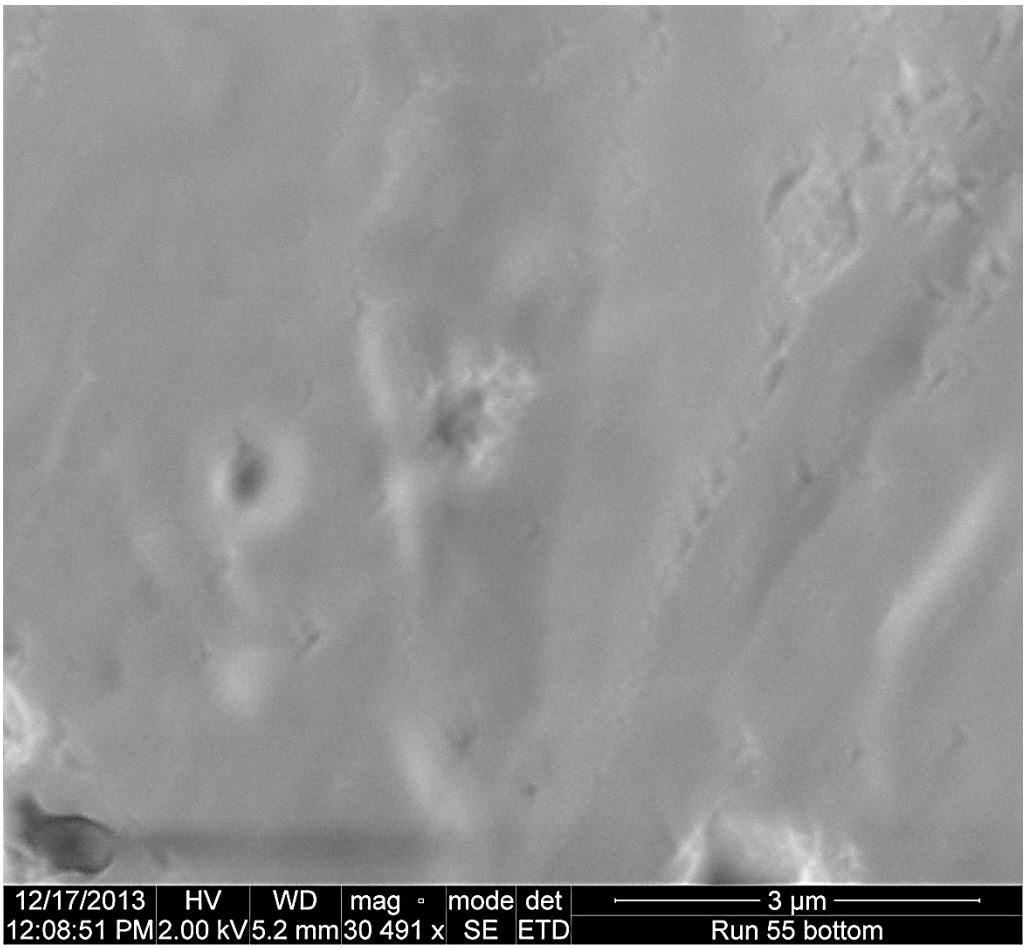

Figure 55: Run 55 bottom of the diamond film and close up of the previous SEM image. Visible width is 8 µm with the smallest structures visible at 50 nm. No visible morphology is present.

To obtain an in-range dead band on the EDS for this sample required a beam at 6.0 keV. At this energy, images obtained are below the surface of the crystal. An exact distance could not be determined. The spectral analysis is shown in figures 56-58.

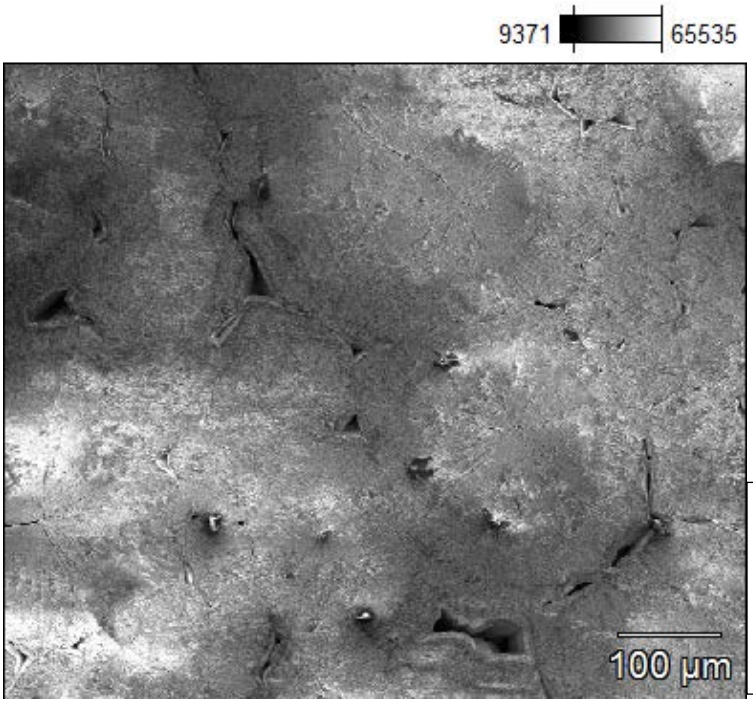


| | |
|---|---|
| Data Type: | Counts |
| Image Resolution: | 512 by 440 |
| Image Pixel Size: | 1.43 µm |
| Map Resolution: | 512 by 440 |
| Map Pixel Size: | 1.43 µm |
| Acc. Voltage: | 6.0 kV |
| Magnification: | 177 |

Figure 56: Run 55. EDS analysis of diamond film. Greyscale image shows area of spectral analysis.

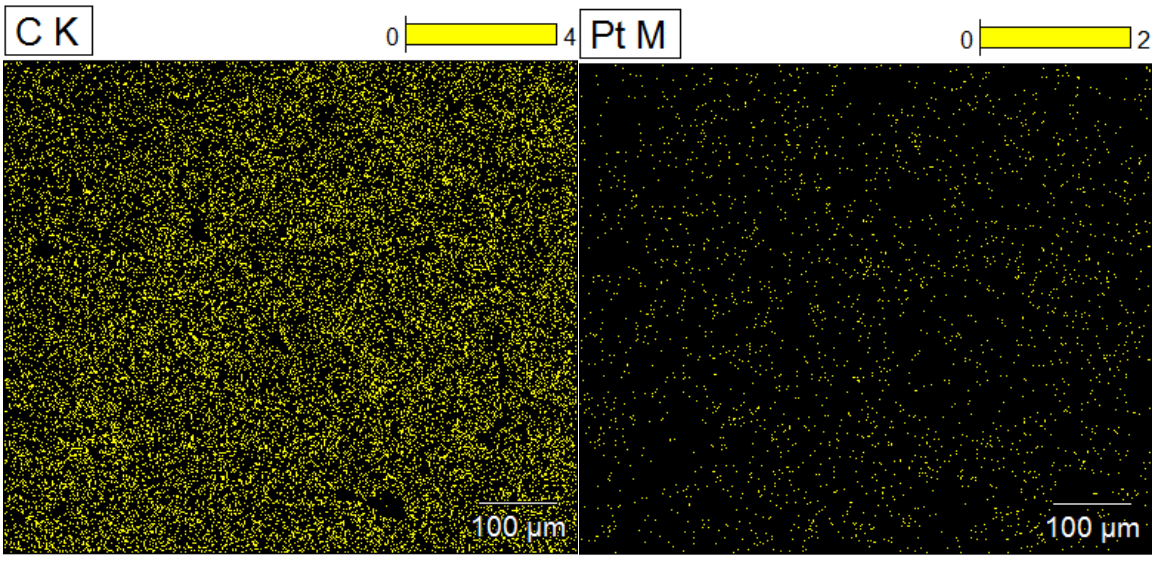


Figure 57: Run 55. EDS spectral mapping of elements found

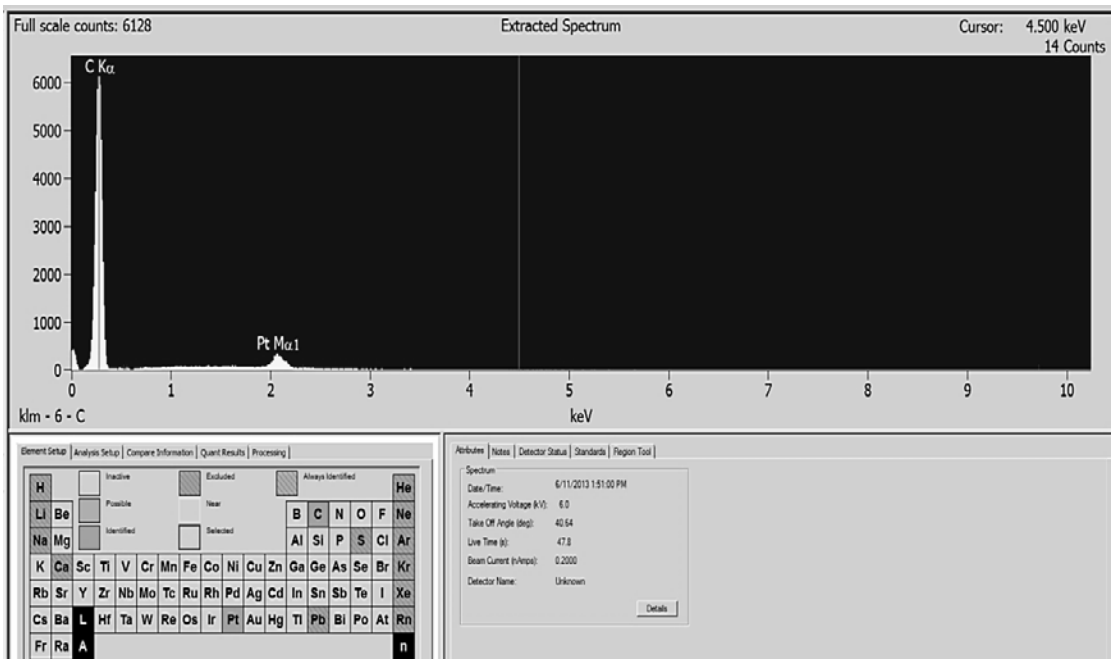

Figure 58: Run 55. EDS spectrum and count

Run 56 had two objectives. First, to determine if modifications to the nozzle could allow for closure of the film in the center of the substrate and determine if modifying the surface topography would allow custom diamond shapes to form. The second objective was tested by pressing a “V” shaped notch into the Pt/Ir foil. If diamond grows according to surface defects, then there should be a complimentary notch in the diamond film. The first objective was achieved as evident in figure 59 where the film closure is 50% greater than in run 55. The run was terminated prior to complete film closure due to slippage of the nozzle which nearly touched the substrate. This caused graphitization and fracture of the final film. Although optical microscopic analysis showed evidence that modification of the surface topography can be used to alter the shape of diamond growth in the film, since the final film fractured conclusive

evidence could not be verified. The “V” that was created in the metal had fractured in the film. Only one-half of the “V” could be reconstructed.

Figure 59: Run 56. Diamond structures as seen as “dots” on the substrate surface directly below the nozzle confirm that reducing the orifice size and maintaining the same linear gas velocity will allow for closure of the film. The nozzle is seen much closer than run 55 due to slippage of the nozzle closer to the substrate. The run was terminated prematurely for this reason.

Runs 57 and 58 were an attempt to increase nucleation density to minimize the piping seen in run 55. This was accomplished by increasing the concentration of seed crystals applied to the substrate. The runs were intentionally terminated early to observe various stages of nucleation. Although nucleation density was observed in run 58 as seen in figure 60, it was not uniform over the entire sample. This indicates conditions for growth were not uniform over the substrate and further modification and study is required.

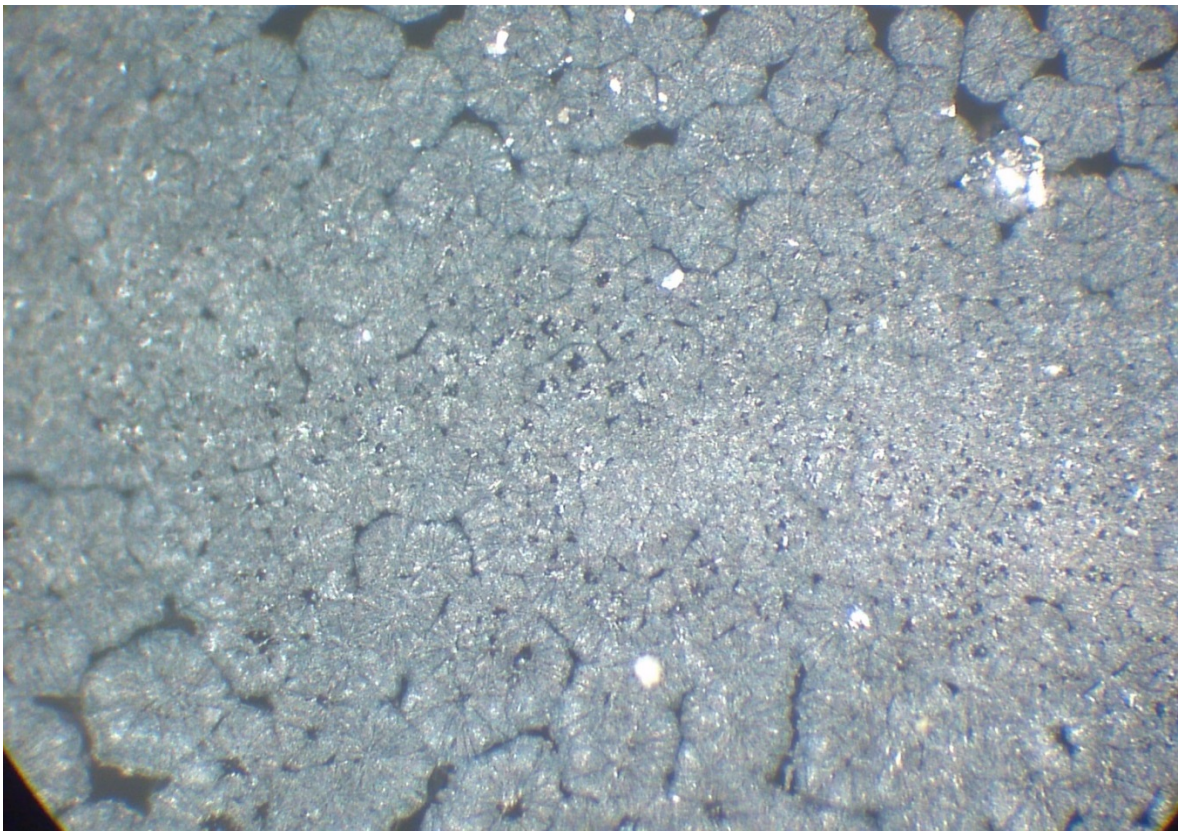

Figure 60: Run 58. Increased nucleation density occurred near the center of the sample which was located 0.5 cm from the center of the substrate. As the sample was observed from top to bottom, nucleation density decreases. 200x magnification.

Runs 59-61 investigated the effect of physical vapor deposition (PVD) of boron nitride on diamond growth. The 5 cm boron nitride (BN) ring that holds the Pt/Ir foil into position was allowed to come within 1 mm of the filaments and in run 61 touched the filaments. This vaporized the BN which was deposited via PVD on the nozzle and copper wire holders. This reduced distance increased the substrate temperature (but still within diamond growth acceptable ranges) and subsequently, the BN cooling block under the substrate. The BN cooling block changed phase from polycrystalline h-BN to strongly oriented h-BN as seen in figure 62. Diamond growth did not occur during these

runs. It was determined based on these observations that PVD interferes with diamond growth.

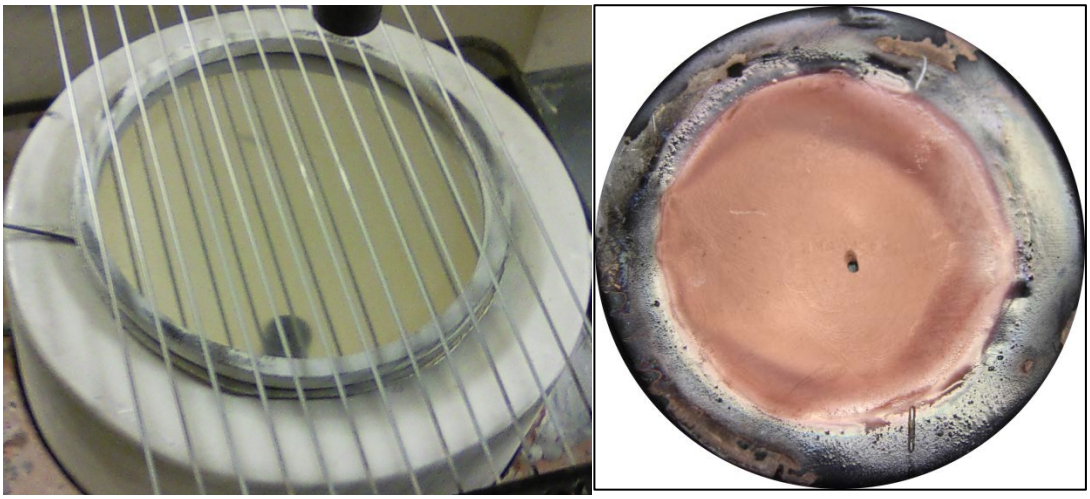

Figure 61: Run 61. Before and after run. Glass structures in right image are oriented crystal hexagonal boron nitride.

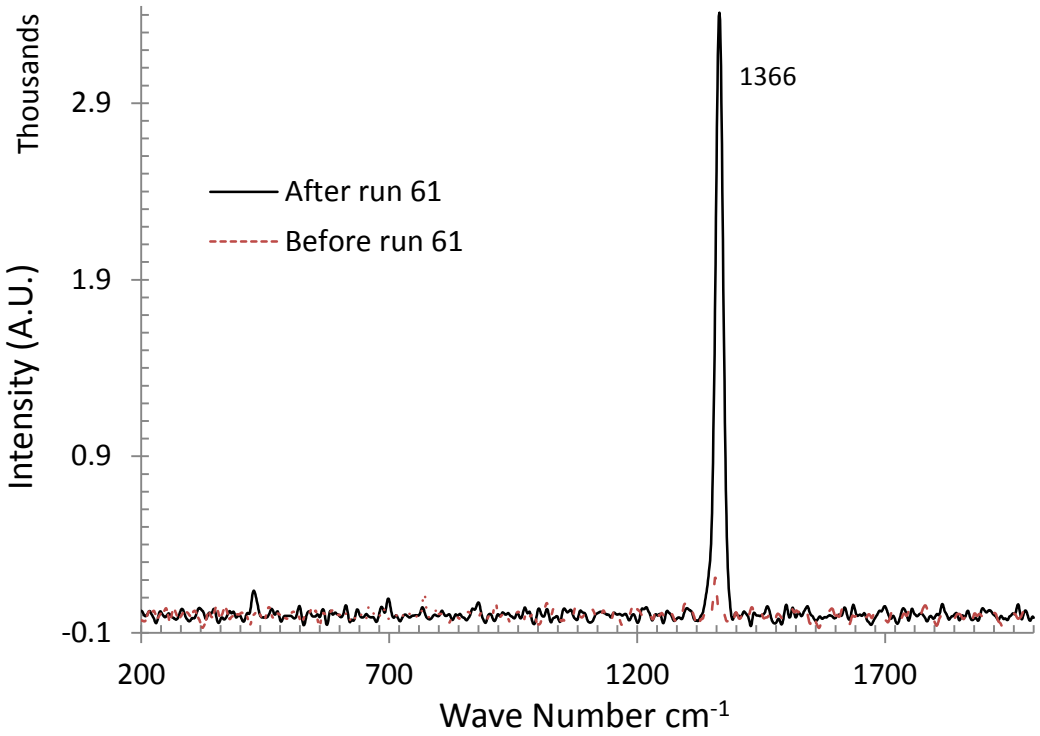


Figure 62: Run 61 Micro Raman spectrograph before and after run. Small peak is indicative of polycrystalline h-BN and is a sample of the boron nitride holder just before the experiment. The organization of the h-BN changed during the run into a textured crystal; as indicated by the sharp peak at 1366 $cm^{-1}$.

Run 64 eliminated the need for boron nitride to be present near the growth zone by replacing the boron nitride ring with a textured (111) tungsten plate with a 44.38 mm hole extruded in the center of the plate. The tungsten plate was carburized along with the wires prior to experiment to minimize contamination. In addition, the plate shown in figure 63 coated with 0-2 µm powder to further prevent tungsten contamination. The extruded hole serves the same purpose as the boron nitride hold down ring; keep the platinum foil flat and provide a lip to alter the gas flow near the substrate.

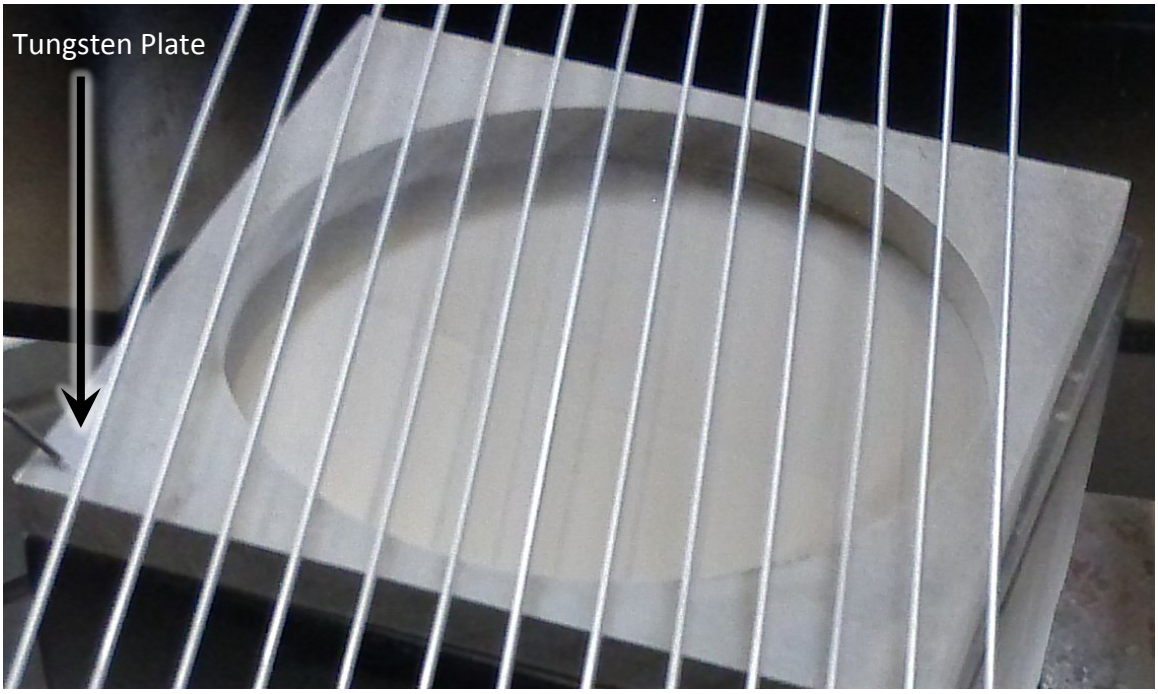

Figure 63: Run 64 shown with tungsten plate and platinum substrate holder.

The objective of the experiment was to verify that a tungsten hold down plate in conjunction with the increased distance to the filaments from the nozzle to 25.4 centimeters could produce a film that covers the entire surface of the substrate. Since

tungsten is nine times denser and its thermal conductivity is over eight times than that of boron nitride, at the time, it was unknown if these facts would negatively affect the resulting film.

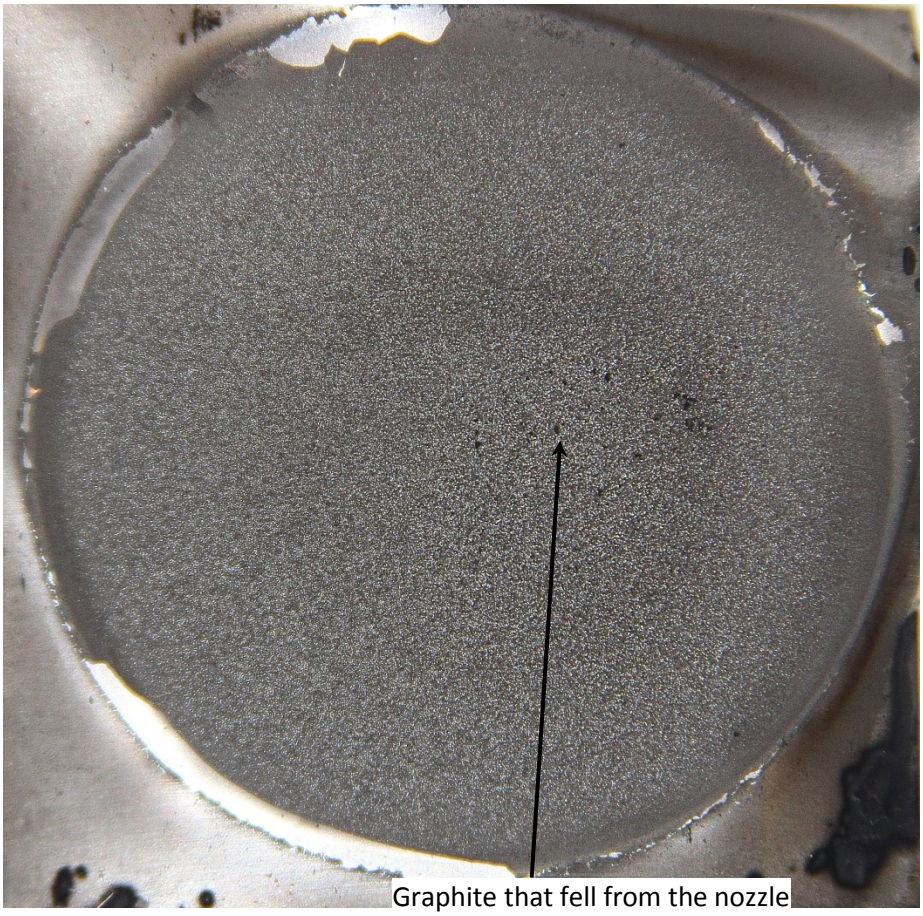

Figure 64: Camera image of run 64 after the completion of the run. Film closure occurred over the entire surface of the growth zone.

The run was terminated after 8 days (as opposed to 14 days) to inspect intermediate results. The Raman spectrograph confirms the film is diamond. The surface area of the film shown in figure 64 is 13.6 $cm^2$ which is the entire growth surface. Unlike the run 55 shown in figure 40, the growth surface shown in figure 66 is completely covered and uniform.

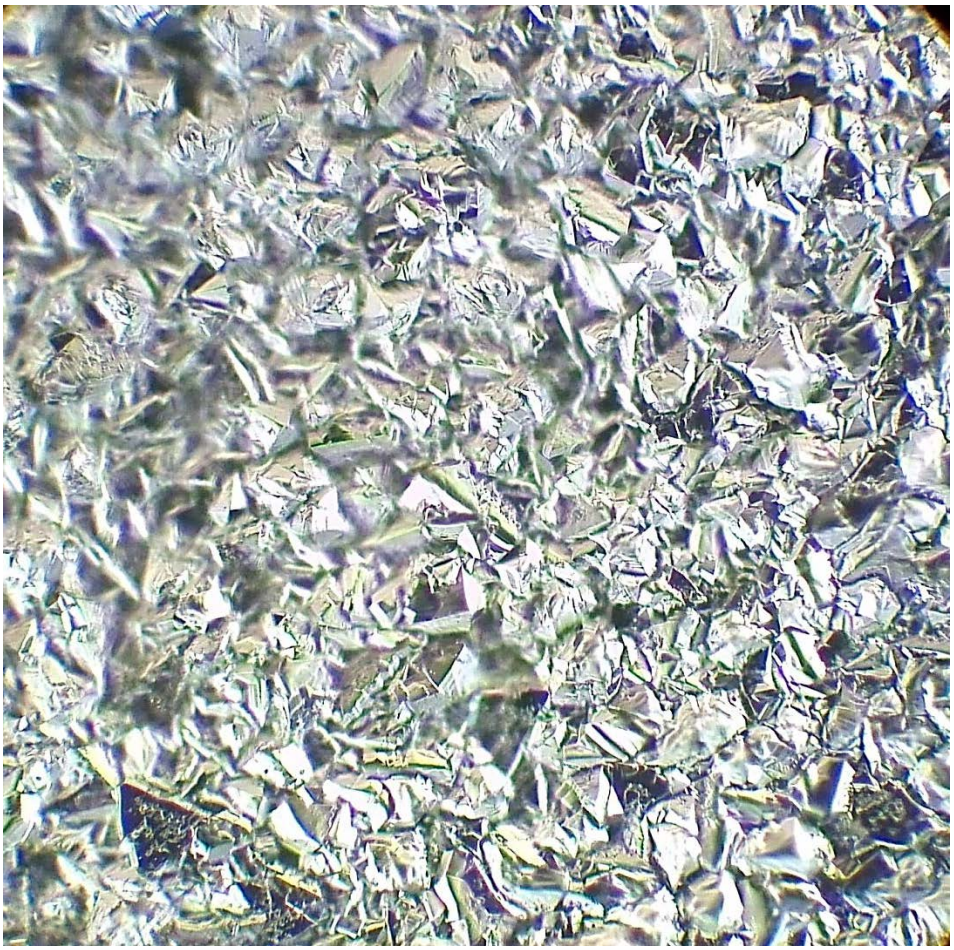

Figure 65: Run 64 optical microscope image of the image in figure 64. Magnification is 400x.

Like run 55, the growth stared at the tungsten ring/substrate interface and proceeded inward. Film closure occurred 4 days after startup. The dark spots on the substrate shown in figures 64 and 67 are graphite that was accumulating on the nozzle that fell onto the substrate.

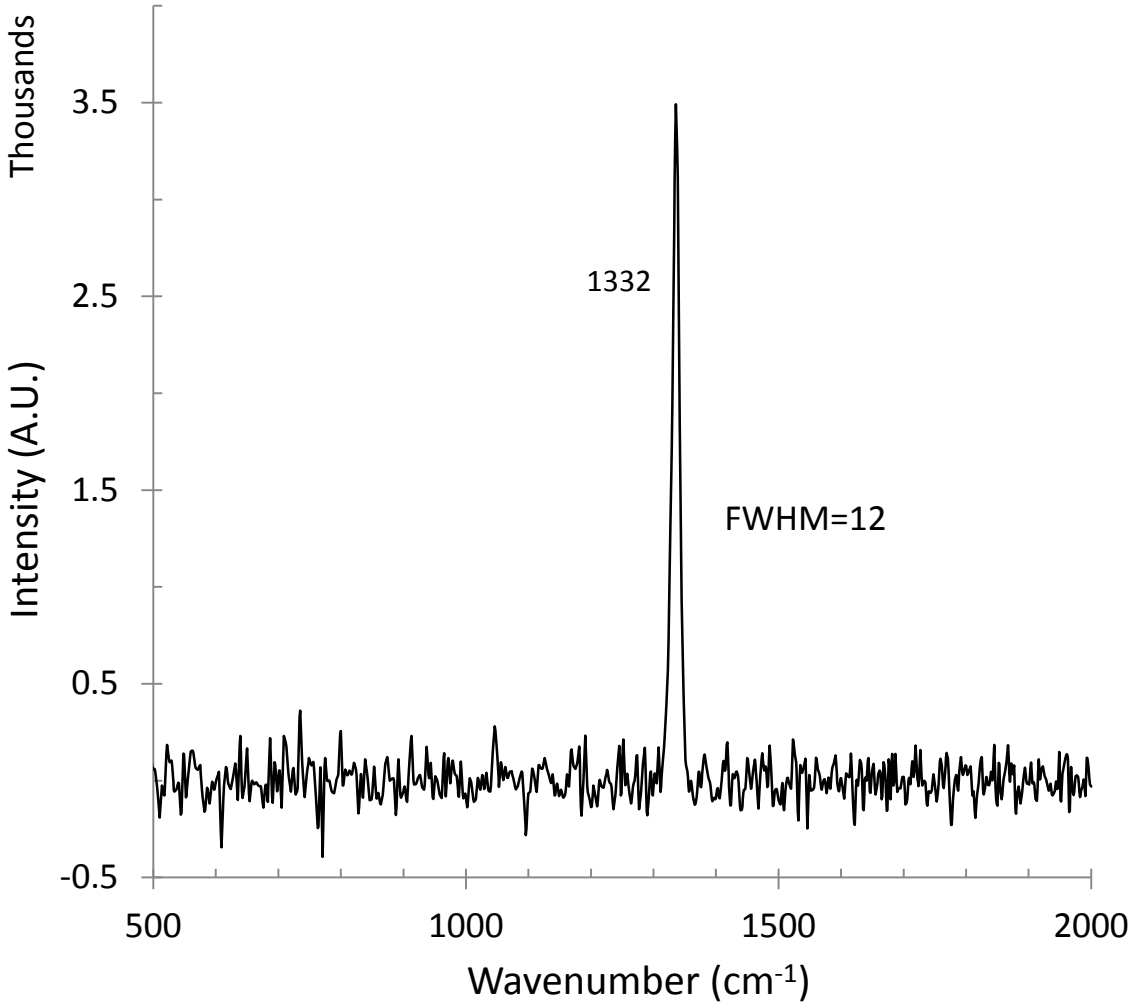


Figure 66: Raman spectrograph for run 64.

This occurred because the methane flow rate was set higher than previous runs to examine the impact on growth rate. From examining this fact and prior runs, the optimal methane flow rate was determined to be 2.70 SCCM.

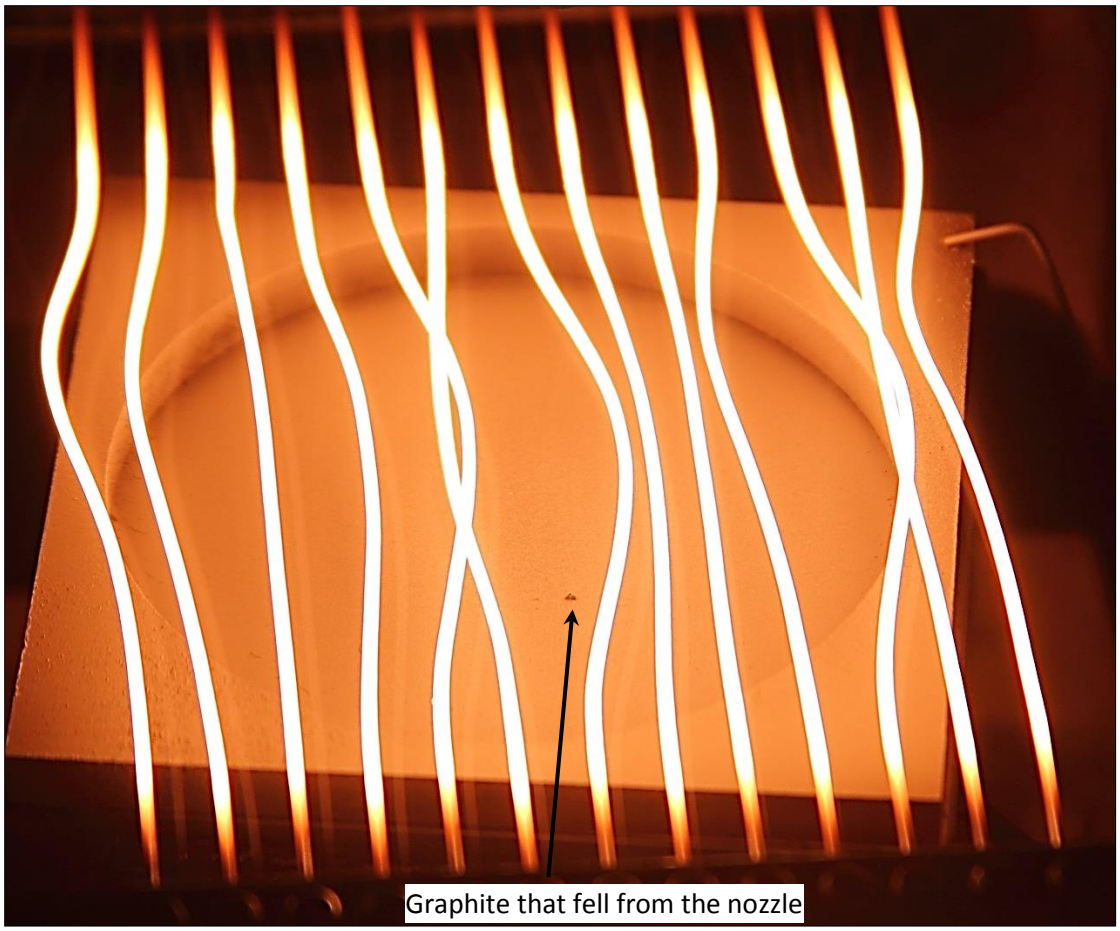

Figure 67: Run 64 growth surface during the experiment.

Reduced growing time and improper polishing of the platinum were responsible for the film not delaminating as in prior runs. It is clear that a well-polished surface is required for the delamination process during cooling. It is important to note that the 0-2 µm (statistical) diamond powder diameter used to initiate nucleation is too small a cross section to register on the DeltaNu Micro Raman. This is advantageous in that new growth on the Raman cannot be confused with the seed material which does not register.

In many of the 64 experiments, the hot filaments would bend in response to thermal stress and gravity. The tungsten wire seems almost semi-fluid and would sag during some experiments. Even heating of the substrate is critical for CVD growth experiments and it was determined by thermal imaging that the center of the substrate temperature is approximately the same as the temperature near the edge. The bending of the wires prompted a new question: does the movement of the wires from a parallel position to a curved position impact the temperature distribution across the substrate. FLIR thermal imaging was used again to answer this question.

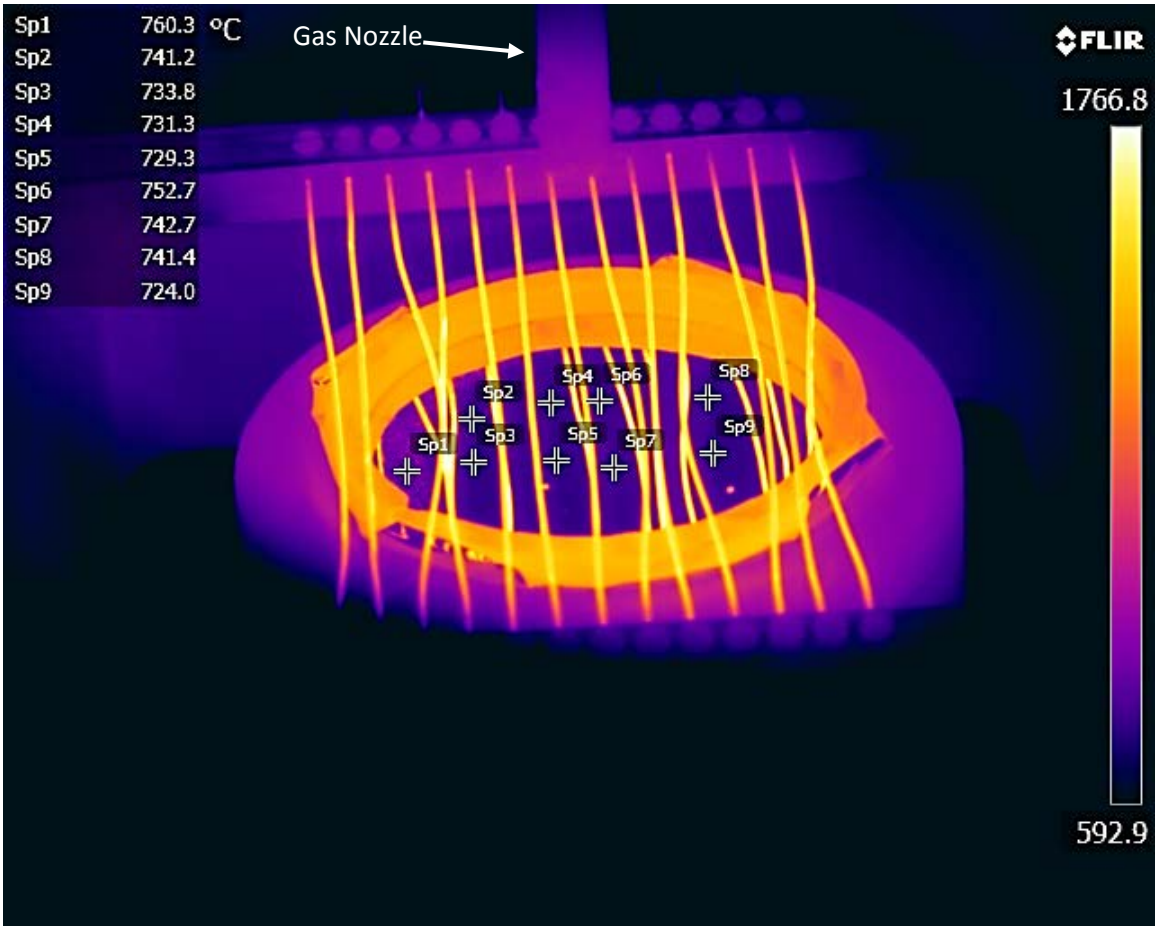


Figure 68: Thermal imaging study of diamond growth to study effect of wire bend on substrate temperature. Emissivity is set for the platinum substrate holder. Wire temperatures shown will therefore be inaccurate.

From figure 68, the average temperature was calculated at 739.6 +/ 11.5 C. The standard deviation of 11.5 C is higher than the 7.2 C recorded in a prior study. The reason for this difference is mostly due to the region designated as Sp1 on the image. The temperature in the region of Sp1 is on average 20 C warmer than the other regions. After the thermal image was taken, that section was examined and diamond growth was found in a higher concentration than on the rest of the substrate. Diamond has a much higher heat capacity and thermal conductivity than platinum and is one reason for this hot spot. In addition, the emissivity of diamond is nearly zero (very reflective) which will interfere with the calculated temperature. The calculated temperature based on Wien's displacement law (as stated in the product literature) requires accurate knowledge of the emissivity of the target. This hot spot was not expected in this region since this is an area where filaments have separated. Removing this region from the calculation yields an average temperature of 737.1 +/- 9.1 C. The standard deviation is within 2 C of the prior study where the wires were parallel. Bending of the wires does not significantly impact the substrate temperature.

A summary of all 64 runs is shown in table 3. In all but 11 experiments, some growth was recorded. The most notable results are experiments 54 and 55 which yielded large-area single-crystal diamond growth.

Table 3: Results of runs 1-64

| Gas flow rate $O_2/CH_4/H_2$ (SCCM) | Run | Substrate holder | Filament temp (Celsius) | Pressure (Torr) | Run Time (Hours) | Results | Bias (volt) | Gas to filament (mm) | Filament to substrate (mm) |
|---|---|---|---|---|---|---|---|---|---|
| 1/2/100 | 1 | Cu 1mm | 2000 | 5 | 2.5 | Nucleated Diamond (ND) | N | 2 | 2.4 |
| 1/2/100 | 2 | Cu 1mm | 2000 | 5 | 2.5 | ND | 65 | 3.5 | 2.5 |
| 1/2/100 | 3 | Cu block | 2000 | 5 | 1.5 | no results | 65 | 2 | 4 |
| 1/2/100 | 4 | Cu 1mm | 2000 | 5 | 1.3 | ND | 60 | 2.5 | 2 |
| 1/2/100 | 4a | Cu 1mm | 2100 | 6 | 3.5 | diamond film (DF) | 65 | 10 | 10 |
| 1/2/100 | 5a | Cu 1mm | 2050 | 6 | 8 | no results | 90 | 3 | 3 |
| 2/4/200 | 5b | Cu 1mm | 2050 | 10 | 3 | Polycrystalline (PCD) | N | 8.9 | 8.9 |
| 2/4/200 | 5c/6 | SS/Cu | 1750 | 10 | 69 | Large area diamond film (LADF) | 100 | 4 init, 0 | 6 |
| 2/4/200 | 7 | SS/Cu | 1830 | 11 | 288 | diamond on SS | 200 | 4 | 5 |
| 1/4/100 | 8 | SS/Cu | 1700 | 10.5 | 72 | no results | N | 5 | 5 |
| 2/4/200 | 9 | SS 1 mm | 1725 | 10.5 | 68 | no results | N | 5 | 5 |
| 2/4/200 | 10 | SS 1 mm | 1725 | 10.5 | 72 | DF | N | 3 | 5 |
| 2/4/200 | 11 | SS 1 mm | 1750 | 11 | 72 | DF | N | 2 | 4.5 |
| 2/4/200 | 12 | SS 1 mm | 1725 | 10 | 72 | Diamond like film | N | 2 | 5 |
| 1/4/200 | 13 | SS/Cu | 1725 | 10 | 68 | Diamond like film | N | 3 | 3 |
| 2/4/200 | 14 | SS/Cu | 1725 | 10 | 70 | ND | N | T | 4 |
| 2/4/200 | 15 | SS/Cu | 1725 | 10.5 | 70 | PCD | N | 1 | 4 |

Table 3: Results of runs 1-64

| Gas flow rate $O_2/CH_4/H_2$ (SCCM) | Run | Substrate holder | Filament temp (Celsius) | Pressure (Torr) | Run Time (Hours) | Results | Bias (volt) | Gas to filament (mm) | Filament to substrate (mm) |
|---|---|---|---|---|---|---|---|---|---|
| 2/4/200 | 16 | SS 1 mm | 1700 | 10.5 | 70 | DF | 100 | T | 4 |
| 4/8/400 | 17 | SS 1 mm | 1725 | 15 | 71 | graphite | 100 | T | 4 |
| 2/4/200 | 18 | Si | 1750 | 10.5 | 69 | SiO2/diamond poly | N | T | 4 |
| 1/4/200 | 19 | SS 1 mm | 1715 | 6.4 | 70.5 | Non-diamond | N | T | 4 |
| 0/4/200 | 20 | Cu only | 1800 | 6.3 | 71 | Diamond fibers | 100 | T | 4 |
| 0.5/2/200 | 21 | Si 0.6 mm | 1725 | 5.5 | 75 | DF | 100 | T | 4 |
| 0.5/2/200 | 22 | Cu only | 1750 | 5 | 27 | graphite | N | T | 4 |
| 0.5/1/200 | 23 | Si 0.6 mm | 1775 | 7.4 | 72 | PCD | 100 | 2 | 4 |
| 0.5/1/200 | 24 | Si 0.6 mm | 1725 | 5.5 | 74 | DF | 100 | 2 | 4 |
| 0.5/1/200 | 25 | Si 0.6 mm | 1750 | 6 | 43.5 | no results | 100 | 2 | 4 |
| 0.5/1/200 | 26 | Si 0.6 mm | 1730 | 5.4 | 70 | ND | 100 | 2 | 4 |
| 0.5/1/200 | 27 | Cu only | 2050 | 20 | 3 | cobalt doped | N | 2 | 4 |
| 0.5/1/200 | 28 | Cu only | 2050 | 22 | 3 | no results | N | 2 | 4 |
| 0/0/200 | 29 | Cu only | 2050 | 24 | 3 | cobalt doped | N | 2 | 4 |
| 0/0/200 | 30 | Cu only | 2050 | 22 | 3 | no results | N | 2 | 4 |
| 0.5/1/200 | 31 | Cu only | 2050 | 21 | 47 | DF | Y | 2 | 4 |
| 0.5/1/200 | 32 | Cu only | 2030 | 20 | 72 | no results | Y | 2 | 4 |
| 0.5/1/200 | 33 | BN | 2050 | 20 | 48 | D-band graphite | N | 2 | 5.5 |

Table 3: Results of runs 1-64

| Gas flow rate $O_2/CH_4/H_2$ (SCCM) | Run | Substrate holder | Filament temp (Celsius) | Pressure (Torr) | Run Time (Hours) | Results | Bias (volt) | Gas to filament (mm) | Filament to substrate (mm) |
|---|---|---|---|---|---|---|---|---|---|
| 0.5/1/200 | 34 | Cu only | 1920 | 25 | 3 | no results | 100 | 2 | 5 |
| 0.5/1/200 | 35 | Cu only | 1920 | 20 | 3 | no results | 100 | 2 | 5 |
| 0.25/1/200 | 36 | Cu only | 2000 | 21 | 3 | D-band graphite | N | 2 | 5 |
| .5/4/400 | 37 | Cu only | 1800 | 13 | 3 | ND | N | 2 | 4 |
| 0.25/4/400 | 38 | Ti | 1800 | 17.5 | 3 | DF | 100 | 2 | 4 |
| 0.25/4/400 | 39 | Cu only | 1925 | 21 | 3 | PCD | 80 | 2 | 4 |
| 0.25/4/400 | 40 | Cu only | 1900 | 20 | 4 | PCD | 65 | 3 | 4.5 |
| 0.25/4/400 | 41 |  | 2000 | 21 | 4 | PCD | 100 | 3 | 5 |
| 0.25/4/400 | 42 | Cu only | 2050 | 21 | 8 | DF | 200 | 3.5 | 5.5 |
| 0.25/4/400 | 43 | Cu only | 1950 | 20 | 6 | DF | 200 | 2.5 | 6 |
| 0.25/4/400 | 44 | Cu only | 1950 | 50 | 7 | DF | 250 | 6.7 | 23.03 |
| 0.25/3.5/400 | 45 | Cu only | 1850 | 20 | 5.5 | DF | 100 | 4.8 | 23.03 |
| 0.25/3.5/400 | 46 | Cu only .25 mm | 1800 | 23 | 70.5 | DF | 100 | 4.8 | 23.03 |
| 0.2/2/200 | 47 | Cu only | 1900 | 20 | 168 | DLC | 100 | 4.8 | 23.03 |
| 0.2/2/200 | 48 | Cu only | 2200 | 20 | 24 | no results | 100 | 4.8 | 23.03 |
| 0.2/2/200 | 49 | Pt/Ir | 2000 | 20 | 178 | LADF, DLC | 100 | 4.8 | 23.03 |
| 0.2/2/200 | 50 | Pt/Ir | 2000 | 20 | 168 | PCD | 100 | 4.8 | 23.03 |

Table 3: Results of runs 1-64

| Gas flow rate $O_2/CH_4/H_2$ (SCCM) | Run | Substrate holder | Filament temp (Celsius) | Pressure (Torr) | Run Time (Hours) | Results | Bias (volt) | Gas to filament (mm) | Filament to substrate (mm) |
|---|---|---|---|---|---|---|---|---|---|
| 0.2/2/200 | 51 | Pt/Ir | 2050 | 20 | 250 | PCD | 100 | 4.8 | 23.03 |
| 0.2/2/200 | 52 | Pt/Ir | 2000 | 20 | 193 | PCD | 100 | 4.8 | 23.03 |
| 0.2/2/200 | 53 | Pt/Ir | 2000 | 22 | 216 | PCD | 100 | 4.8 | 23.03 |
| 0.2/2/200 | 54 | Pt/Ir | 2000 | 20 | 121 | LA single crystal | 100 | 4.8 | 23.03 |
| 0.2/2/200 | 55 | Pt/Ir | 2000 | 18 | 411 | LA single crystal | 100 | 4.8 | 23.03 |
| 0.2/2/200 | 56 | Pt/Ir | 2000 | 19 | 243 | LADF, DLC | 100 | 8.0 | 23.03 |
| 0.2/2/200 | 57 | Pt/Ir | 2000 | 10 | 1 | Equipment Error | 100 | 8.0 | 23.03 |
| 0.2/2/200 | 58 | Pt/Ir | 2000 | 20 | 151.5 | DF | 100 | 8.0 | 23.03 |
| 0.2/2/200 | 59 | Pt/Ir | 2000 | 20 | 576 | h-BN recrystallize | 100 | 7.0 | 25.0 |
| 0.2/2/200 | 60 | Pt/Ir | 2000 | 20 | 200 | h-BN recrystallize | --- | 7.0 | 35.6 |
| 0.2/2/200 | 61 | Mo | 1995 | 20 | 341 | h-BN recrystallize | 100 | 6.0 | 25.4 |
| 0.2/2/200 | 62 | Pd | 2000 | 20 | 362.5 | Diamond fibers | 100 | 7.0 | 25.4 |
| 1.0/2/200 | 63 | Pd | 2000 | 20 | 338.5 | PCD | 100 | 7.0 | 25.4 |
| 0.5/3.3/200 | 64 | Pt/Ir | 2000 | 20 | 169 | LADF | 100 | 7.0 | 25.4 |

# 9. CONCLUSION

The Raman spectrograph of a diamond film produced using the HFCVD equipment described in this work is consistent with a single crystal film with a FWHM within one $cm^{-1}$ of electronic grade single crystal diamond. Optical microscope images reveal a glassy surface consistent with single crystal diamond films. However, scattering of light by the contaminated layer limits the quality of the image that can be captured digitally. FESEM and SEM analysis confirm the lack of texturing and provide evidence of layering of the sample. Careful analysis of the XRD spectrograph also indicates layering of the sample and furthers the evidence of a single-crystal portion of the film.

The challenges in obtaining a representative XRD plot associated with the layering of the sample can be overcome by polishing, annealing, ablating, or etching the top layer containing the platinum contamination. Approximately 10-50 μm deep and an area of at least one-half centimeter would need to be removed from the sample to improve optical and XRD qualities of the film. Polishing is risky because the sample is curved and does possess at least one mechanical partial fracture. In addition, polishing was attempted on a film of similar quality on a prior run without success. The natural diamond polishing powder was unable to scratch the surface. Annealing may be accomplished in the HFCVD chamber where the bottom surface is exposed to 500-600 C temperatures for 1-2 hours. Incorrect annealing may lead to graphitization and further contamination of the sample. Ablating through Focused Ion Beam (FIB) is time

consuming as the beam only penetrates at a maximum of 100 nm at a length of 1 µm. A raster pattern based on the curvature of the sample would need to be developed. FIB is typically utilized for small samples where a thin layer of material, typically 5-20 nm needs to be removed. Therefore, FIB is not the ideal solution. Etching can be performed in the HFCVD reactor in this work at 2200 C for 12-24 hours using a hydrogen stream. Hydrogen ions will etch the surface at approximately 1 µm per hour. Based on the initial estimates of the top layer, this would require approximately one or two days. Incorrect etchant parameters will lead to graphitization and possibly fracture of the sample. Because all of the techniques described above are destructive with little chance of success, microanalysis of the intact sample was used to obtain the conclusions. By observing the differences (stronger (111) and weaker (220) peak in the Gonio scan) and similarities (lacking peak broadening) between the Gonio scan and the thin film scan, the conclusion that the XRD pattern is for two layers in the sample is reasonable. Moreover, it is concluded that the bulk of the sample is single crystal and is in the (111) orientation.

Horizontal crystal growth was seen eighteen times on four different substrates. The lack of diamond seed directly below the horizontal growth suggests what is necessary for this type of growth to occur. First, properly oriented both mechanically and electrically during the run with the positive bias seed crystal is necessary to start the growth of new diamond. Secondly, a scratch free surface for the film to extend should be provided in the direction of growth. This may require some sub-µm polishing and

verification via optical microscope. Finally, the run should proceed long enough to allow the film to coalesce fully into a film at least 200 μm thick. If the film is too thin, it will crack during cooling and complicate analysis. From experience during the runs, this should take at least 8 days and preferably 14 days. The 5 cm substrate should be covered by diamond seed stock uniformly 1 cm to the outside. The inner circle should be kept clear of all material to allow the diamond to move horizontally across the surface free from obstruction. If diamond grows in the manner suggested, the entire portion of the inner surface should be covered in the film.

This reactor appears to allow diamond to grow horizontally faster than vertically, a phenomenon that has not been reported to date. The mechanism that allows this to happen is the nozzle/ring assembly. Gas exits the nozzle and is excited by the hot filaments, producing an ion stream accelerated by the positive bias toward the substrate. The gas strikes the substrate and is pushed radially outward by the incoming gas. This turbulence is compounded by a ring of boron nitride that is 3 mm deep that recesses the substrate. This configuration allows for the ion stream to make contact with the substrate longer than other reactor designs; effectively increasing the probability of interaction with the surface and suppressing the vertical growth rate. It is also possible that when the gas changes direction after striking the substrate, some of the ions re-approach the filaments and are redirected back to the substrate via pressure from radiative heating.

## Future Work

Since the nozzle is directly over the recessed substrate, the incoming gas perturbs the gas in the growth zone and reduces the overall filament temperature. Based on observations while running the reactor, the gas flow direction has been plotted and may look something like what is shown in figure 69.

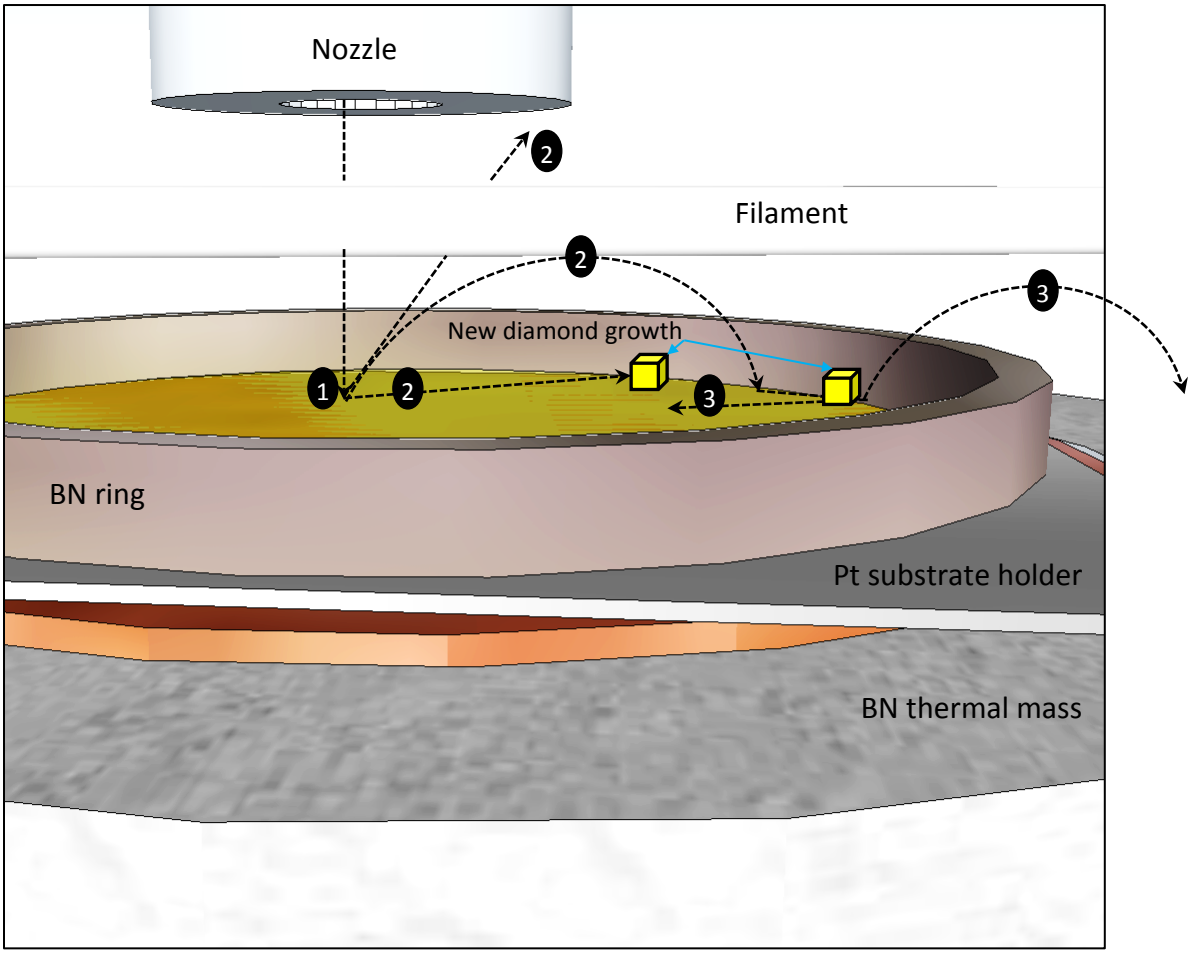


Figure 69: Suspected gas flow direction based on experimental observation.

First, the fully mixed hydrogen, methane, and oxygen are ejected from the nozzle at approximately 2 feet per second. Upon proximity to the filaments, thermal

cracking occurs and the molecules become ions. The positive bias from the filaments to the substrate accelerates the ions toward the substrate where they will either move along the surface of the substrate or rebound toward the filaments. The radiative convection will redirect some of the ions back toward the substrate where they will either strike the wall of the boron nitride ring and reverse direction or spill over the ring and leave the growth zone. As can be seen in figure 69, it is likely that when ions encounter a diamond molecule, it will be horizontally in at least two of the four possible impacts. Impacts (1) and (2) are vertical and impacts (2) and (3) are horizontal. Of course, this is just one flow stream and the flow pattern is a solid cone which will further complicate the flow beyond what is shown here. What is known for certain is that some of the gas makes a second pass on the filaments and that diamond grows faster horizontally than vertically on the substrate.

A more complete conclusion may be provided experimentally by varying the operational parameters that directly relate to gas flow. However, based on the 14 parameters required for diamond growth, the number of experimental permutations is prohibitive. Therefore, it is reasonable to presume the answer may lie in modeling the current system to gain insight into how the flow mechanics affects the growth mechanics. This should be an iterative process where the model is matched to the current design parameters and then the model parameters altered to simulate new experimental conditions. Favorable conditions for diamond growth will be those that allow large contact time between the ions and substrate surface. Based on the recent

success with growth in the horizontal plane, there likely exists an optimal depth or design configuration for the substrate holder. Simulation may also provide additional insight not currently being considered. The simulation should also be used to revisit run 55 which yielded the 4.4 cm diameter single crystal.

Another important question is why, during runs where the bias was reversed from positive to negative; the bias interacted with the thermocouple in the center of the boron nitride substrate holder. There is a 1 mm layer of sub-µm natural diamond powder between the negative bias and thermocouple which was placed there to prevent the thermocouple from shorting out the bias. The negative bias was started one hour into the run at 260 volts. The thermocouple reading slowly decreased without a decrease in actual temperature, gradually increasing the DC current until the bias shorted out at approximately 25 mA DC. The DC power supply was reset and reapplied at a lower DC value until, after one hour; the bias could only be set to 20 volts and still produced a 25 mA DC current. Diamond is non-conductive so this result, which has been reproduced four times, is not easy to explain. One possible explanation is that diamond was becoming doped with copper making the powder conductive. This speculation has been partially confirmed through Micro Raman analysis where the diamond powder was shifted from 1332 to 1316, 1320, and 1324 $cm^{-1}$ in three regions of the sample. Although less likely, it is possible that the interference observed in the thermocouple is a complex, non-steady state galvanic interaction which has been reported in thermocouples of this type. This interaction can occur with the dyes used in

the insulation of the thermocouple wires but have only been reported in the presence of water.[68] Visible and ultraviolet spectroscopy of the diamond powder before and after the run should indicate whether the diamond has been doped.

Recent success in forming large area single crystal diamond has led to the question of why diamond forms in this reactor as a single crystal through self-alignment. Investigation of the film will yield how the film was created but the "why" may not be answerable without some assistance from simulation. To perform a simulation of the system of this magnitude requires a 3-D model of the system and a program that can account for flow mechanics, transport, and ion exchange and deposition. The program Fluent by Ansys®, Inc. may be the solution. Moreover, the mass, momentum, and energy balances must be at least understood and possibly solved by using a finite method to verify the simulation has been configured correctly. For this configuration, the mass balance is simply

$$\frac{\partial \rho}{\partial t} = -\nabla \cdot (\rho \vec{v}) \quad (1)$$

And the momentum balance is

$$\frac{\partial (\rho \vec{v})}{\partial t} = \nabla \cdot \vec{T} + \rho g - \nabla \cdot (\rho \vec{v} \vec{v}) \quad (2)$$

where $\vec{T}$ is the viscous stress tensor and is given by

$$\vec{T} = -\left\{\left[P + \frac{2}{3}\mu(\nabla \cdot \vec{v})\right]\delta_{ij} + 2\mu(\nabla \vec{v} + \nabla \vec{v}^{T}\right\} \quad (3)$$

$\delta_{ij}$ is Kronecker's delta. For the derivation of these balances, it was necessary to make certain assumptions: 1. The gas flow is monoatomic, laminar, continuous, ideal, and

Newtonian. 2. The viscous mixing of the fluid does not alter the temperature of the gas (the viscous loss is reversible). The energy balance is given by

$$c_p \frac{\partial}{\partial t}(\rho T) = -\sum_{i=1}^{R}\sum_{g=1}^{G} H_g v_{ig}\left(r_{g,f}^{g} - r_{g,r}^{g}\right) - c_p \nabla \cdot (\rho \vec{v} T) + \sum_{i=1}^{R} \frac{H_i}{m_i} \nabla \cdot \vec{J}_i + \nabla \cdot (k \nabla T) + \nabla \cdot \left[RT \sum_{i=1}^{R} \frac{D_i^T}{m_i} \nabla (ln f_i)\right] \quad \text{.....(4)}$$

The terms on the right hand side are chemical reaction, convection, inter diffusion, thermal conductivity, and the Dufour effect respectively.[69] The Dufour effect as shown in the last term for equilibrium systems is quite small and can usually be neglected.[70] However, in this situation where ions can exhibit large chemical potential gradients, the thermal conductivity of the gas can be greatly influenced and therefore, cannot be neglected.[71] Perhaps a more common way to state the Dufour effect is the change in the enthalpy of activation for a gas phase reaction during diffusion. Under equilibrium conditions, the gases are fully mixed and therefore this term is often neglected. The CVD reactor is not an equilibrium system. It is uncertain whether this relation can be used in this system because diffusion relations do not generally model low pressure systems well.

# 10. SUMMARY

Large-area diamond crystal films were created through coalescing nucleation sites in this HFCVD reactor chamber. Careful pre-treatment of the substrate and growth zone was necessary for organized, oriented growth. Noble metals such as platinum provided an adequate support for the diamond growth but lift off creates challenges as well as the presence of piping in the final film. The gas inlet flow mechanics need to be fully characterized.

For this film to be utilized as a substrate in MPACVD growth, the growth face must be single crystal with low defects. Additional work is needed to improve crystal quality and elimination of lift off site defects, but results of this work clearly indicate a viable method for producing large area single-crystal diamond.

# APPENDIX A

## Carburization Procedure

*Underlined items are critical safety and operational steps and should not be skipped under normal circumstances*

**Pre-startup checklist:** This checklist is to be performed only after the filament loading procedure has been conducted. This involves distributing the filaments across the threads and verifying tension on the springs.

1. Open pressure chamber and verify that all relevant internal surfaces are free of visible contamination
2. If apparatus surfaces are not clean of debris, use a particulate-free wipe (such as Kimwipe) with acetone to wipe down surface. Be sure to wear the appropriate PPE for handling of chemicals.
3. Verify pressure vessel dome gasket is in place
4. If buildup is visible around the gasket, remove gasket, wipe down as in step 2, replace gasket and apply Apezion high temperature grease to dome gasket.
5. Verify sufficient pressure in the helium/nitrogen and methane tanks (>500 psi)
6. Verify vacuum pump operation by reducing the pressure to 1 torr, isolating the system using the isolating valve, and waiting 10 minutes to see if the pressure holds at 1 torr.
7. Verify vacuum pump ventilation is correctly connected.

8. Start optical pyrometer and move it into position over the view port. Aim the FOV at one of the filaments.
9. Verify all power leads are securely connected and free of burn or fray marks
10. Protect/cover high voltage leads going into the vessel
11. Verify oil level in vacuum pump

**Carburization Procedure:**

1. Turn on pressure controller. This type of pressure transducer is heated and should be operational several hours prior to startup.
2. Close pressure control valve fully.
3. Turn on vacuum pump
4. Slowly open the pressure control valve.
5. Estimate time to reach 10 torr. Time to reach this from atmospheric is less than 5 minutes. This is accomplished to verify pump performance to anticipate pump problems.
6. Reduce pressure to approximately 1 Torr.
7. Close pressure control valve.
8. Open methane valve slowly (purging operation)
9. Allow pressure to reach 100 Torr.
10. Close methane valve slowly.
11. Open pump isolation valve
12. Reduce pressure to approximately 1 Torr.

13. Repeat steps 5-10 two more times.
14. Turn on HP 6682A power supply. Set voltage to 0.06 Volts and current to 1 amp.
15. Depress the Output on/off button to turn on the power.
16. If power supply has an arrow by cc, rotate the current knob clockwise. If the arrow is by the cv, then rotate the voltage knob clockwise. The power supply will "rock" back and forth up the power curve. Keep turning up the voltage and current until the pyrometer reads the right value.
17. Monitor pyrometer for temperature readings. Minimum pyrometer reading is 900 C.
18. Repeat step 14 until pyrometer reads 1800 C. Based on temperature ramp-up, this should take just under 10 minutes.
19. Open methane valve slowly. Stabilize the pressure in the vessel at 20-30 Torr. It may be necessary to increase the power setting due to convective cooling of the gas flow (even though the flow of gas is laminar). Steps 18 and 19 can be reversed (experimenter preference). *Do not overflow the gas!!!* Very little flow is required to provide fresh methane to carburize. It just takes a trickle of gas (<500 sccm). Overflowing the gas will result in graphite formation on the wires which will be visible once carburization is complete. If graphite forms on the surface, remove the wires and start over. Hydrogen bond thermal cracking will not occur if the tungsten surface is graphitized.

20. Upon reaching the desired pressure, record the time and hold these conditions for 20-40 minutes.

21. Slowly reduce the power to the power supply by turning the cc or cv knob counterclockwise.

22. Fully open the pressure control valve.

23. Terminate gas flow.

Allow 1 hour for system to return to ambient conditions before starting crystal growth experiment.

# APPENDIX B

CVD Reactor Operating Instructions

Example Operating Conditions Are For Diamond Growth

Startup and Operating Procedure

1. Carburization procedure must be complete prior to operating the reactor.

   Follow carburization procedure prior to operation

2. Turn on MKS type 247D readout

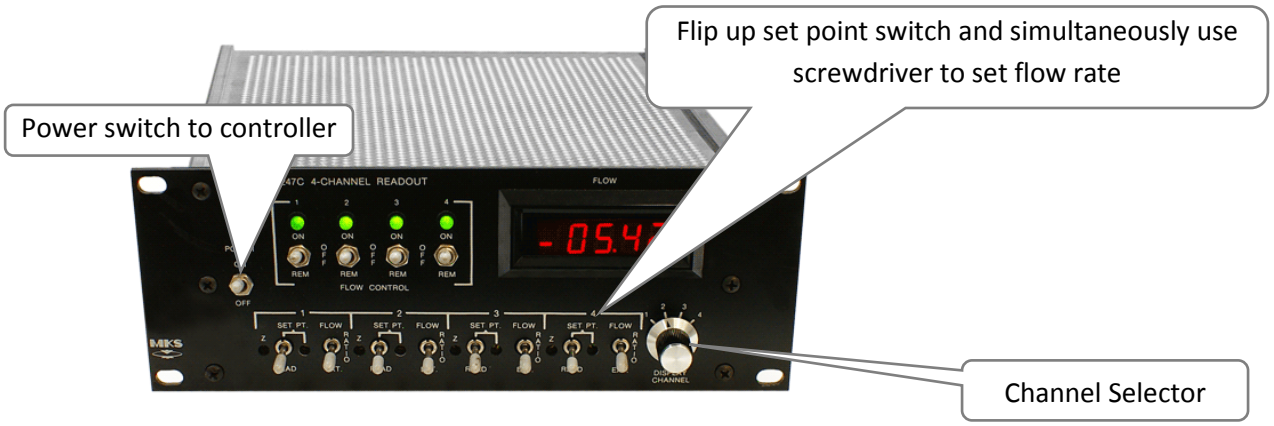


3. Set flow rate to zero on all three flow rates
4. Channel 3 is currently connected to UHP Hydrogen, channel 2 is UHP methane, and channel 1 is UHP oxygen. After zero set, turn on feed to $H_2$ and rotate the valve open on top of the tank. Applied pressure should be 50 psi. Note the tank pressure in the tank.
5. Turn the selector on the MSK readout to 2 and follow step above. Do the same for 1. It takes 30 minutes for the controllers to warm up after they are turned on.

6. You can determine the volume left in the tanks using this simple formula:

   **$cm^3$ left at atmospheric pressure = tank pressure * physical volume of tank**.

   Use DOT# on tank and the internet to get the volume of the tank. Example: If the US DOT spec is 2AA2400, the volume is 49,900 $cm^3$. If the pressure on the gauge is 1000 psi (68 atm), that is about 3.3 million cubic centimeters of gas. So if the flow rate is 100 sccm, you can run for about 23 days. You can use this link: http://en.wikipedia.org/wiki/Gas_cylinder

7. Place sample in the reactor. For diamond growth, the optimal distance from the gas distribution head to the filaments is 2 mm and the optimal distance from the filament to the substrate is less than 5 mm.

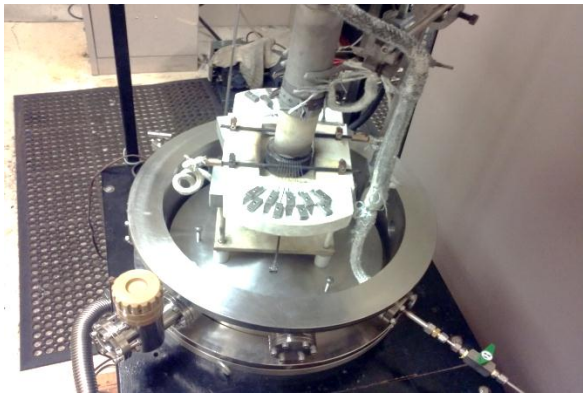

8. Verify the power poles connected to the filament assembly are connected.

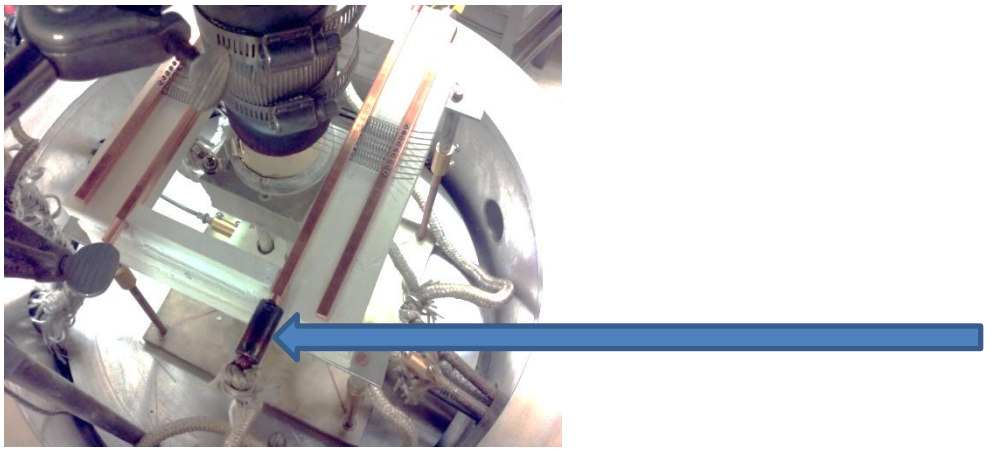

9. Verify thermocouples read room temperature (currently shown at 547 C, 136 C)


10. Close reactor vessel top

11. Verify that the pressure regulator valve is closed (currently shown in the closed position)

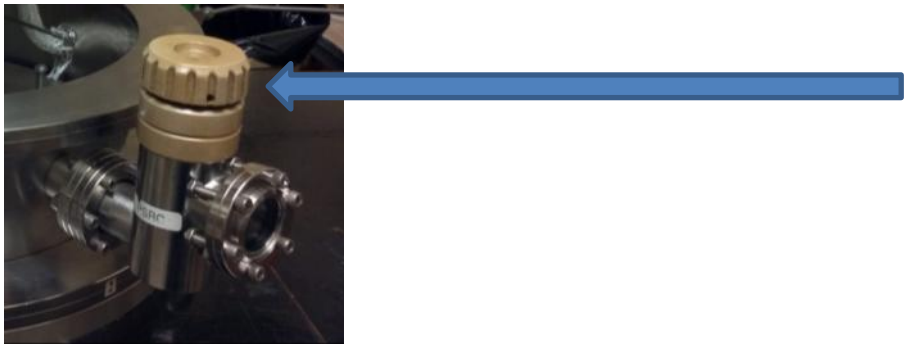

12. Turn on the pump

13. SLOWLY open the valve counterclockwise. Listen to the pump; it will begin to change pitch as you open the valve. Continue to open the valve slowly and wait for the pitch returns to its starting point.
14. Reduce the pressure in the vessel to below 1 Torr. The readout is in voltage. Mentally move the decimal two places to the right to read in Torr. Pressure shown is 6.7 Torr.


15. Close the pressure regulator valve
16. Open the helium valve. This is a purge operation intended to exchange the air with an inert gas
17. Bring the pressure to 100 Torr (1 volt)
18. Close the helium valve
19. Slowly open the pressure regulator valve to bring the pressure back down to below 1 Torr
20. Close the pressure regulator valve

21. The MKS type 247D readout should be warmed up by now. Set the flow rate of each gas to the proper flow rate
22. Allow the pressure to climb to 3 times the intended operating pressure
23. Open the pressure regulator valve slowly
24. Slowly open the pressure regulator valve to bring the pressure back down to below 1 Torr. This is a purge operation to replace the helium with the intended gas mixture. For better results, the charge and purge should be done 3 times.
25. Allow the pressure to climb to the intended operating pressure
26. Open the pressure regulator valve slowly. Open/close the value until the pressure is stable
27. Turn on the HP 6681A high amp power supply

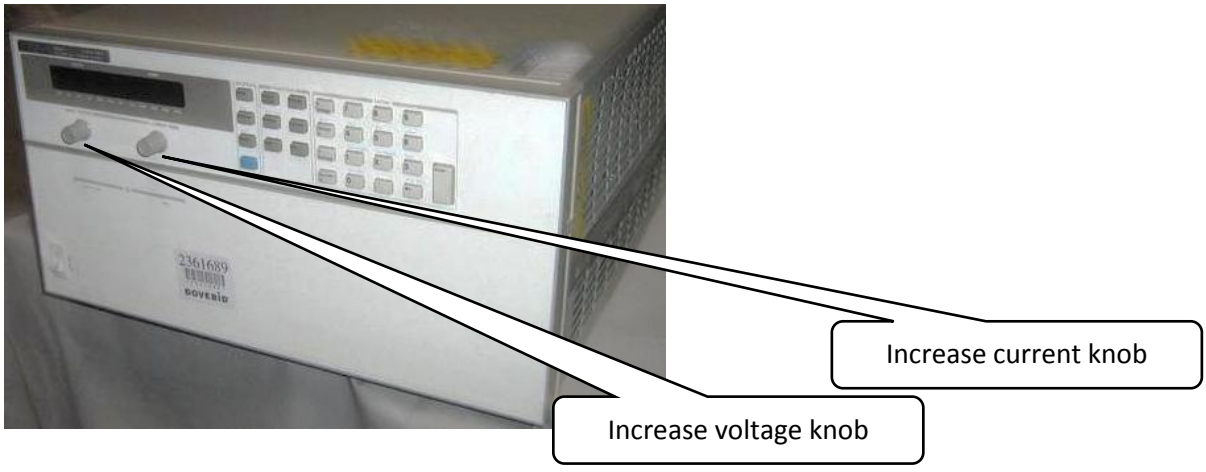

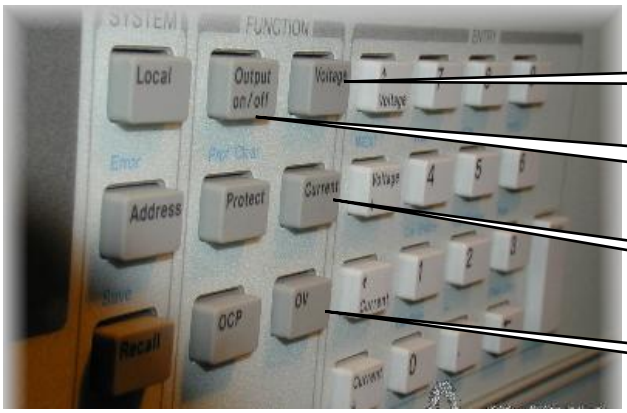


28. Set the voltage set point (for diamond CVD, recommended is .06 volts to start)

29. Set the amp set point (start with 1 amp)

30. Set the Over voltage to 8.5 volts

31. Press the Output on/off to turn on the power. CAUTION: **The filaments are now energized**


32. CV (constant voltage) OR CC (constant current) will be on (look for the arrow next to the CC or CV

33. If the display is on CC, turn the current knob clockwise to the desired current. The system will "walk" up the C/V curve. The system may go to constant voltage before you reach your target voltage. If this happens, turn clockwise the voltage knob to the desired voltage. If the system goes to

constant current, turn up the current knob. Continue until the desired power is reached.

34. If the system is on CV, turn the voltage knob clockwise and follow the procedure in the prior step
35. As the temperature of the system increases, the system pressure will increase. Adjust the pressure back down to the desired pressure. Some adjustment between pressure and power to the filaments may be necessary to stabilize temperature and pressure. Filament life is approx. 500-700 hours
36. Temperature/pressure steady state should be reached within 1-2 hours of startup.

***SHUTDOWN OPERATION***

1. Open pressure regulator valve fully
2. Reduce power to HP power supply to operating temperature. As the pressure drops, the temperature will climb. Be prepared to turn down the power. If it system is on CC, turn down the current. If the system is on CV, turn down the voltage.
3. Reduce power slowly (about 25 amps or 1 volt per minute)
4. Close pressure regulator valve fully. Turn off pump. Allow system to cool (use internal thermocouples to see that the highest temperature is less than

100 C) prior to venting the system. Cooling down is required to prevent filaments and other components from oxidizing.

5. Vent the system. The vent is connected to the helium tank (not shown). Disconnect the helium tank at the needle valve shown to bring air into the vessel.

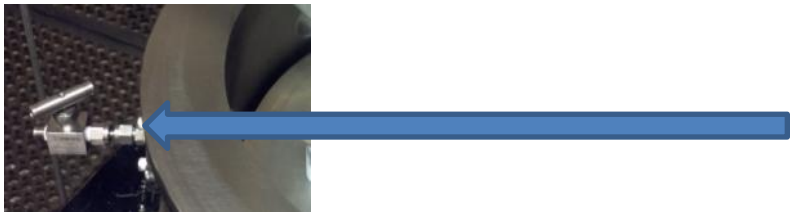

6. Open the vessel and remove the sample

# APPENDIX C

## Substrate preparation methods- homoepitaxial growth

1. Manual dry alignment, 50 µm
    a. Copper appears to be the only material suitable for adequate heat transfer away from the seed crystals to prevent evaporation. Distribute a sufficient quantity of seed crystals across the surface to create layer 5-10 crystals thick.
    b. Use a mechanical adaptation method such as mechanical vibration. The goal is to distribute sufficient crystals across the surface such that the surface of the copper is not visible.

Figure 70: Manual dry alignment of 50 µm diamond

2. Fluidized bed, 30-50 µm, canola oil

    a. Place sufficient amount of oil to barely cover the surface of the copper.

    b. Using a 50 µm sifter, place diamond seeds onto the surface of the liquid.

    c. Apply electrostatic field several inches above the surface of the liquid. Use 1000 volt potential with 4 mA current. The electrostatic field will cause to diamond seeds to connect.

    d. Remove the bulk of the oil with burette.

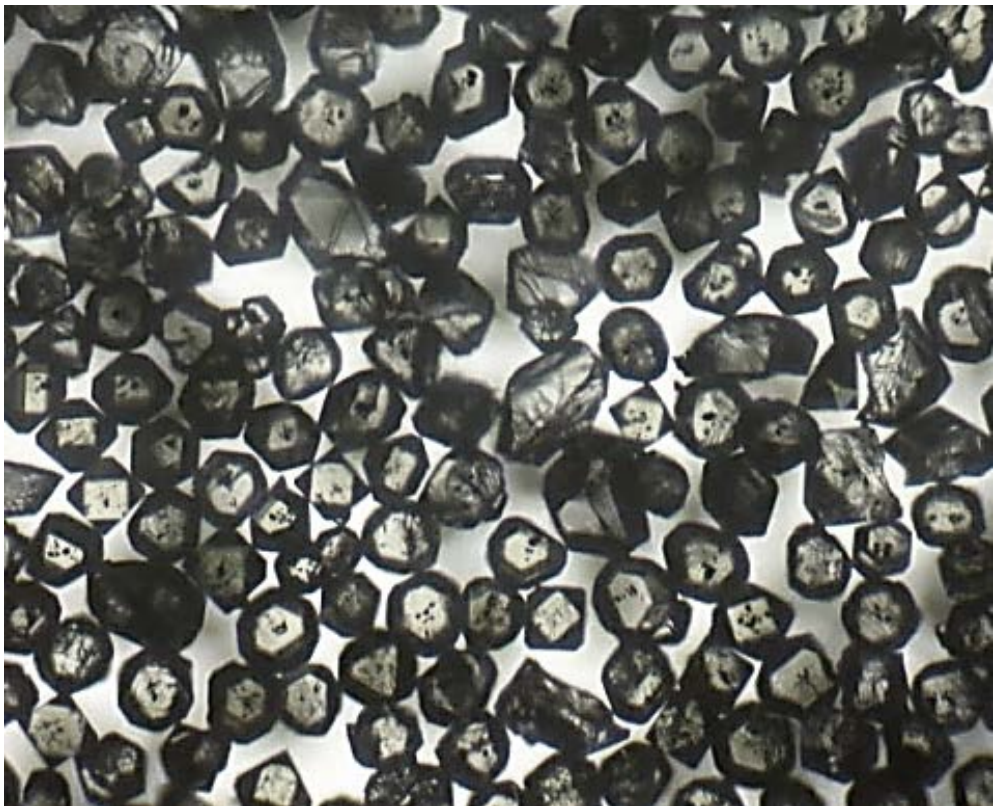

Figure 71: Canola oil fluidized bed technique

3. Fluidized bed, 30-50 µm, deionized water

    a. Brush on nano-diamond to lightly cover the surface.

b. Apply deionized water to the surface of the copper.

c. Using a 50 µm sifter, place diamond seeds onto the surface of the liquid.

d. Using a burette, remove the water from the copper. During the burette procedure, do not remove diamond from the surface.

e. Allow the remainder of the water to dry naturally by applying a vacuum with the reactor to dry the rest of the way.

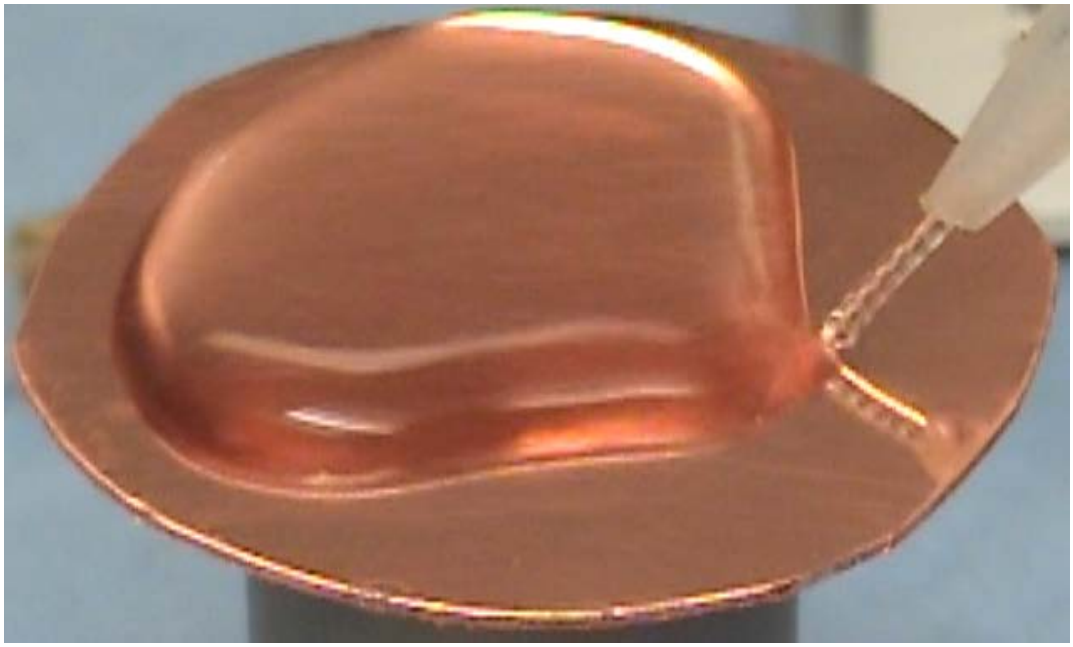

Figure 72: Without Nano-Diamond Pretreatment: Application of DI water on a copper surface. High surface tension and low adhesion creates a near 90 degree angle between the copper and water

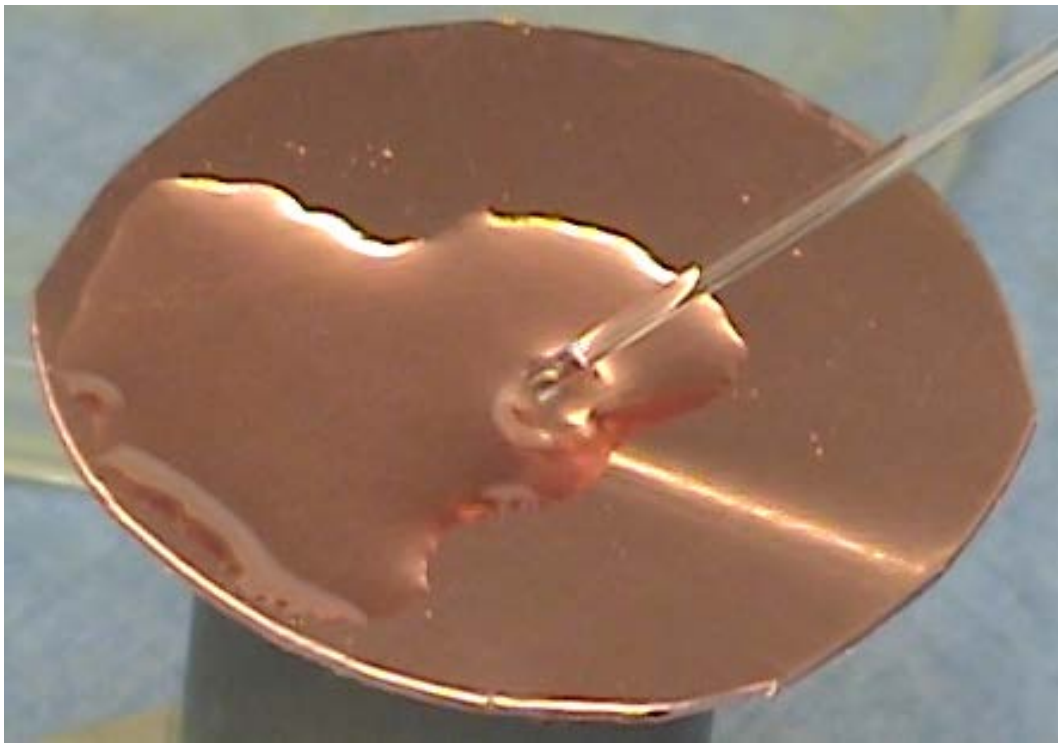

Figure 73: Without Nano-Diamond Pretreatment: As the water is removed, the water retracts due to poor adhesion with the copper surface.

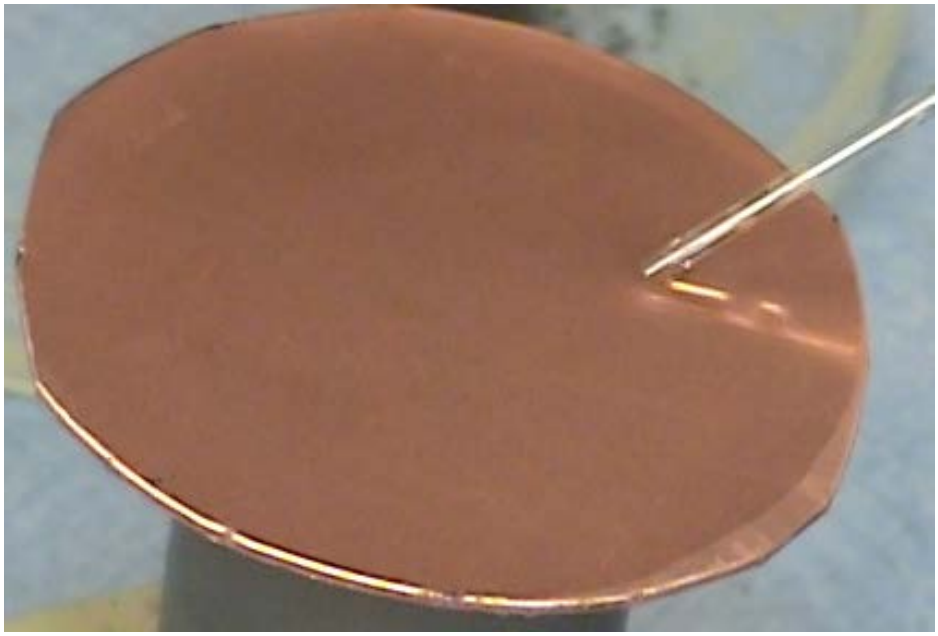

Figure 74: With Nano-Diamond Pretreatment: After pretreatment of the copper surface with nano-diamond, contact angle is nearly 0 degrees. This process is reversible by removing the coating with any organic solvent.

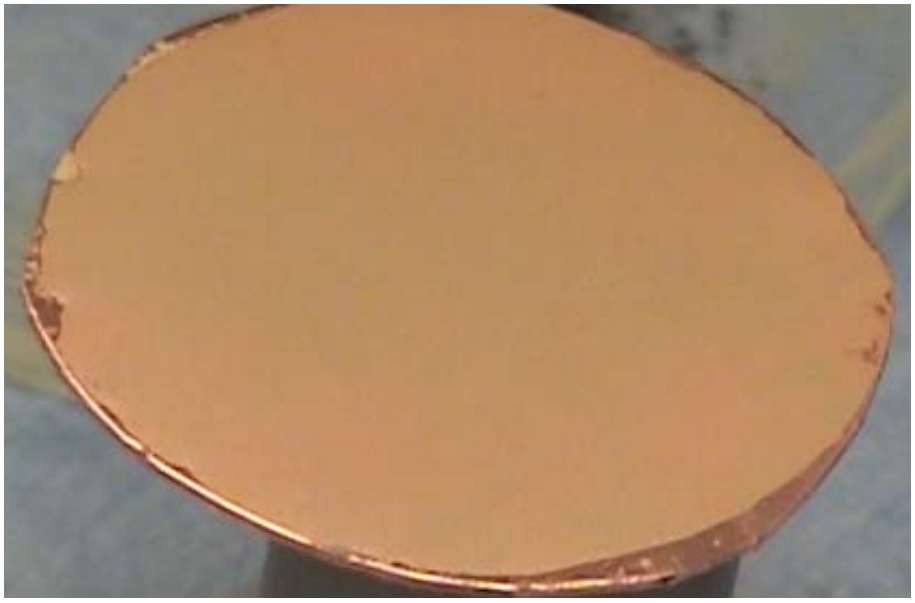

Figure 75: With Nano-Diamond Pretreatment: Diamond film applied to the DI water surface

Figure 76: alignment final result. A single layer of crystals deposited on top of a metal holder. Crystals shown are 50 µm +/- 10%

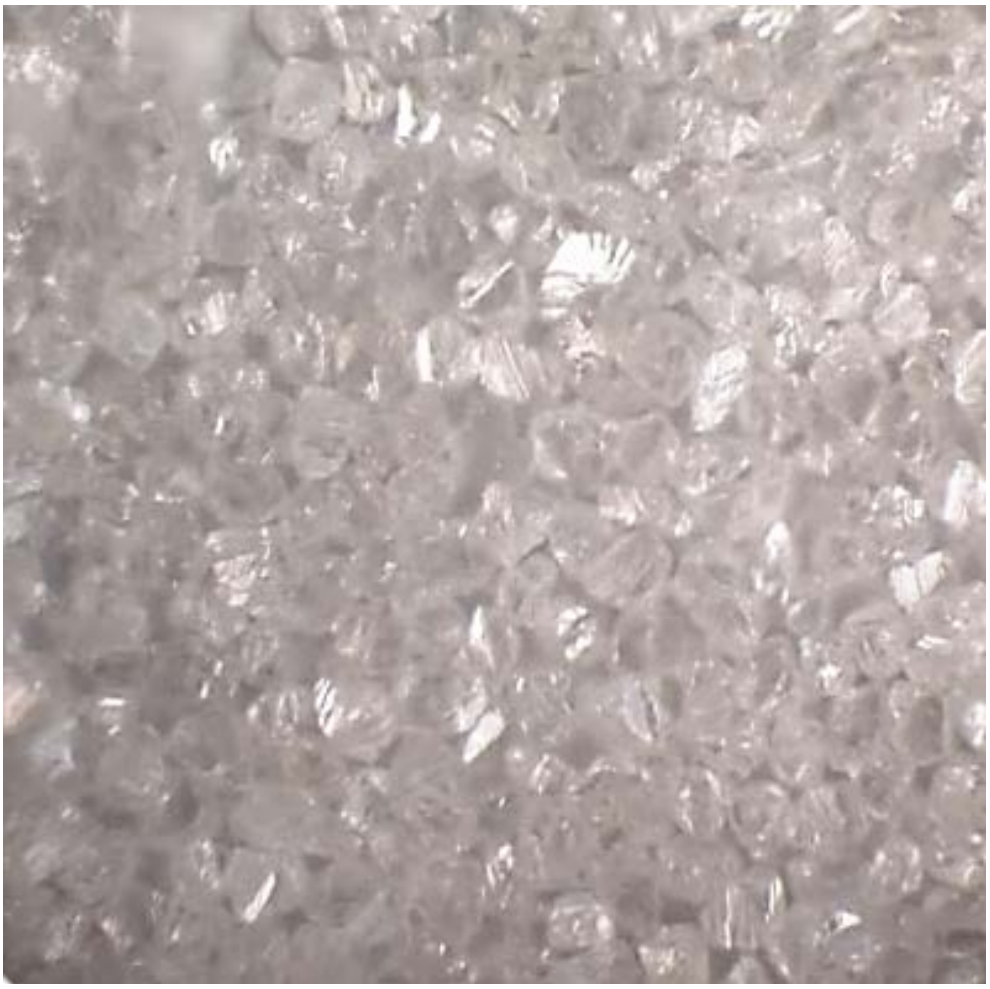

Figure 77: Increased magnification of alignment final result. A single layer of crystals deposited on top of a metal holder. Diamond crystals shown are 50 µm +/- 10%

4. Brush- on nano-diamond on copper
    a. Brush on nano-diamond.
    b. Apply n-hexane to the surface sufficient to wet the surface.
    c. Allow n-hexane to dry naturally

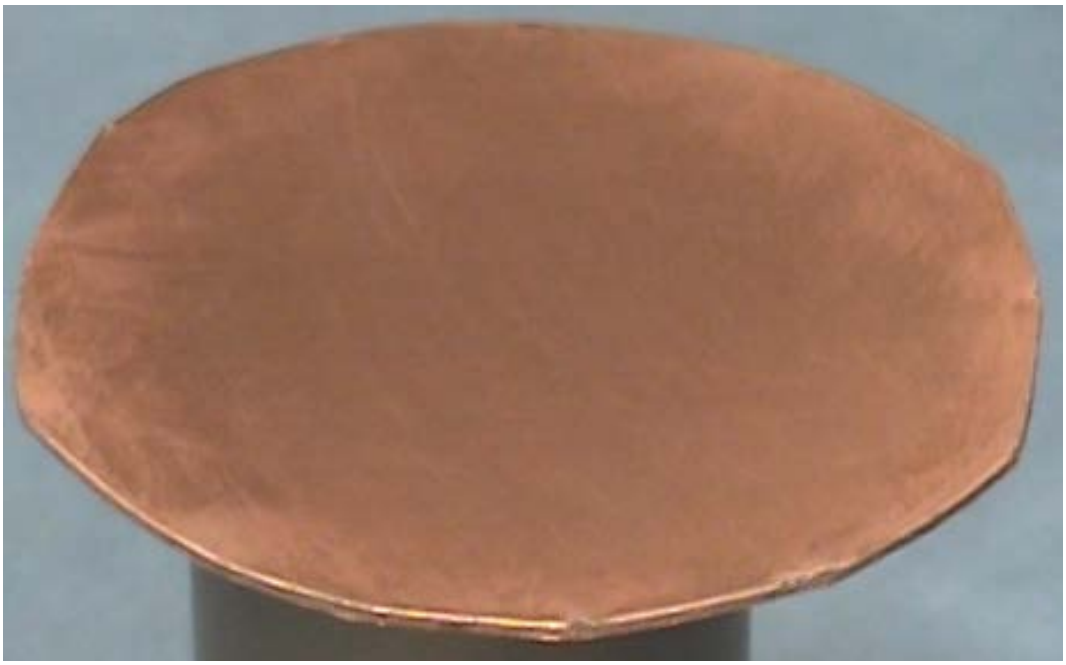

Figure 78: Brush on nano-diamond technique macro image on copper

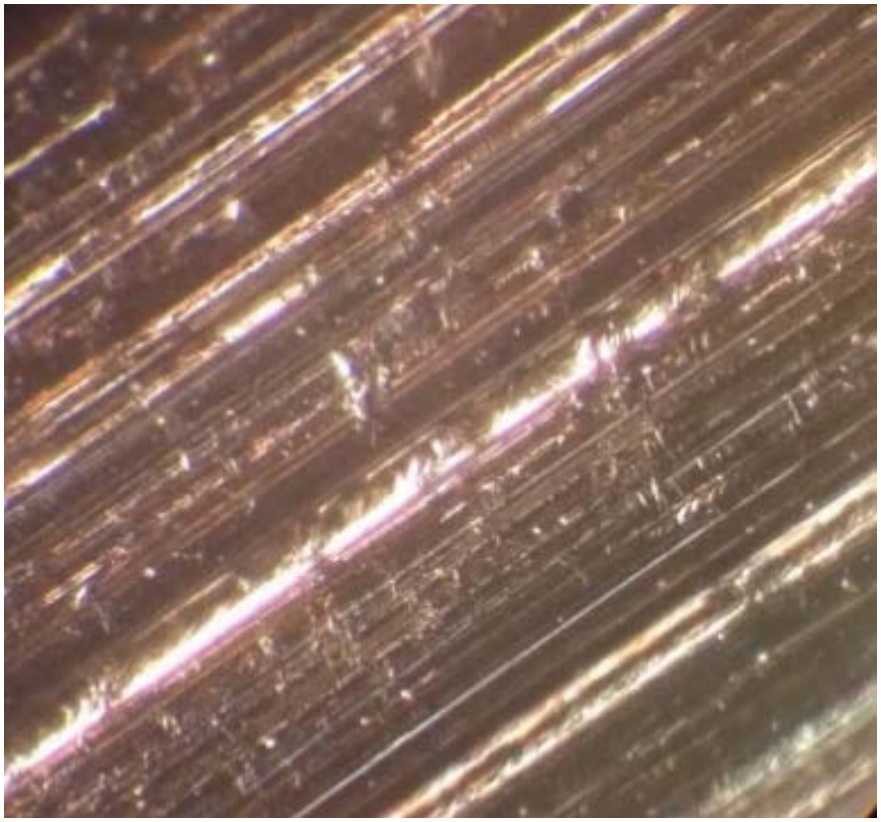

Figure 79: Without Nano-Diamond brush on technique optical microscope image. Magnification is 200x

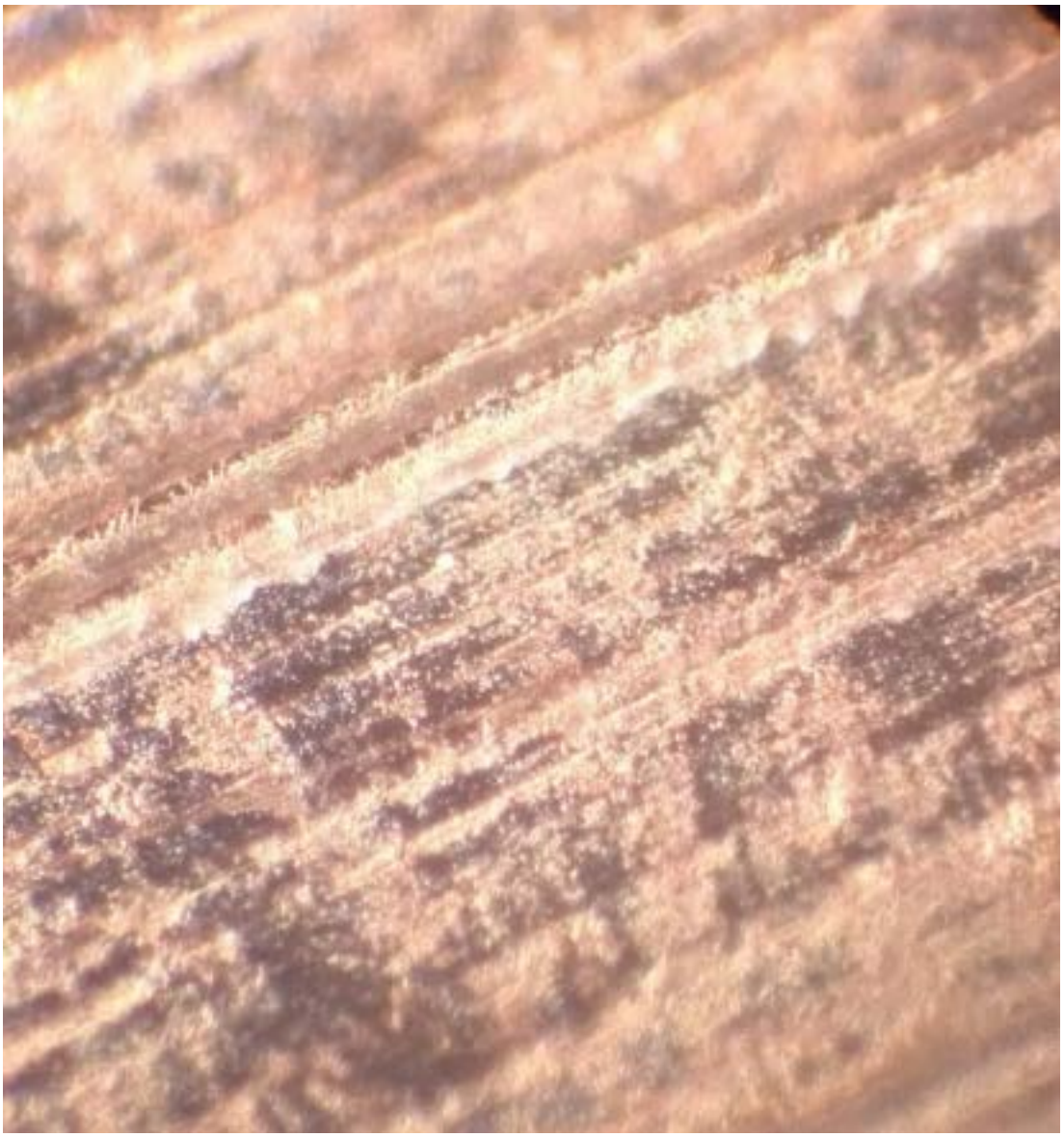

Figure 80: Brush on technique with Nano Diamond powder on copper. Magnification is 300x.

5. Brush- on nano-diamond with Pt/Ir
    a. If necessary, mechanically polish Pt/Ir with 5-8 µm diamond polishing powder
    b. Apply 0-2 µm diamond powder to Pt/Ir surface with electrostatic brush

c. Apply 1 kV, 2 mA electrostatic field 10 mm above Pt/Ir surface

d. Apply toroidal, 1.5 inch diameter, 1 Hz, 50 gauss max pulsing electromagnet 10 mm above metal surface

e. Observe alignment under optical microscope. If the distributed diamond powder is not uniform, remove diamond powder with DI and repeat procedure.

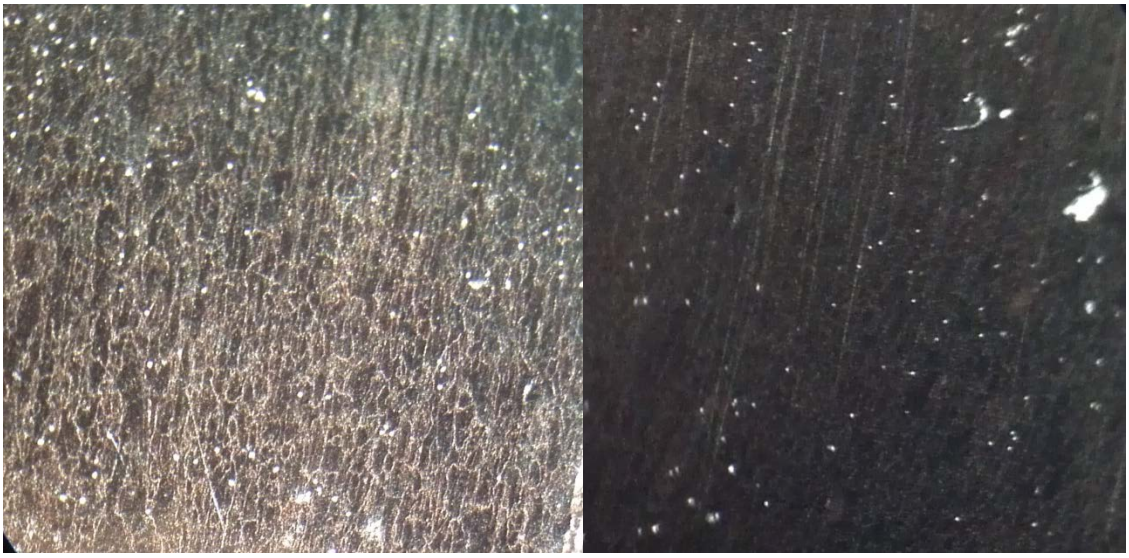

Figure 81: Unpolished and polished Pt/Ir example. Magnification is 200x.

Note: In this technique, 5-8 µm seeds may be also added to ensure that complete etching does not occur during nucleation.

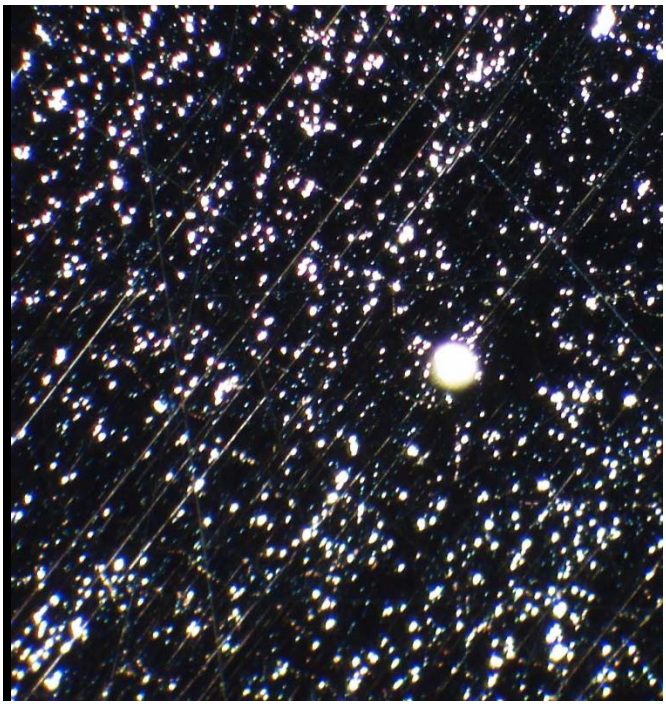

Figure 82: Distributed crystals before electrostatic and electromagnetic fields were applied. Larger crystals are 5-8 µm seeds applied in this technique. Crystals are closer sporadically distributed. Magnification is 200x.

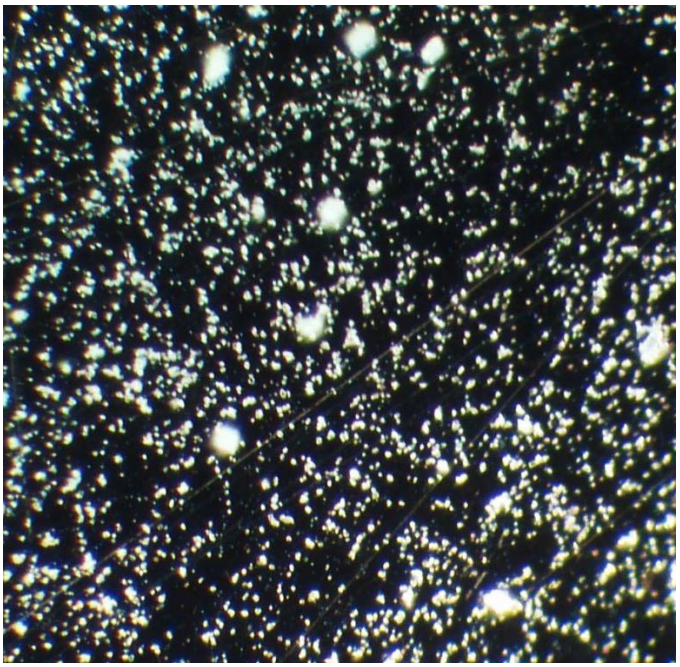

Figure 83: Distributed crystals after electrostatic and electromagnetic fields were applied. Larger crystals are 5-8 µm seeds applied in this technique. Crystals are closer together and more evenly distributed. Magnification is 200x.

# APPENDIX D

**Adobe Photoshop® CC 14.2.1 procedure for computing open area**

The image must be in focus and lighting must be consistent across surface.

1. Copy the background layer
2. On the top layer, apply the highpass filter to the image. The highpass radius should be set to accentuate the edges of the image and changes based on the image.
3. Change the display for the highpass layer to overlay. This is referred to as the highpass/overlay method. It is commonly used in photography to sharpen an image non-destructively. Toggle the highpass layer on/off to view the effect of the filter.
4. Create threshold layer and select threshold based on visual of original image. The "white space" should represent the crystal coverage. The black space should show where the spaces are.
5. Create selection using color range. Select black area on threshold layer with no fuzziness. Make sure the image is highlighted on the layers list and not the adjustment layer.
6. Use histogram to determine number of pixels selected. This is the open area with no crystals. Save the selection.
7. Select all. This is the total area of the crystals.
8. Use histogram to determine number of pixels selected.
9. Divide open area by total area.

# BIBLIOGRAPHY


1 Horowitz, F., Brandão, L. E., Camargo, K. C., Michels, A. F., & Balzaretti, N. M. , 'Nano-Microstructured, Superhydrophobic, and Infrared Transparent Polytetrafluoroethylene/Diamond Films', *Journal of Nanophotonics,* 7 (2013), 8.

2 Obraztsov, A. N., Kopylov, P. G., Loginov, B. A., Dolganov, M. A., Ismagilov, R. , et al., 'Single Crystal Diamond Tips for Scanning Probe Microscopy', *Review of Scientific Instruments,* 81 (2010), 5.

3 Zhang, M., Xia, Y., Wang, L., & Gu, B. , 'Cvd Diamond Devices for Charged Particle Detection', *Semiconductor science and technology,* 20 (2005), 5.

4 Lukosi, E., Prelas, M., & Palsmeier, J. , 'Monte Carlo Simulations of Multiplexed Electronic Grade Cvd Diamond for Neutron Detection', *Radiation Measurements,* 47 (2012), 8.

5 Lommatzsch, U. , Wahl, E. H. , Owano, T.G. , Kruger, C.H. , Zare, R.N. , 'Spatial Concentration and Temperature Distribution of Ch Radicals Formed in a Diamond Thin Film Hot-Filament Reactor', *Chemical Physics Letters,* 320 (2000), 339-44.

6 Tallaire, A., Achard, J., Silva, F., Brinza, O., & Gicquel, A., 'Growth of Large Size Diamond Single Crystals by Plasma Assisted Chemical Vapour Deposition: Recent Achievements and Remaining Challenges', *Comptes Rendus Physique,* 14 (2013), 16.

7 Matsumoto, Seiichiro, Yoichiro Sato, Masayuki Tsutsumi, and Nobuo Setaka. , 'Growth of Diamond Particles from Methane-Hydrogen Gas', *Journal of Materials Science,* 17 (1982), 6.

8 Kamo, Mutsukazu, Yoichiro Sato, Seiichiro Matsumoto, and Nobuo Setaka, 'Diamond Synthesis from Gas Phase in Microwave Plasma', *Journal of Crystal Growth,* 62 (1983), 3.

9 Tachibana, T., Ando, Y., Watanabe, A., Nishibayashi, Y., Kobashi, K., et al., 'Diamond Films Grown by a 60-Kw Microwave Plasma Chemical Vapor Deposition System', *Diamond and Related Materials,* 10 (2001), 4.

10 Yan, C. S., Vohra, Y. K., Mao, H. K., & Hemley, R. J., 'Very High Growth Rate Chemical Vapor Deposition of Single-Crystal Diamond', *Applied Physical Sciences,* 99 (2002), 3.

11 Silva, F., Achard, J., Brinza, O., Bonnin, X., Hassouni, K., et al., 'High Quality, Large Surface Area, Homoepitaxial Mpacvd Diamond Growth', *Diamond and Related Materials,* 18 (2009), 5.

12 Silva, F., Hassouni, K., Bonnin, X., & Gicquel, A. , 'Microwave Engineering of Plasma-Assisted Cvd Reactors for Diamond Deposition', *Journal of Physics: Condensed Matter,* 21 (2009), 17.

13 Yamada, H., Chayahara, A., Mokuno, Y., Tsubouchi, N., & Shikata, S. I. , 'Uniform Growth and Repeatable Fabrication of Inch-Sized Wafers of a Single-Crystal Diamond', *Diamond and Related Materials,* 33 (2013), 5.

14 Chayahara, A., Mokuno, Y. Tsubouchi, N. Yamada, H., 'Development of Single-Crystalline Diamond Wafers', *Synthesiology,* 3 (2010), 8.

15 Fischer, M., Gsell, S., Schreck, M., Brescia, R., & Stritzker, B., 'Preparation of 4-Inch Ir/Ysz/Si (001) Substrates for the Large-Area Deposition of Single-Crystal Diamond', *Diamond and Related Materials,* 17 (2008), 7.

16 Tallaire, A., Achard, J., Brinza, O., Mille, V., Naamoun, M., Silva, F., et al., 'Growth Strategy for Controlling Dislocation Densities and Crystal Morphologies of Single Crystal Diamond by Using Pyramidal-Shape Substrates', *Diamond and Related Materials,* 33 (2013), 7.

17 Hei, L. F., Liu, J., Li, C. M., Song, J. H., Tang, W. Z., et al., 'Fabrication and Characterizations of Large Homoepitaxial Single Crystal Diamond Grown by Dc Arc Plasma Jet Cvd', *Diamond and Related Materials,* 30 (2012), 13.

18 Vaissiere, N., Saada, S., Bouttemy, M., Etcheberry, A., Bergonzo, P., & Arnault, J. C. , 'Heteroepitaxial Diamond on Iridium: New Insights on Domain Formation', *Diamond and Related Materials,* 36 (2013), 10.

19 Kobashi, K., Nishibayashi, Y., Yokota, Y., Ando, Y., Tachibana, T., et al., 'R&D of Diamond Films in the Frontier Carbon Technology Project and Related Topics', *Diamond and Related Materials,* 12 (2003), 8.

20 Lee, D. G., & Singh, R. K., 'Synthesis of (111) Oriented Diamond Thin Films by Electrophoretic Deposition Process', *Applied Physics Letters,* 70 (1997), 1542.

21 Komiyama, H., Shimogaki, Y., & Egashira, Y., 'Chemical Reaction Engineering in the Design of Cvd Reactors', *Chemical engineering science,* 54 (1999), 16.

22 E. Zeiler, S. Schwarz, S.M. Rosiwal, R.F. Singer, 'Structural Changes of Tungsten Heating Filaments During Cvd of Diamond', *Materials Science and Engineering A335,* 335 (2002), 10.

23 Bachmann, P. K., Leers, D., & Lydtin, H., 'Towards a General Concept of Diamond Chemical Vapour Deposition ', *Diamond and Related Materials,* 1 (1991), 12.

24 Angus, J. C., Argoitia, A., Gat, R., Li, Z., Sunkara, M., Wang, L., & Wang, Y. , 'Chemical Vapour Deposition of Diamond', *Philosophical Transactions of the Royal Society of London. Series A: Physical and Engineering Sciences,* 342 (1993), 13.

25 Hu, Q., 'Diamond Based-Materials: Synthesis, Characterization and Applications' (University of South Florida, 2011), p. 160.

26 Popovici, G., Khasawinah, S. , Sung, T. , Prelas, M. A. , Spitsyn, B. V. , 'Raman Scattering Characterization of (100) and (111) Oriented Diamond Films Grown in the Same Run by Hot Filament Chemical Vapor Deposition', *Journal of Materials Research,* 9 (1994), 5.

27 Popovici, G., & Prelas, M. A., 'Nucleation and Selective Deposition of Diamond Thin Films', *Physica Status Solidi (a),* 132 (1992), 233-52.

28 Tolt, L. , Heatherly, L. , Ciausing, R. E. , Shaw, R. W., Feigerle, C. S. , 'Hfcvd of Diamond at Low Substrate and Low Filament Temperatures', (Department of Chemistry, University of Tennessee Knoxville, TN: National Science Foundation, Materials Sciences of the U.S. Department of Energy, 1995), p. 8.

29 Asmussen, J. , Reinhard, D., *Diamond Films Handbook* (New York, New York: Marcel Dekker, Inc, 2002).

30 Chao, C. H., Popovici, G., Charlson, E. J., Charlson, E. M., Meese, J. M., et al., 'Smooth Diamond Films Grown by Hot Filament Chemical Vapor Deposition on Positively Biased Silicon Substrates', *Journal of Crystal Growth,* 140 (1994), 454-58.

31 Jiang, X. C. P. R. M. H. J., Klages, C. P., Zachai, R., Hartweg, M., & Fusser, H. J. , 'Epitaxial Diamond Thin Films on (001) Silicon Substrates', *Applied physics letters,* 62 (1993), 3.

32 Liu, X., Yu, T., Wei, Q., Yu, Z., & Xu, X., 'Enhanced Diamond Nucleation on Copper Substrates by Employing an Electrostatic Self-Assembly Seeding Process with Modified Nanodiamond Particles', *Colloids and Surfaces A: Physicochemical and Engineering Aspects,* 412 (2012), 8.

33 Tachibana, Takeshi, et al., 'Diamond Films Heteroepitaxially Grown on Platinum (111)', *Physical Review B,* 56 (1997), 14.

34 Yarbrough, W. A., & Messier, R., 'Current Issues and Problems in the Chemical Vapor Deposition of Diamond', *Science,* 247 (1990), 8.

35 W. Zhu, P. C. Yang, and J. T. Glass, 'Oriented Diamond Films Grown on Nickel Substrates', *Applied Physics Letters,* 63 (1993), 3.

36 Lee, S. , Lin, Z. , Jiang, X. , 'Cvd Diamond Films: Nucleation and Growth', *Materials Science and Engineering: R: Reports,* 25 (1999), 32.

37 Kwon, Thomas J., 'Carbon Crystal Growth Using Electric Emission Enhanced Showerhead Hot Filament Chemical Vapor Deposition' (University of Missouri-Columbia, 2000), p. 90.

38 Prelas, M. A. , Popovici, G. , Bigelow, L. K. , *Handbook of Industrial Diamonds and Diamond Films* (New York, New York: CRC Press, 1997), p. 1232.

39 Chih-shiue Yan, Yogesh K. Vohra, Ho-kwang Mao, and Russell J. Hemley, 'Very High Growth Rate Chemical Vapor Deposition of Single-Crystal Diamond', *Proceedings of the National Academy of Sciences of the United States of America* 99 (2002), 3.

40 Zeiler, E., Schwarz, S., Rosiwal, S. M., & Singer, R. F., 'Structural Changes of Tungsten Heating Filaments During Cvd of Diamond', *Materials Science and Engineering A335,* 335 (2002), 10.

41 Schwarz, S., Rottmair, C., Hirmke, J., Rosiwal, S., Singer, R. F., 'Cvd-Diamond Single-Crystal Growth', *Journal of Crystal Growth,* 271 (2004), 425-34.

42 Mainak, R., 'Heterogeneous Growth of Diamond Films: Some Key Issues Resolved', ed. by BARC, Chemistry Division of (2007).

43 Mokuno, Y., Chayahara, A., Soda, Y., Horino, Y., & Fujimori, N., 'Synthesizing Single-Crystal Diamond by Repetition of High Rate Homoepitaxial Growth by Microwave Plasma Cvd', *Diamond and Related Materials,* 14 (2005), 4.

44 Shiomi, H., Tanabe, K., Nishibayashi, Y., & Fujimori, N., 'Epitaxial Growth of High Quality Diamond Film by the Microwave Plasma-Assisted Chemical-Vapor-Deposition Method', *Japanese journal of applied physics,* 29 (1990), 6.

45 Tallaire, A., Achard, J., Boussadi, A., Brinza, O., Gicquel, A., , et al., 'High Quality Thick Cvd Diamond Films Homoepitaxially Grown on (111)-Oriented Substrates', *Diamond and Related Materials,* 41 (2014), 7.

46 Mokuno, Y., Chayahara, A., & Yamada, H., 'Synthesis of Large Single Crystal Diamond Plates by High Rate Homoepitaxial Growth Using Microwave Plasma Cvd and Lift-Off Process', *Diamond and Related Materials,* 17 (2008), 4.

47 Mokuno, Y., Chayahara, A., Yamada, H., & Tsubouchi, N. , 'Improving Purity and Size of Single-Crystal Diamond Plates Produced by High-Rate Cvd Growth and Lift-Off Process Using Ion Implantation', *Diamond and Related Materials,* 18 (2009), 4.

48 Chen, Y. C., 'Diamond Chemical Vapor Deposition and Practical Applications' (Auburn University, 2009).

49 Wahl, E. H., 'Laser-Based Diagnostics of Diamond Synthesis Reactors' (Stanford University, 2001), p. 123.

50 Singh, J., 'Novel Techniques for Selective Diamond Growth on Various Substrates', *Journal of Materials Engineering and Performance,* 3 (1994), 7.

51 Chao, C. H., Popovici, G., Charlson, E. J., Charlson, E. M., Meese, J. M., and Prelas, M. A., 'Smooth Diamond Films Grown by Hot Filament Chemical Vapor Deposition on Positively Biased Silicon Substrates', *Journal of Crystal Growth,* 140 (1994), 454-58.

52 S.-Tong Lee, Zhangda Lin, Xin Jiang, 'Cvd Diamond Films: Nucleation and Growth', *Materials Science and Engineering: R: Reports,* 25 (1999), 32.

53 Ohtsuka, K., Fukuda, H., Suzuki, K., & Sawabe, A. , ' Fabrication of Epitaxial Diamond Thin Film on Iridium', *Jpn. J. Appl. Phys. ,* 36 (1997), 3.

54 M. Vedawyas, G. Sivananthan, Ashok Kumar, 'Textured Polycrystalline Diamond Films on Cu Metal Substrates by Hot Filament Chemical Vapor Deposition', *Materials Science and Engineering B78,* 78 (2000), 5.

55 Chen, Yu-Chun, 'Diamond Chemical Vapor Deposition and Practical Applications' (Auburn University, 2009).

56 Dong-Gu Lee, Rajiv K. Singh, 'Synthesis of (111) Oriented Diamond Thin Films by Electrophoretic Deposition Process', *Applied Physics Letters,* 70 (1997), 3.

57 Reginald B. Little, Xu Wang and Robert Goddard, 'Nano-Diamond Synthesis in Strong Magnetic Field', *JOURNAL OF CLUSTER SCIENCE,* 16 (2004), 10.

58 Galina Popovici, M. A. Prelas, 'Nucleation and Selective Deposition of Diamond Thin Films', *Solid State Physics, physica status solidi (a),* 132 (1992), 20.

59 Geis, M. W., 'Growth of Textured Diamond Films on Foreign Substrates from Attached Seed Crystals', *Applied Physics Letters,* 55 (1989), 3.

60 C.H. Chao, G. Popovici, E.J. Charlson, E.M. Charlson, J.M. Meese, M.A. Prelas, 'Smooth Diamond Films Grown by Hot Filament Chemical Vapor Deposition on Positively Biased Silicon Substrates', *Journal of Crystal Growth,* 140 (1994), 4.

61 P Bachmann, D Leers, H Lydtin, 'Towards a General Concept of Diamond Chemical Vapour Deposition ', *Diamond and Related Materials,* 1 (1991), 12.

62 Feng, Z. B., Chayahara, A., Mokuno, Y., Yamada, H., & Shikata, S. , 'Raman Spectra of a Cross Section of a Large Single Crystal Diamond Synthesized by Using Microwave Plasma Cvd', *Diamond and Related Materials,* 19 (2010), 3.

63 Jes Asmussen, D Reinhard, *Diamond Films Handbook* (New York, New York: Marcel Dekker, Inc, 2002).

64 Shenderova, Olga A., and Dieter M. Gruen., *Ultrananocrystalline Diamond: Synthesis, Properties and Applications* (Norwich, New York, U.S.A.: William Andrew, 2012).

65 Ferrari, A. C., & Robertson, J., 'Raman Spectroscopy of Amorphous, Nanostructured, Diamond–Like Carbon, and Nanodiamond', *Philosophical Transactions of the Royal Society of London. Series A: Mathematical, Physical and Engineering Sciences,* 362 (2004), 37.

66 Sumiya, H., & Irifune, T., 'Synthesis of High-Purity Nano-Polycrystalline Diamond and Its Characterization', *SEI Technical Review,* 59 (2005), 8.

67 Ungár, T., & Gubicza, J., 'Nanocrystalline Materials Studied by Powder Diffraction Line Profile Analysis', *Zeitschrift fur Kristallographie,* 223 (2007), 15.

68 'Practical Temperature Measurements', in *Agilent Technologies, Inc.* (2000).

69 Lin, Jeong-long ; Taylor, William L., 'Thermodynamics of Thermal Diffusion', (University of Cincinnati, Cincinnati, OH: U.S. Department of Energy, 1988).

70 R. Byron Bird, Warren E. Stewart, Edwin N. Lightfoot, *Transport Phenomena* (Wiley 2001), p. 914.

71 Eyring, Robert G. Mortimer and Henry, 'Elementary Transition State Theory of the Soret and Dufour Effects', *Proceedings of the National Academy of Sciences USA,* 77 (1980), 4.

# VITA

Paul Mason was born on October 4, 1971 in Parma, Ohio. He attended Holy Name High School and played football, wrestled, and ran track. He later attended Cleveland State University where he obtained his bachelor's and master's in science degrees in Chemical Engineering. From there he attended the University of Missouri to attain his Doctorate of Philosophy in Nuclear Engineering with an emphasis in Health Physics.

The views expressed in this dissertation are those of the author and do not reflect the official policy or position of the United States Air Force, Department of Defense, or the U.S. Government